Investigating the Function of *Drosophila* MAPs

Msd1 and dTD-60 in Mitotic Spindle Assembly

Submitted to the Degree of Doctor of Philosophy



Tommy Duncan B.A. (Hons)

Keble College
Oxford

Acknowledgements

A number of people have supported me throughout my D.Phil. First, I would like to thank Dr. James G. Wakefield primarily for his unwavering optimism throughout my project, but also for everything I have learned from him. I wish him well at the University of Exeter.

A major influence in my development as a scientist has been Dr. Alan Wainman, who, without obligation, has supported me constantly from the moment I entered the Lab until my thesis was submitted, despite leaving the Wakefield Lab halfway through. I am very grateful to him for helping me over the finish line.

A very big thank you to Dr. Stephen Kearsey and every member of his lab for accommodating and supporting me towards the end of my project.

Dr. David Sharp and his lab gave me an invaluable opportunity in New York to build upon my project. Thank you for being so welcoming, and for literally accommodating me.

Thank you also to my friends, notably the Darwin's Crew, who almost never discussed science with me at lunch time. Thanks to Matt, for struggling with me all the way, and to Mark, whose own scientific curiosity quite possibly hindered my progression.

Thanks to my wonderful girlfriend Zinnie, who now understands how to build a mitotic spindle using matchsticks.

Finally, thank you to my parents, whose lifelong support has enabled me to follow every one of my ambitions.

Abstract

Mitosis is the process by which new cells are formed. Following accurate duplication of chromosomes, a cell must segregate its chromosomes into separate daughter cells with great accuracy. Failure to do so can result in genomic instability. Thus, entry into mitosis is tightly regulated via complex protein interactions. Microtubules (MTs) are versatile Tubulin polymers that constitute a considerable portion of the cytoskeleton, and it is the dramatic rearrangement of MTs upon mitotic entry that is required to build the mitotic spindle – the structure responsible for segregating the duplicated sister chromatids. MTs are modulated by MT-Associated Proteins (MAPs) that enact major MT rearrangements during mitosis. Identifying and understanding the role of MAPs is essential to the study of MT behaviour during mitosis.

Recently, an RNAi screen for *Drosophila* MAPs identified two proteins that are the subject of this thesis; Msd1 and dTD-60. This thesis demonstrates that Msd1 is a novel MAP that is a component of the recently identified Augmin complex – the action of which is to generate a novel and redundant population of MTs within the mitotic spindle from existing MTs. Experiments described below demonstrate that Msd1 is required for Augmin-directed MT generation, and further investigate the role of this novel population of MTs within the developing fruit fly. Furthermore, a role for Msd1 in central spindle formation during anaphase in *Drosophila* is identified.

dTD-60, the *Drosophila* homologue of human TD-60 (hTD-60), is the subject of another study described in this thesis. While hTD-60 has a role in metaphase progression through interaction with the Chromosomal Passenger Complex, a contrasting role for dTD-60 is investigated here. This thesis describes both a divergent localisation and phenotype of dTD-60, and further investigates the role of dTD-60 and its interactors in mitotic spindle formation.

Table of Contents

1. Introduction 12

1.1. Microtubules & Mitosis 12
1.1.1. MT Structure & Assembly 12
1.1.2. Dynamic Instability 13
1.1.3. G2/M 13
1.1.4. Chromosome Attachment to the Spindle 14
1.1.5. Anaphase – Cytokinesis 15
1.2. Building the Mitotic Spindle 18
1.2.1. Introduction 18
1.2.2. Centrosome-nucleated MTs 19
1.2.3. Ran-dependent, chromatin directed MT generation 23
1.2.4. Kinetochore-driven MT generation 25
1.2.5. CPC-directed MT generation 26
1.2.6. MT-Templated MT-Nucleation 27
1.2.7. Cytoplasmic MTs 29
1.2.8. Relative contributions of each pathway 30
1.3. *Drosophila* Development 33
1.3.1. Oogenesis 33
1.3.2. The Syncytial Blastoderm 33
1.3.3. Mitosis Post-Cellularisation 34
1.4. Msd1 and dTD-60 as MAPs 34

2. Materials & Methods 36

2.1. Resources Used in this Thesis 36
2.2. Fly Stocks 39
2.2.1. Keeping Fly Stocks 39
2.2.2. Deficiency Complementation 39
2.2.3. Fertility Tests 39

2.2.4. Collecting Embryos 40
2.2.5. GFP Expression in Embryos 40
2.2.6. Hatch Rates 43
2.2.7. Recombination 43
2.2.8. FRT-Directed Recombination 43
2.2.9. Imprecise Excision of P-elements 43
2.3. Molecular Techniques 48
2.3.1. Isolation of gDNA 48
2.3.2 Isolation of gDNA from Individual Males 48
2.3.3. Isolation of mRNA 49
2.3.4. Production of cDNA 49
2.3.5. Production of dsRNA 49
2.3.6. PCR 50
2.3.7. Purification of PCR Products 50
2.3.8. Sequencing 51
2.3.9. Cloning GFP Fusion Proteins 51
2.3.10. Restriction Digests 52
2.4. Biochemistry 53
2.4.1. SDS PAGE 53
2.4.2. Western Blotting 53
2.4.3. MT Spin-down (MTSD) 54
2.4.4. Coupling of Antibodies to Protein A Beads 54
2.4.5. Antibody Co-Immunoprecipitation 55
2.4.6. Antibody Co-Immunoprecipitation with Chromotek α-GFP Beads 55
2.4.7. Sucrose Gradients 56
2.5. Cytology 57
2.5.1. Fixing Embryos 57
2.5.2. Culturing *Drosophila* S2 Cells 57
2.5.3. Transient Transfection of S2 Cells 57
2.5.4. S2 Cell RNAi 58
2.5.5. Fixing S2 Cells 58
2.5.6. Antibody Staining of Fixed Tissues 59
2.5.7. Imaging Fixed S2 Cells 60
2.5.8. Imaging Live S2 Cells 60

2.5.9. FRAP in S2 Cells 60
2.5.10. Imaging Fixed Embryos 61
2.5.11. Imaging Live Embryos 61

3. Results 62

3.1. Msd1 and the Augmin Complex 62
3.1.1. Msd1 is a MAP 62
3.1.2. *msd1* RNAi Significantly Reduces Mitotic Spindle Density 64
3.1.3. Duration of *msd1* RNAi Exposes a Phenotypic Progression 67
3.1.4. *msd1* RNAi Eliminates γ-Tubulin Staining from Spindle MTs, Independently of the Centrosome 69
3.1.5. Msd1 is Required for the Localisation of Dgt6 to the Spindle 72
3.1.6. Msd1 Co-Fractionates with the Augmin Complex 72
3.1.7. Msd1 Co-Precipitates with the Augmin Complex 75
3.1.8. Large Scale Co-Immunoprecipitation Shows Msd1 Interactors via Mass-Spectrometry 77
3.1.9. Discussion 78
3.2. Msd1 and *Drosophila* Development 81
3.2.1. $msd1^{ex51}$ is a Hypomorphic Allele Causing Maternal Effect Lethality 81
3.2.2. $msd1^{ex51}$ Meiotic Spindles Appear Normal 83
3.2.3. $msd1^{ex51}$ Phenotype is Intensified Over Deficiency 83
3.2.4. $msd1^{ex51}$ is Rescued by Msd1-GFP in Embryos 87
3.2.5. $msd1^{ex51}$ Phenotype is Consistent with S2 Cells 87
3.2.6. $msd1^{ex51}$ has a Significantly Reduced Mitotic Spindle Density in Early Embryos Expressing α-Tubulin-GFP 90
3.2.7. $msd1^{ex51}$ Embryos Are Delayed in Metaphase Progression 94
3.2.8. $msd1^{ex51}$ Nuclei Have Errors in Chromosome Congression and Aneuploidy 96
3.2.9. $msd1^{ex51}$ has a Significantly Reduced Spindle/Centrosome Ratio of γ-Tubulin-GFP in Early Embryos 96
3.2.10. Live Analysis of Moesin-GFP Reveals No Clear Defects in Actin Organisation in $msd1^{ex51}$ embryos 101
3.2.11. Discussion 104
3.3. Mitotic Spindle Dynamics After Metaphase 107
3.3.1. The Central Spindle is Disrupted in $msd1^{ex51}$ Early Embryos 107

3.3.2. *msd1* RNAi Causes Central Spindle Defects in Live S2 Cells Expressing α-Tubulin-GFP 109
3.3.3. *msd1* RNAi Affects EB1-GFP Localisation at the Central Spindle in Anaphase 109
3.3.4. *msd1* RNAi Reduces Turnover of MTs During Central Spindle Formation 110
3.3.5. Discussion 116
3.4. Characterisation of dTD-60 119
3.4.1. CG9135 Shows Homology to hTD-60 119
3.4.2. dTD-60 Localisation Differs from hTD-60 121
3.4.3. GFP-dTD-60 Localises Dynamically in the Early Embryo 121
3.4.4. *dTD-60* RNAi Shows No Clear Phenotype 125
3.4.5. *dTD-60* RNAi Does Not Disrupt INCENP Localisation 129
3.4.6. Double Knock-Down of *dTD-60* and its Orthologue, *bj1* Shows No Clear Phenotype 130
3.4.7. Large Scale Co-Immunoprecipitation Shows dTD-60 Interactors via Mass-Spectrometry 134
3.4.8. Preliminary RNAi screen of dTD-60 interactors 134
3.4.9. Mutant Generation Using FRT-Directed Recombination 138
3.4.10. Imprecise Excision of P-element P{GawB}NP2466 141
3.4.11. Discussion 141

4. Discussion 143

4.1. Msd1 – A novel MAP required for MT-templated MT nucleation 143
4.2. A divergent role for TD-60 in *Drosophila* 148

5. References 150

List of Figures

Figure 1-1. MT nucleation in the mitotic spindle……22
Figure 2-1. Crosses to express UAS-fusion constructs that are on the 2nd chromosome……41
Figure 2-2. Crosses to express UAS-fusion constructs that are on the 3rd chromosome……42
Figure 2-3. Crosses to generate *msd1*^{ex51};γTub-GFP chromosome……44
Figure 2-4. Recombination crosses to generate *msd1*^{ex51};*mad2* chromosome……45
Figure 2-5. FRT-based recombination of P-elements PBac^{f03307} and P[HA5045}……46
Figure 2-6. Crosses to generate a P-element excision using a Δ2-3 source……47
Figure 3-1. Msd1 is a MAP……63
Figure 3-2. *msd1* RNAi reduces mitotic spindle density……65
Figure 3-3. *msd1* RNAi reduces spindle/centrosome α-Tubulin intensity……66
Figure 3.4. Duration of *msd1* RNAi causes different phenotypes……68
Figure 3.5. Msd1 is required to localise γTubulin specifically to the spindle……70
Figure 3-6. *msd1* RNAi significantly reduces spindle/centrosome γ-Tubulin intensity……71
Figure 3-7. Msd1 is required for the localisation of Augmin subunit Dgt6 to spindle MTs……73
Figure 3-8. Msd1 co-fractionates with the Augmin complex……74
Figure 3-9. Msd1 co-precipitates with the Augmin complex……76
Figure 3-10. *msd1*^{ex51} is a hypomorphic allele that is maternal effect lethal……82
Figure 3-11. Spindle bipolarity is not disrupted in *msd1*^{ex51} meiotic spindles……85
Figure 3-12. *msd1*^{ex51} developmental failure is intensified over deficiency……86
Figure 3-13. *msd1*^{ex51} embryos are rescued by Msd1-GFP……88
Figure 3-14. *msd1*^{ex51} embryos show a phenotype comparable to S2 cells……89
Figure 3-15. α-Tubulin-GFP shows a phenotype consistent with Augmin in *msd1*^{ex51} embryos……92
Figure 3-16. *msd1*^{ex51} embryos have a significantly reduced spindle/centrosome α-Tubulin intensity……93
Figure 3-17. *msd1*^{ex51} embryos are delayed in metaphase progression……95

Figure 3-18. *msd1*^{ex51} embryos show errors in chromosome congression and aneuploidy……98
Figure 3-19. γ-Tubulin-GFP is absent from spindles in *msd1*^{ex51} embryos……99
Figure 3-20. *msd1*^{ex51} embryos have significantly reduced spindle/centrosome γ-Tubulin-GFP intensity.. ……100
Figure 3-21. *msd1*^{ex51} embryos have no clear defects in Actin dynamics……103
Figure 3-22. The Central Spindle is disrupted in *msd1*^{ex51} embryos……108
Figure 3-23. *msd1* knock-down causes anaphase defects in live S2 cells……112
Figure 3-24. Fluorescence recovery is diminished as a result of *msd1* knock-down in S2 cells……113
Figure 3-25. Fluorescence recovery of α-Tubulin-GFP is diminished at the central spindle in the absence of Msd1……114
Figure 3-26. Kymographs show that Msd1 is required for a specific population of MTs within the central spindle……115
Figure 3-27. CG9135 shows homology to human TD-60……120
Figure 3-28. dTD-60 localises to chromatin and the spindle in metaphase, and the mid-body in late telophase……123
Figure 3-29. dTD-60-GFP localises dynamically in the early embryo……124
Figure 3-30. *dTD-60* RNAi reduces dTD-60 protein levels……126
Figure 3-31. *dTD-60* RNAi has no effect on mitotic index……127
Figure 3-32. *dTD-60* RNAi shows no clear phenotype……128
Figure 3-33. *dTD-60* RNAi does not disrupt INCENP localisation in metaphase……..131
Figure 3-34. *dTD-60* RNAi does not disrupt INCENP localisation in telophase……..132
Figure 3-35. Double knock-down of *dTD-60* with *bj1* has no clear phenotype……133
Figure 3-36. RNAi analysis of dTD-60 interactors……136
Figure 3-37. dTD-60 interactors have a role in spindle length regulation……137
Figure 3-38. Genetic elements utilised at the *CG9135* locus……140
Figure 4-1. Redundancy of MT nucleation pathways in the mitotic spindle……..144

List of Abbreviations

APC/C	Anaphase Promoting Complex/Cyclosome
CPC	Chromosomal Passenger Complex
CPP	Chromosomal Passenger Protein
EDTA	Ethylenediaminetetraacetic Acid
EGTA	Ethylene glycol tetraacetic Acid
GFP	Green Fluorescent Protein
GTP	Guanosine Triphosphate
HEPES	N-2-Hydroxyethylpiperazine-N'-2-Ethanesulphonic Acid
kMT	Kinetochore Microtubule
LB	Luria-Bertain Broth
MAP	Microtubule Associated Protein
MT	Microtubule
MTOC	Microtubule Organising Centre
NEB	Nuclear Envelope Breakdown
PAGE	Poly-Acrylamide Gel Electrophoresis
PBS	Phosphate Buffered Saline
PCR	Polymerase Chain Reaction
SAC	Spindle Assembly Checkpoint
SDS	Sodium Dodecyl Sulphate
SEM	Standard Error of the Mean
γ-TuRC	γ-Tubulin Ring Complex
γ-TuSC	γ-Tubulin Small Complex

1. Introduction

1.1. Microtubules & Mitosis

1.1.1. MT Structure & Assembly

MTs are polymers of α/β-Tubulin heterodimers – GTPases of approximately 50kDa that comprise a significant proportion of the cell cytoskeleton. Lateral association of 12-15 α/β-Tubulin protofilaments results in a polarised MT polymer that has numerous roles throughout the cell cycle (Nogales *et. al,* 1998). This polarity is governed by the organisation of α/β-Tubulin dimers within the MT. β-Tubulin is oriented towards the plus-end, and α-Tubulin toward the minus-end. This organisation means that GTP that is bound to α-Tubulin cannot be hydrolysed, and is thus a structural component of a MT. β-Tubulin subunits account for GTP-hydrolysis within the MT. Thus, MTs have a structural polarity that is reflected in their polymerisation dynamics.

MTs originate via nucleation, and grow in a plus-end directed manner. While MT nucleation can occur *in vitro* from pure α/β-Tubulin dimers (Desai *et. al,* 1997), MT polymerisation is highly regulated throughout the cell cycle. γ-Tubulin is considered the primary MT nucleating protein. As part of the γ-Tubulin Ring Complex (γ-TuRC), γ-Tubulin is present at MT minus-ends and directs the polymerisation of new MTs (Luders *et. al,* 2007). During mitosis, accurate modulation of MT stability is essential for mitotic spindle assembly, and thus for the fidelity of sister chromatid segregation.

Crucial to this process are Microtubule Associated Proteins (MAPs), which bind to, and modulate, MTs depending on cell cycle specific signalling.

1.1.2. Dynamic Instability

Dynamic instability of MTs was first observed *in vitro.* Within a population of MTs, no single MT exhibits a steady state length, instead transitioning regularly between growth and shrinkage phases (Mitchison & Kirschner 1984, Horio & Hotani 1986). Growth of a MT plus end is dependent on the concentration of free GTP-Tubulin, which caps the growing MT plus end. Shrinkage of a MT is initiated by GTPase activity of β-Tubulin. Hydrolysis of GTP results in GDP-bound tubulin within the MT, resulting in an unstable MT conformation, and subsequent catastrophe. Moreover, these depolymerising MTs are occasionally rescued by the addition of GTP-bound tubulin (Desai & Mitchision 1997). This transient transitioning from MT growth to shrinkage is termed dynamic instability – a phenomenon that is highly modulated by MAPs and increases dramatically as the cell enters mitosis.

1.1.3. G2/M

Mitotic entry ultimately depends upon the activation of Cyclin Dependent Kinase 1 (CDK1) by Cyclin B. CDK1 phosphorylates multiple mitotic targets, initiating mitotic spindle assembly via positive feedback loops with downstream effectors – notably Polo and Aurora A kinases. Polo-like kinase 1 (Plk1) is required for correct bipolar spindle assembly via its localisation to the centrosome at the onset of mitosis. Here, Plk1 organises centrosomal components such as Cnn and γ-Tubulin to generate MT asters (Dobbelaere *et. al,* 2008; Lane *et. al,* 1996). Furthermore, Aurora A localisation

to the centrosome is dependent upon Plk1 activity – a mechanism that is essential for spindle bipolarity (Gonzalez *et. al,* 1998). Accurate mitotic progression depends upon regulation of these upstream kinases. Aurora A kinase activity is modulated by reversible phosphorylation. DNA damage at the G2 checkpoint inactivates Cyclin B-CDK1 complexes through the action of Wee1 kinase, in turn inactivating Aurora A to prevent the onset of mitosis (Marumoto *et. al,* 2002). At the onset of mitosis, MAPs such as Msps and TPX2 are employed as downstream effectors of these major mitotic kinases to promote spindle assembly and accurate chromosome segregation. Notably, spindle assembly factors (SAFs) become active, and are the subject of Section 1.2 of this thesis.

1.1.4. Chromosome Attachment to the Spindle

Accurate chromosome attachment and congression to the metaphase plate is essential to avoid genomic instability. Following nuclear envelope breakdown (NEB), sister chromatids must achieve bioriented attachments to the mitotic spindle to satisfy the Spindle Assembly Checkpoint (SAC). The kinetochore - a large, multiprotein complex is assembled at the centromeres of replicated sister chromatids – is integral to chromosome attachment to the mitotic spindle. Ndc80, a conserved, 4-subunit component of the KMN network, localises to the outer kinetochore and is a key component for generating spindle MT attachments. Ndc80 binds to MTs (Cheeseman *et. al,* 2006) and is required for stable kinetochore MT attachment, and for SAC signalling (McCleland *et. al,* 2003).

Biorientation of sister kinetochores on the spindle is a dynamically regulated process. Both syntelic (both sister chromatids attaching to one pole) and merotelic (both poles attaching to a single chromatid) attachments to the spindle result in lagging chromosomes and aneuploidy. By regulating Kinetochore MT (kMT) stability depending upon kinetochore attachment status, cells negatively regulate this process until biorientation is achieved. Aurora B Kinase, a component of the Chromosomal Passenger Complex (CPC) that is required for spindle bipolarity and cytokinesis, localises to the inner centromere and is essential for correcting improper attachments in experimentally induced monopolar spindles (Lampson *et. al,* 2004; See section 1.2.5). Aurora B becomes enriched at merotelic attachments where it regulates MT depolymerising enzymes such as MCAK to correct these errors (Andrews *et. al,* 2004). Moreover, Aurora B negatively regulates improper attachments by phosphorylating the Ndc80 complex, reducing its affinity to MTs (Cheeseman *et. al,* 2006). Although this mechanism is unclear, tension across sister kinetochores appears to spatially segregate Aurora B at the inner centromere from its substrates at the kinetochore, suggesting that bioriented kinetochores physically limit the MT destabilising capacity of Aurora B (Liu *et. al,* 2009).

1.1.5. Anaphase – Cytokinesis

When the SAC is satisfied, activation of the Anaphase Promoting Complex/Cyclosome (APC/C) initiates chromosome segregation in anaphase, initially via destruction of Cyclin B. Liberation of separase by proteolytic destruction of securin results in cleavage of the cohesin complex that binds sister chromatids together, in a process that can be separate from Cyclin B destruction (Stratmann *et.*

al, 1996). A further dramatic reorganisation of spindle MTs, regulated by MAPs, accurately co-ordinates the formation of identical daughter cells. Numerous Kinesin MT motors in addition to Dynein contribute to anaphase, modulating MT dynamics to generate poleward force to separate chromatids during anaphase A, and sliding interpolar MTs as the cell extends during anaphase B (Sharp *et. al,* 2000).

The Central Spindle, composed primarily of MT bundles and MAPs, forms after chromosome segregation, and is required for abscission during cytokinesis in a number of cell types (Wheatley *et. al,* 1996). Dynamic relocalisation of the Chromosomal Passenger Complex (CPC) to the spindle mid-zone during anaphase is required for central spindle assembly. Phosphorylation of numerous central spindle components including MKLP1/Pav and PRC1 by Aurora B occurs at the central spindle to initiate MT bundling (Wheatley *et. al,* 2001, Ban *et. al,* 2004). MKLP1/Pav is a component of the tetrameric Centralspindlin motor complex that contributes to bundling and regulates RhoA to organise the contractile ring (Glotzer 2005). PRC1 is a MAP that has MT bundling activity but also interacts with the essential MT motor Kif4a at the central spindle (Zhu *et. al,* 2005). Loss of PRC1 results in a diffuse localisation of Centralspindlin during anaphase (Verni *et. al,* 2004). Evidently, complex and inter-dependent interactions between these components facilitate central spindle assembly.

The contribution of MT polymerisation to central spindle assembly is not clear. Photobleaching experiments identified a role for MT turnover during spindle elongation in anaphase, although the rate of tubulin exchange is markedly reduced

relative to metaphase spindles (Saxton *et. al,* 1987). Furthermore, rapid incorporation of fluorescently labelled tubulin is observed throughout the spindle mid-zone in anaphase (Shelden *et. al,* 1990), an observation that is consistent with the presence of plus-end markers here (Rosa *et. al,* 2006). The origin of these new MTs, and their role in central spindle assembly is not understood.

1.2. Building the Mitotic Spindle

The majority of the following section (1.2) has been submitted as part of a review article (in press).

1.2.1. Introduction

The accurate segregation of duplicated chromosomes, essential for the development and viability of a multi-cellular organism, requires the formation of a robust MT-based spindle apparatus. Entry into mitosis or meiosis initiates a cascade of signalling events which result in the activation of pathways responsible for a dramatic reorganisation of the MT cytoskeleton; through changes in the properties of MAPs, local concentrations of free tubulin dimer, and through enhanced MT nucleation. The latter is considered to be driven by localisation and activation of γ-Tubulin-containing complexes (γ-TuSC and γ-TuRC) at specific sub-cellular locations. For example, upon entering mitosis, animal cells concentrate γ-Tubulin at centrosomes to tenfold the normal level during interphase, resulting in aster-driven search and capture of chromosomes, and bipolar mitotic spindle formation (Khodjakov *et. al,* 1999). Thus, in these cells, centrosomes have traditionally been perceived as the primary microtubule organising centre (MTOC) during spindle formation. However, studies in meiotic cells, plants, and cell-free *Xenopus* extracts have revealed the existence of complementary mechanisms of spindle formation; mitotic chromatin, kinetochores, the spindle matrix and existing MTs can all contribute to a bipolar spindle apparatus.

1.2.2. Centrosome-nucleated MTs

Early experiments in animal cells unequivocally established centrosomes as the primary MTOCs during mitosis. For example, unfertilised *Xenopus* embryos, which do not ordinarily contain a centrosome, will undergo cell cycle oscillations when pricked with a needle. However, these embryos will not undergo cell division unless a centrosome is coinjected (Maller *et. al,* 1976). Centrosomes consist of a pair of perpendicular centrioles that organise the surrounding pericentriolar material (PCM; Bobinnec *et. al,* 1998). The PCM is an electron dense structure consisting of many proteins, including γ-Tubulin in the form of the γ-Tubulin ring complex (γ-TuRC; Hannak *et. al,* 2002). Increased nucleation of MTs by centrosomes at the onset of mitosis or meiosis depends on the co-ordinated action of centriolar and PCM components that recruit and anchor increased amounts of γ-Tubulin at the spindle pole. In human cells this is facilitated, at least in part, by the centrosomal protein Pericentrin (Zimmerman *et. al,* 2004). In flies, where the pathway of centrosome maturation has been more extensively studied, the Pericentrin-like Protein (D-PLP) shares this role with centrosomin (Cnn). The localisation of both these PCM proteins is dependent upon the presence of the core centriolar component D-Spd2 (Dix *et. al,* 2007, Giansanti *et. al,* 2008), while the phosphorylation of Cnn by the mitotic kinase, Polo, correlates with centrosome maturation (Dobbelaere *et. al,* 2008), suggesting a hierarchical pathway in which γ-Tubulin is targeted and maintained at the PCM in step-wise fashion.

Interestingly, centrosome maturation does not fully account for the increase in astral MTs nucleated early in mitosis. Centrosomal MTs, once formed, do not remain

tightly bound to γ-Tubulin, but are nonetheless held in the vicinity of the PCM (Mastronade *et. al.* 1993). Whether the detachment of newly nucleated MTs from the γ-TuRC template is a passive process or whether an active severing of MTs close to the minus end occurs, it is clear that maintaining an interaction between MTs and the PCM is crucial for centrosome function; the loss of centrosomal MAPs such as Asp leads to centrosomes that continue to nucleate short astral MTs, but that detach from the bulk of MTs that have already contributed to the growing spindle (Gonzalez *et. al,* 1990).

The dramatic increase in centrosome-driven MT nucleation at the onset of mitosis leads to the astral arrays so familiar in textbooks (See Figure 1-1). Although initially radial, the centrosome-derived MTs begin to grow with directional bias, such that the density of MTs between the centrosomes and the mitotic chromatin is greater than between the centrosomes and the cell cortex. It is clear that the assembly of a bipolar spindle is achieved through many additional MAPs, and MT motor proteins, working in concert with one another. For example, dynamics at the spindle pole are regulated by MAPs including D-TACC and Msps/XMAP215, a complex required for proper astral MT function (Gergely *et. al,* 2000, Lee *et. al,* 2001).

Despite the well-characterised and diverse functions of centrosomes during spindle formation, ablation of both centrosomes during prophase in Monkey CVG-2 cells by laser microsurgery does not disrupt bipolar spindle assembly (Khodjakov *et. al,* 2000). This is perhaps unsurprising, given the accumulated evidence of acentrosomal meiotic systems in mouse (Calarco-Gillam *et. al,* 1983), *Xenopus* (Heald *et. al,* 1996)

and *Drosophila* (Matthies *et. al,* 1996). Furthermore, while some basal land plants exhibit mitotic spindles with centriole-containing centrosomes, it is clear that higher plants do not employ this mechanism (Shimamura *et. al,* 2004, Brown *et. al,* 2004).

Drosophila cnn null mutants fail to recruit PCM, thus reducing the MT nucleating capacity of the centrosome. Nonetheless, spindles in *cnn* null mutants are formed in the absence of astral MTs, these flies develop to adulthood with near-normal timing and few observable defects in morphology or developmental timing (Megraw *et. al,* 2001). Moreover, a null mutant in *DSas-4*, a centriole duplication factor, was also shown to develop into a morphologically normal adult. Although severe co-ordination defects due to a lack of cilia are ultimately lethal for these adults, and larval brain cells commonly show both a delay in mitosis and a failure to establishing asymmetry, bipolar mitotic spindles capable of chromosome segregation form (Basto *et. al,* 2006).

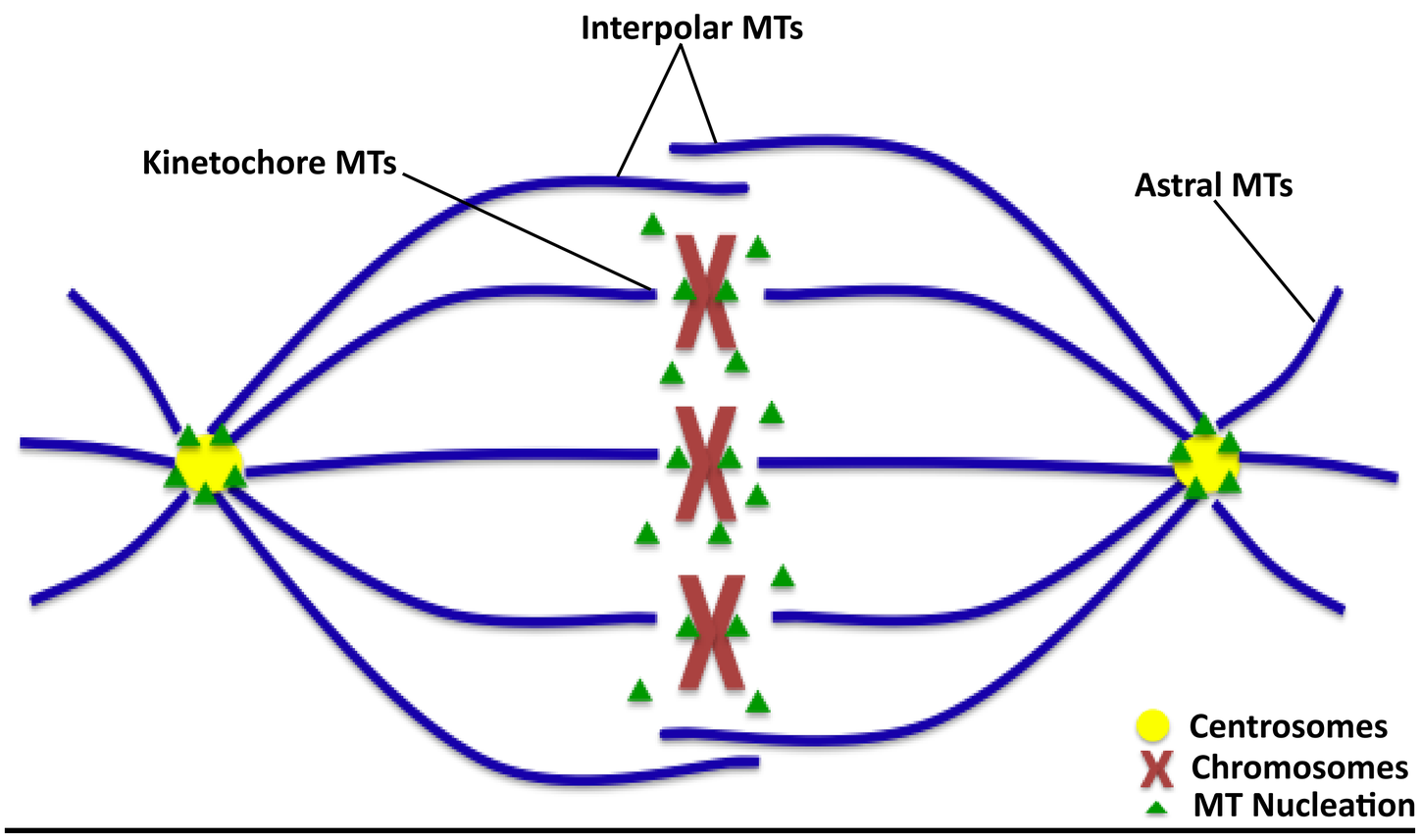


Figure 1-1. MT nucleation in the mitotic spindle.
MTs are known to be nucleated (Green) from 2 distinct regions of the mitotic spindle. New MTs form at both the centrosomes (Yellow) and in the vicinity of the chromatin (Maroon) in a diffuse manner surrounding chromatin and at the kinetochores**.**

1.2.3. Ran-dependent, chromatin directed MT generation

The ability of cells to build a spindle in the absence of centrosomes implies that redundant mechanisms must exist to generate and organise MTs (Rebollo *et. al,* 2004). Many mitotic and meiotic animal cells that divide in the absence of centrosomes, such as *Drosophila* female meiotic spindles, organise MTs in the vicinity of condensed chromatin and arrange them in a bipolar array (Theurkauf *et. al,* 1992).

The ability of condensed chromatin to form a bipolar spindle has been described most clearly in an *in vitro* system using *Xenopus* egg extracts. When sperm nuclei (containing centrosomes) are added to such extracts, focused spindles form primarily via centrosomal nucleation of MTs followed by the concerted action of motor proteins such as cytoplasmic dynein and MAPs such as NuMA (Sawin *et. al,* 1991, Heald *et. al,* 1997). However, the addition of beads coated with mitotic chromatin to activated extracts lacking centrosomes, similarly initiates the formation of bipolar spindles with two focused poles, and a similar distribution of spindle lengths as those with centrosomes. Interestingly however, these spindles take much longer to form, and pass through a number of intermediate structures not seen when centrosomes are present (Heald *et. al,* 1996).

This chromatin-directed MT assembly is dependent upon the small GTPase Ran, via the localisation of its guanine nucleotide exchange factor, RCC1. Upon nuclear envelope breakdown, RCC1 binds to condensing chromatin. This generates a well-

characterised gradient of Ran.GTP in the vicinity of the chromosomes. First described in the *Xenopus in vitro* system using FRET reporters (Kalab *et. al,* 2002), this gradient has also been shown to be present in human somatic cells (Kalab *et. al,* 2006).

MT organisation by Ran.GTP relies upon its liberation of cargo proteins from the nuclear import factor Importin-β, and an excess of Importin-β inhibits spindle formation. These liberated cargoes, termed spindle assembly factors (SAFs), include TPX2, a spindle pole protein required for the targeting of XKlp2 to MT minus ends (Wittmann *et. al,* 2000, Gruss *et. al,* 2001), and HURP (Wong *et. al,* 2006). TPX2 induces aster formation at the spindle poles via a physical interaction with Aurora A, which contributes to activation of the kinase (Trieselman *et. al,* 2003). Active Aurora A can stabilise MTs via phosphorylation of a protein complex containing Msps/XMAP215, Eg5 and HURP (Koffa *et. al,* 2006). In the absence of pre-polymerised MTs, HURP has also been shown to act independently of this complex. HURP is active in a Ran.GTP-dependent manner, and is required for bipolar spindle formation via an action that is distinct from TPX2 (Casanova *et. al,* 2008).

However, *Xenopus* extracts with the Ran.GTP gradient experimentally flattened (via titration of dominant negative Ran (RanT24N) with a constitutively active form (RanQ69L) throughout the extract) can support bipolar spindle formation when sperm nuclei (containing kinetochores and centrosomes), are added, thus implicating additional spatial signals for guiding MT growth (Maresca *et. al,* 2009).

1.2.4. Kinetochore-driven MT generation

For over 30 years, it has been known that kinetochores can initiate MT polymerisation *in vivo* independently of centrosomes (Witt *et. al,* 1980) and, for over 20 years that they can modulate the stability of MTs that are kinetochore-bound (Hyman *et. al,* 1990). Live imaging of MTs has conclusively shown that in normal mitotic cells these kinetochore-generated MTs exist, incorporating into the growing, centrosome-driven spindle via their capture by astral MTs (Khodjakov *et. al,* 2003, Maiato *et. al,* 2004). Different populations of MTs are thus incorporated into a single bipolar spindle.

However, the mechanisms underlying kMT generation and their contribution to spindle assembly in normal cells have been difficult to elucidate. This is mainly due to the relationship between MTs and kinetochores. In the classical search-capture model of chromosome alignment (Nicklas *et. al,* 1994) astral MTs from opposing centrosomes attach to kinetochores, facilitating chromosome congression. However, if MTs from the same pole attach to sister kinetochores the interaction is selectively destabilised such that correct MT-kinetochore relationships can be established. Thus, kinetochores must contain MT binding sites, and act as a read-out of merotely and syntely, in addition to themselves generating MTs.

Furthermore, the relationship between kinetochore-driven and Ran.GTP chromatin-driven MT generation is unclear. Kinetochores clearly reside in the chromatin and, while the original experiments in the *Xenopus in vitro* system lacked canonical kinetochores (Heald et. al, 1996), injection of Importin-β, and depletion of TPX2

diminishes MT formation at kinetochores following nocodazole treatment (Tulu *et. al,* 2006;). Conversely, live analyses of cells undergoing Mitosis with Unreplicated Genomes (MUG) suggest that kinetochores can support bipolar spindle formation without the direct influence of chromosome arms. Following treatment with Hydroxyurea (HU) kinetochores become uncoupled from chromosomes, forming a bipolar spindle and completing the full complement of mitotic movements while unreplicated chromatin is excluded from the spindle (Brinkley *et. al,* 1988). During MUG, RCC1 binds chromatin, but not kinetochores, and generates a Ran.GTP gradient that does not correspond to the polarity of spindles that form around kinetochores (O'Connell *et. al,* 2009).

1.2.5. CPC-directed MT generation

The Chromosomal Passenger Complex (CPC), consisting of Aurora B, INCENP, Survivin and Borealin/Dasra-B, is required for spindle bipolarity, chromosome alignment and cytokinesis. The presence of the CPC at the chromosome arms during prophase implicates it in MT stabilisation. Re-localisation of the CPC to the inner centromeres at prometaphase enables it to regulate the stability of kinetochore-kMT interactions (for review, see Ruchaud *et. al,* 2007), while its presence along the spindle suggests a more general role in MT generation during spindle formation (Tseng et. al, 2010).

Undoubtedly, the CPC has a role in modulating MT dynamics to facilitate spindle bipolarity. Op18/Stathmin inhibits MT polymerisation *in vitro*, and is negatively regulated in the vicinity of chromatin during spindle formation (Andersen *et. al,* 1997). Inhibition of Op18/Stathmin depends on hyperphosphorylation by Aurora B

(Gadea *et. al,* 2006), while chromatin beads cannot form bipolar spindles in the absence of CPC activity in *Xenopus* extracts – an effect that is reversed by co-depletion of INCENP with the MT depolymerising enzyme MCAK (Sampath *et. al,* 2004).

However, there is increasing evidence that the CPC has a direct role in generating a population of MTs that incorporate into the growing spindle. Reconstitution of active CPC on beads supports MT assembly in the absence of Ran.GTP (Kelly *et. al,* 2007). However, sperm nuclei containing kinetochores and centrosomes, which generate bipolar spindles in the absence of a Ran.GTP gradient, cannot promote local MT generation after either INCENP immunodepletion or chemical inhibition of Aurora B in this system (Maresca *et. al,* 2009). Furthermore, the association of active Aurora B with spindle MTs (as opposed to kinetochores) is essential for spindle assembly. Spindle-associated Aurora B effectively transmits a spatial signal from chromosomes to promote bipolar spindle formation (Tseng *et. al,* 2010).

Whatever the precise mechanisms of CPC-directed MT generation, the importance of MT organisation by the CPC in *Drosophila* is demonstrated by a drastic delay in female meiotic spindle formation in *incenp* mutants (Colombié *et. al,* 2008).

1.2.6. MT-Templated MT-Nucleation

Fluorescence speckled microscopy of anastral meiotic spindles in *Xenopus* reveals a distribution of MT minus ends throughout the spindle, concentrated primarily at spindle poles (Burbank *et. al,* 2006). Thus, new MTs nucleated near chromatin would

be incorporated into the spindle and moved poleward via a flux mechanism. However, live cell imaging of the plus-end associated protein, EB1, in cells without functional centrosomes shows MT plus ends originating throughout the spindle (Mahoney *et. al,* 2006), suggesting that new MTs are generated at sites distant from chromatin during mitosis.

Indeed, recent work has uncovered a set of MAPs, originally identified in *Drosophila*, that appear to have a role in MT generation from within the spindle (Goshima et. al, 2007; Hughes et. al, 2008). These proteins localise a sub-population of γ-Tubulin to existing spindle MTs and their absence leads to spindles of lower density with an increased astral population (Goshima *et. al,* 2008; Hughes et. al, 2008). Termed Augmin, or HAUS (Homologous to Augmin Subunits (HAUS); Lawo *et. al,* 2009; Uehara *et. al,* 2009), this conserved hetero-octomeric complex has been shown to directly interact with the γTuRC subunit, NEDD1 (Zhu *et. al,* 2008), a result that has been independently verified (Teixido-*Travesa et. al,* 2010). Thus a model has been proposed in which Augmin binds existing spindle MTs during prometaphase, and targets active γTuRC, facilitating intra-spindle MT nucleation (Goshima et. al, 2008; Uehara et. al, 2009).

Similarly to the centrosomal contribution of MTs to spindle formation, MTs generated by Augmin are dispensable for animal development. Null mutants of the Augmin subunit, *wac*, are viable, albeit showing a small, but significant, impact on somatic mitosis (Meireles *et. al,* 2009). However, Augmin is essential for the fast and synchronous early embryonic divisions that occur in the embryo of the fly. Mitotic

spindles from embryos laid by mothers mutant for the gene encoding either *wac* or another Augmin subunit, *msd1*, are larger and less dense than their wild-type counterparts, failing in chromosome alignment and segregation (Meireles *et. al,* 2009; Wainman *et. al,* 2009).

1.2.7. Cytoplasmic MTs

Evidently, MT assembly throughout the cell cycle is contingent upon numerous MTOCs that exist with a degree of redundancy. In *Drosophila* S2 cells, the centrosome is not the primary MTOC during interphase. Although duplicated centrioles are present, recruitment of PCM components, including γ-Tubulin does not occur. Strikingly, the interphase MT cytoskeleton assembles independently of γ-Tubulin, from numerous discrete sites in the cytoplasm, and is not associated with centrioles (Rogers *et. al,* 2008). Noncentrosomal nucleation of MTs has been observed in plants. MTs appear to originate from sites adjacent to existing MTs, but also from regions devoid of detectable MTs during interphase in *Arabidopsis* (Shaw *et. al,* 2003). The origin of these MTs is unclear.

The significance of these noncentrosomal MTOCs during mitosis is not well established. Live analysis of γ-Tubulin during mitosis in acentriolar S2 cells lacking DSas-4 demonstrated a novel MTOC that forms in the absence of centrioles. γ-Tubulin aggregates in the cytoplasm colocalise with γ-TuRC components and Cnn, and are capable of nucleating new MTs. In the absence of centrioles, these aggregates originate near both the chromatin and the cytoplasmic periphery, before moving towards the spindle poles as they form. Effectively, acentriolar MTOCs

(aMTOCs) can substitute for the centrosome-organising function of centrioles – an effect that is dependent upon MT bundling by Ncd (Moutinho-Pereira *et. al,* 2009). The self-organising capacity of centrosomal components in the absence of centrioles clearly accounts for a significant portion of MT organisation throughout mitosis.

1.2.8. Relative contributions of each pathway

The centrosomal contribution to mitotic spindle formation is thus not necessary for *Drosophila* development. However, centrosomal asters appear to facilitate important spindle characteristics including organising the cleavage furrow and maintaining mitotic timing. Furthermore, errors in the establishment and maintenance of asymmetry in division are linked to centrosome deregulation. Over-expression of SAK in *Drosophila* results in centrosome amplification. Although spindle bipolarity is maintained, this process requires an active SAC and supernumerary centrosomes disrupt the establishment of asymmetry in larval neural stem cells. This population of cells has the capacity to produce stable, ectopic tumors in the abdomens of wild-type flies (Basto *et. al,* 2008). These data further support evidence of a causal link between centrosome deregulation and cancer (for review see Nigg *et. al,* 2009).

Disruption of centrosomes eliminates astral MTs, in turn causing defects in spindle length (Goshima *et. al,* 2005), chromosome segregation (Gergely *et. al,* 2000) and also central spindle formation during anaphase (Riparbelli *et. al,* 2002).

It is not clear whether Ran.GTP directly induces MT nucleation. TPX2 alone appears to nucleate MTs, promote aster formation and bundle MTs in pure Tubulin solutions (Schatz *et. al,* 2003). This process is enhanced by the addition of the TPX2 binding partner XRHAMM, although the dependence of this process on γ-Tubulin is uncertain (Groen *et. al,* 2004). Furthermore, ISWI has MT nucleation and bundling activity in pure Tubulin solutions (Yokoyama *et. al,* 2009). Ran.GTP evidently exerts a tight regulatory role on the cell cycle. Modulation of nuclear import/export factors via mitotic chromatin directs the formation of a population of MTs that is distinct from those produced at the centrosome (Gruss *et. al,* 2002) while also governing both the centrosomal contribution of MTs and to an extent, kMT stability via modulation of HURP (Silljé *et. al,* 2006).

The conserved KNL-1/Mis12/Ndc80 (KMN) network is regulated by Aurora B at kinetochores to modulate MT stability (Cheeseman *et. al,* 2006). Xorbit, a plus-end stabilising factor, is localised at kinetochores via an interaction with the kinetochore-associated motor CENP-E, and promotes MT stabilisation (Hannak *et. al,* 2006). Here, MT growth from kinetochores relies to an extent on γ-Tubulin-dependent MT nucleation. Nup107-160, the 9-subunit nucleoporin complex dissociates from the Nuclear Pore Complex (NPC) during mitosis and localises to kinetochores. Nup107-160 is required to recruit γTuRC and nucleate MTs in a manner dependent on Ran.GTP (Mishra *et. al,* 2010). Furthermore, the Augmin subunit Dgt6 is partly required for γ-Tubulin localisation to kinetochores, and subsequent KMT regrowth (Bucciarelli *et. al,* 2009).

Clearly, a multitude of mechanisms exist that work both redundantly, and in concert with each other to produce a robust bipolar mitotic spindle.

1.3. *Drosophila* Development

1.3.1. Oogenesis

Drosophila oogenesis begins with four incomplete mitotic divisions from a stem cell in the ovary that produces a 16-cell cyst of cells whose cytoplasm is shared via ring canals. Here, one cell that is connected by four ring canals becomes the oocyte. The remaining 15 cells differentiate into polyploid nurse cells (Theurkauf *et. al,* 1994). Meiosis begins as the oocyte matures, and is subsequently arrested in metaphase I. This meiotic arrest is only reversed upon activation of the oocyte as it enters the oviduct (Gonzalez *et. al,* 1993).

1.3.2. The Syncytial Blastoderm

Following fertilisation, the somatic nuclei undergo 13 rounds of synchronous division in a shared cytoplasm known as a syncytium. After 8 divisions, the majority of nuclei have migrated to the periphery of the cell, originating first at the posterior and extending towards the anterior to form a cortical monolayer. At this point, some posterior nuclei cellularise to become the pole cells whose division is decoupled from the syncytium and become the germ cell progenitors. 5 further cortical cycles complete the syncytial stage, and nuclei cellularise via membrane invagination during interphase of cycle 14 to form distinct somatic cells. Until this point, nuclear cycles are completely dependent upon the maternal complement of RNA and protein. Zygotic transcription increases following cellularisation and somatic cells are then patterned relative to spatial cues throughout the embryo (Foe *et. al,* 1983).

1.3.3. Mitosis Post-Cellularisation

In the syncytial blastoderm, nuclear morphologies and cell cycle lengths do not vary significantly between nuclei in a given cycle. Following cellularisation, however, cell cycles within the embryo become asynchronous as tissue differentiation begins. At this stage, 'mitotic domains' are evident as discrete groups in the embryo, and are bilaterally symmetrical across the embryo midline. Each domain enters its 14^{th} mitotic cycle depending upon embryo patterning, and this cycle is tightly linked to morphogenetic movements during gastrulation (Foe *et. al,* 1989).

1.4. Msd1 and dTD-60 as MAPs

A dramatic rearrangement of the cytoskeleton occurs upon entry into mitosis - a process that is reliant on the co-ordinated action of MAPs to assemble a mitotic spindle that attaches to, and segregates, duplicated chromosomes with great fidelity. This project focuses on two proteins identified in a screen for MAPs (Hughes *et. al,* 2008). *Drosophila* 0-3h embryo extracts were used due to their enrichment in mitotic proteins. A MT-spindown was performed (See Section 2.4.3) on polymerised MTs to precipitate MAPs from the extract. This sample was subjected to Mass Spectrometry and hits were identified as having a score higher than 50. Subsequently, an RNAi screen was performed on MAPs to identify mitotic phenotypes. From this screen, the proteins Msd1 and dTD-60 were chosen for further study in this thesis (Hughes *et. al,* 2008).

First, an RNAi screen identified mitotic spindles that had a reduced microtubule density in the absence of Msd1. Further characterisation of this protein would reveal the mechanism that underlies this phenotype. This project provides an initial characterisation of the role of Msd1 in the assembly of the mitotic spindle in S2 cells using biochemical, cell and molecular biological methods, before further investigating the role of Msd1 in the developing fruit fly. Finally, the role of Msd1 in the formation and maintenance of the central spindle during anaphase is investigated.

The identification of dTD-60 as a MAP, in addition to the role of the homologous human TD-60 as a putative component of the Chromosomal Passenger Complex (CPC), suggested that dTD-60 might have a role in mitosis. This project focuses on the role of dTD-60 in *Drosophila,* investigating the relationship between dTD-60 and the CPC, in addition to a preliminary characterisation of other proteins that interact with dTD-60.

2. Materials & Methods

2.1. Resources Used in this Thesis

Fly Stock	Reference	Comments
w^{1118} ; Tft/Cyo	Lab Stock	Balancer Stock
w^{1118}; TM3/TM6B	Lab Stock	Balancer Stock
w^{1118}; Tft/Cyo;MKRS/TM6B	Lab Stock	Balancer Stock
w^{1118}; GFP-dTD-60	BestGene	GFP
w^{1118}; Msd1-GFP	BestGene	GFP
w^{1118}; *msd1*^{ex51} / TM6B	Wainman *et. al,* 2009	P-element excision
w^{1118}; HisGFP/SM6a	Bloomington 24163	UAS-GFP
w^{1118}; α-Tubulin-GFP/Cyo	J.Raff Stock	GFP (Ncd promoter)
w^{1118}; γ-Tubulin-GFP/TM6B	S.Endow Stock	GFP (γ-Tub promoter)
w^{1118}; Moesin-GFP/Cyo	J.Bloor Stock	UAS-GFP
w^{1118}; *mad2*^{p} / *mad2*^{p}	R.Karess	P-element - Null
w^{67}; P$^{[EY11673]}$	Bloomington 20814	P-element in *CG13914*
w^{1118}; Df(2L)ED343	Bloomington 9185	Deficiency for *CG9135*
w^{1118}; Df(2L)ED343	Bloomington 9186	Deficiency for *CG9135*
w^{1118}; Df(3L)bab-PG	Bloomington 5412	Deficiency for *CG13914*
w[*];P{w+matα-4-GAL}V2H	Bloomington 7062	GAL4
w^{1118};PBac$^{\{CG9135f03307\}}$	Bloomington 18638	FRT in *CG9135*
w^{1118};P{RS5}CG139955-HA-5045	Bloomington 125807	FRT in *CG9135*
*w**; P{GawB}NP2466 / CyO	Kyoto DGRC 104209	P-element in *CG9135*
w[*]; wg/CyO; Sb P{Δ2-3}/TM6B	Bloomington 3629	Δ2-3 Source

Table 1. Fly Stocks

Primer	Sequence	Comments
msd1 Forward	CAC CAT GTC AGA CGC TGT GGA CAA AAT GTT G	TOPO cloning
msd1 Reverse	GGG GGA ATC CTC GCT GGC AT	TOPO Cloning
msd1 RNAi Forward	CGA CTC ACT ATA GGG AGA AAT GGA GCG GTC GAA CAA	RNAi; partial T7; 400bp
msd1 RNAi Reverse	CGA CTC ACT ATA GGG AGA ATC CTC GCT GGC ATA CTG	RNAi; partial T7; 400bp
dTD-60 RNAi Forward	GCG TTA ATA CGA CTC ACT ATA GGG ACC GCA AGA ACG	RNAi; T7
dTD-60 RNAi Reverse	GCG TTA ATA CGA CTC ACT ATA GGG AAT GTT AGC ATG	RNAi; T7
RFP Forward	GCT GCG CGG CAC CAA CTT CC	Sequencing from 3' of RFP/GFP
RFP Reverse	GGA CAG CTT CAA GTA GTC GG	Sequencing from 5' of RFP/GFP
β-lac Forward	GCG TTA ATA CGA CTC ACT ATA GGG TTC CTG TTT TTG CTC ACC	RNAi control; T7, 400bp
β-lac Reverse	GCG TTA ATA CGA CTC ACT ATA GGG AGT GAG GCA CCT ATC TCA	RNAi control; T7, 400bp
bj1 RNAi Forward	TAA TAC GAC TCA CTA TAG GGA GAC GGT CGG CTT GGT CTG GG	RNAi; T7
bj1 RNAi Reverse	TAA TAC GAC TCA CTA TAG GGA GAC CGC CCC GCT TGG CAG C	RNAi; T7
ssp4 RNAi Forward	TAA TAC GAC TCA CTA TAG GGA GAA CTA GTT GGT GAC ATT GCT CCC	RNAi, T7
ssp4 RNAi Reverse	TAA TAC GAC TCA CTA TAG GGA GAC AAT CTC ACC TAT CGC ATA CCC	RNAi, T7
6084 RNAi Forward	TAA TAC GAC TCA CTA TAG GGA GAT AGC CTC CTC TAG GAT GAC CG	RNAi, T7
6084 RNAi Reverse	TAA TAC GAC TCA CTA TAG GGA GAA GCT CCC TGA AGC TGA AGT ACC	RNAi, T7
1943 RNAi Forward	TAA TAC GAC TCA CTA TAG GGA GAG GAC ACA CCA ATA TCT TCT CGG	RNAi, T7
1943 RNAi Reverse	TAA TAC GAC TCA CTA TAG GGA GAT GAT TCT TAT GTC GGT CTG AGG	RNAi, T7
5791 RNAi Forward	TAA TAC GAC TCA CTA TAG GGA GAA GTA GCG TGA GAG TCG ATA CGG	RNAi, T7
5791 RNAi Forward	TAA TAC GAC TCA CTA TAG GGA GAC GCC ACT ACC GTC ATT TCC	RNAi, T7
*9135*_3'UTR Forward	CTC GCT ATC TAC ATA CTA TAC	P-element diagnostic
GAL4_541Reverse	AGC GAC ACT CCC AGT TGT TC	P-element diagnostic
*13995*_5' Reverse	GAC AGG ACC ACG GCG GAA GAC T	P-element diagnostic

Table 2. Primers

Antibody	Type	Conc.	Reference
α-Tubulin, DM1A	Ms monoclonal	1:1000	Sigma
γ-Tubulin, GTU88	Ms monoclonal	1:1000	Roche
GFP	Ms monoclonal	1:1000	Roche
GFP-TrapA	Camel monoclonal	N/A	Chromotek
dTD-60	Rb polyclonal	1:1000	Invitrogen
INCENP	Rb polyclonal	1:100	Invitrogen
Dgt4	Rb polyclonal	1:1000	Goshima et. al, 2008
Dgt5	Rb polyclonal	1:1000	Goshima et. al, 2008
Dgt6	Rb polyclonal	1:1000	Bucciarelli et. al, 2009
Wac	Rb polyclonal	1:20	Meireles et. al, 2009
PNUT	Rb polyclonal	1:1000	Hughes et. al, 2008
eIF-4E	Rb polyclonal	1:1000	Wakefield Lab Stock

Table 3. Antibodies

2.2. Fly Stocks

2.2.1. Keeping Fly Stocks

Fly stocks were kept on yeast/dextrose medium (5.5% Glucose, 5% Yeast Extract, 3.5% Wheat Flour, 1% Pen/Strep, 0.75% Agar, 0.4% Propionic Acid, 0.25% Nipagin) in either 30ml vials or 250 ml bottles, plugged with bonded dense weave cellulose acetate flugs (Fischer). Stocks and crosses were kept at 25°C as standard, but reduced to 18°C to slow development where appropriate. Fly pushing techniques used were as described in Greenspan (1997). Fly stocks used are shown in table 2.1. Balancer Chromosomes used are described in Lindsley and Zimm (1992).

2.2.2. Deficiency Complementation

Flies of the experimental genotype were crossed to flies with deletions in known genomic regions that covered the gene of interest (Bloomington). The resulting progeny was scored for the ability to phenocopy the homozygous phenotype. The genomic locus of a given aberration was confirmed if the experimental phenotype was still evident in these progeny.

2.2.3. Fertility Tests

Male fertility of flies was tested by crossing 3 males of the experimental genotype with 5 w^{67} virgin females and scoring for the ability to produce a progeny. Female fertility was tested by crossing 5 virgin females of the experimental genotype with 3 w^{67} males, and scored in the same way.

2.2.4. Collecting Embryos

Embryos were collected from flies in egg laying chambers on 25mm Petri dishes containing approximately 3ml fruit juice agar (25% Raspberry & Cranberry Juice, 2.25% Agar Powder, 2.5% Sucrose, 0.25% Nipagin).

2.2.5. GFP Expression in Embryos

DNA constructs of both N-Terminal and C-terminal GFP fusion proteins were cloned as described in Section 2.3.8. Purified constructs were then coinjected into w^{1118} embryos at 1mg/ml with a transposase source helper plasmid by BestGene Inc. Flies carrying the UASp construct were selected for the presence of red/orange eyes. Red-eyed flies were balanced and crossed to the Maternal α-TubulinGAL4 (mat-α-TubGAL4 hereafter) driver to drive expression in embryos, as described in Figure 2-1 and 2-2.

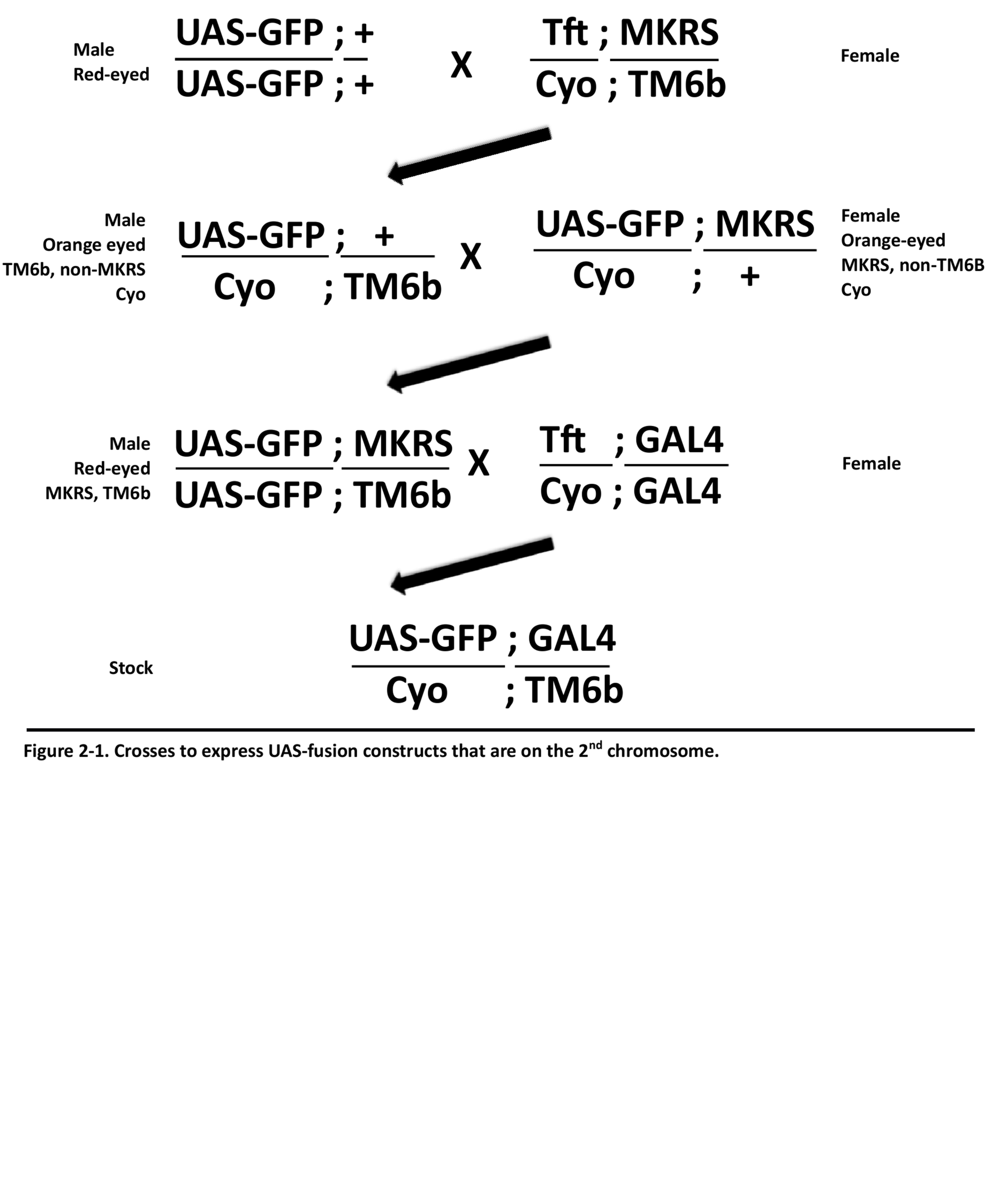


Figure 2-1. Crosses to express UAS-fusion constructs that are on the 2nd chromosome.

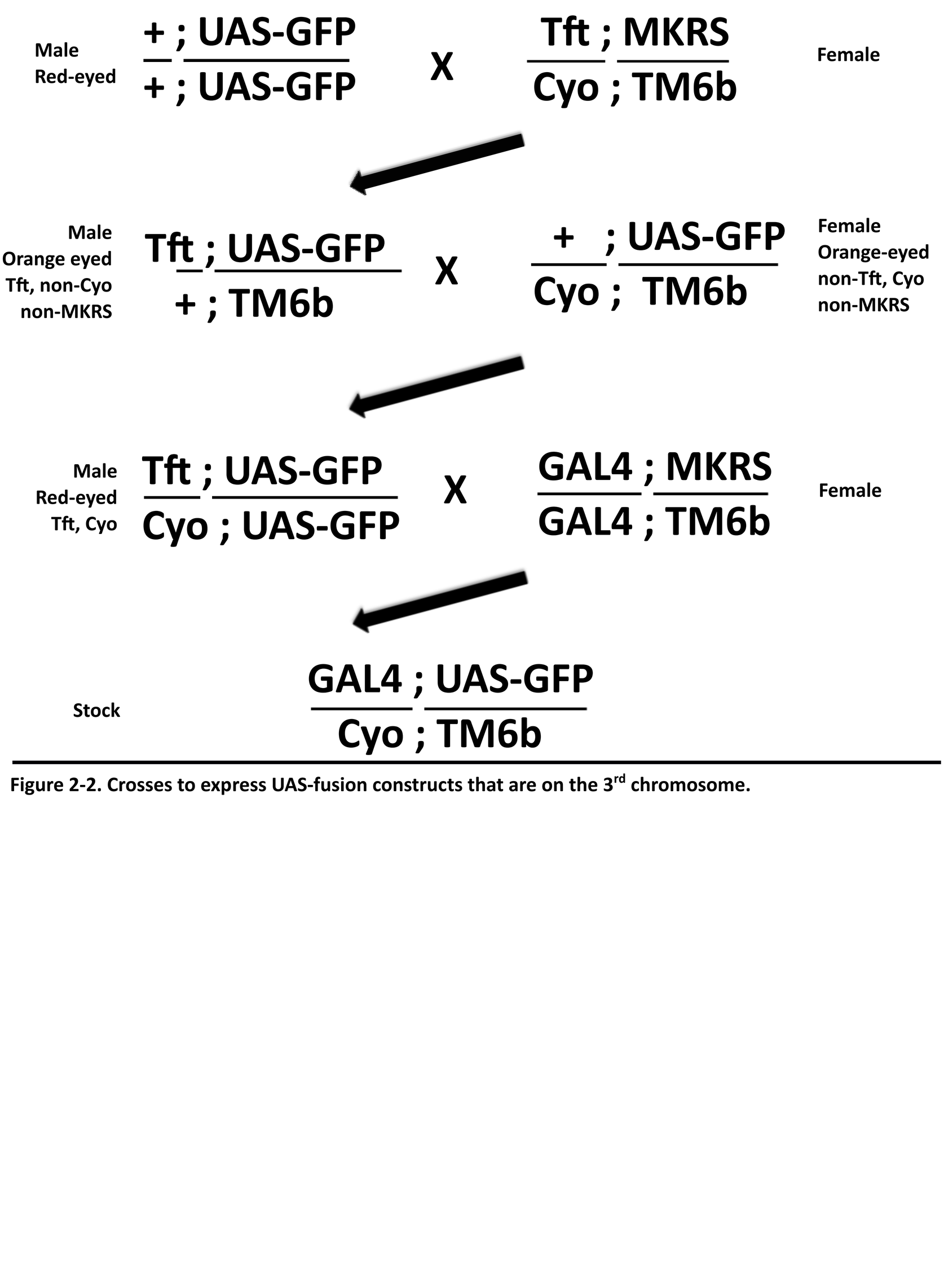


Figure 2-2. Crosses to express UAS-fusion constructs that are on the 3rd chromosome.

2.2.6. Hatch Rates

Flies of the experimental genotype and w^{67} flies were transferred to egg laying cages and allowed to lay on fruit juice agar plates overnight. Plates were aged for 24h at 25°C and were scored for the number of embryos that hatched. Differences in hatch rates were tested by 2-tailed t-test.

2.2.7. Recombination

Recombination crosses were carried out via the cross described in Figure 2-3 and 2-4. Recombinants in both cases were selected by testing lines for female sterility.

2.2.8. FRT-Directed Recombination

FRT-Directed recombination of P-elements was carried out via the cross described in Figure 2-5. Elements were cross-referenced for suitability using the DrosDel database (Parks *et. al,* 2004).

2.2.9. Imprecise Excision of P-elements

Imprecise excision of P-elements was carried out via the cross described in Figure 2-6. Individual white eyed males were selected and mated to virgin females before isolation of individual gDNA for molecular analysis (See section 2.3.2).

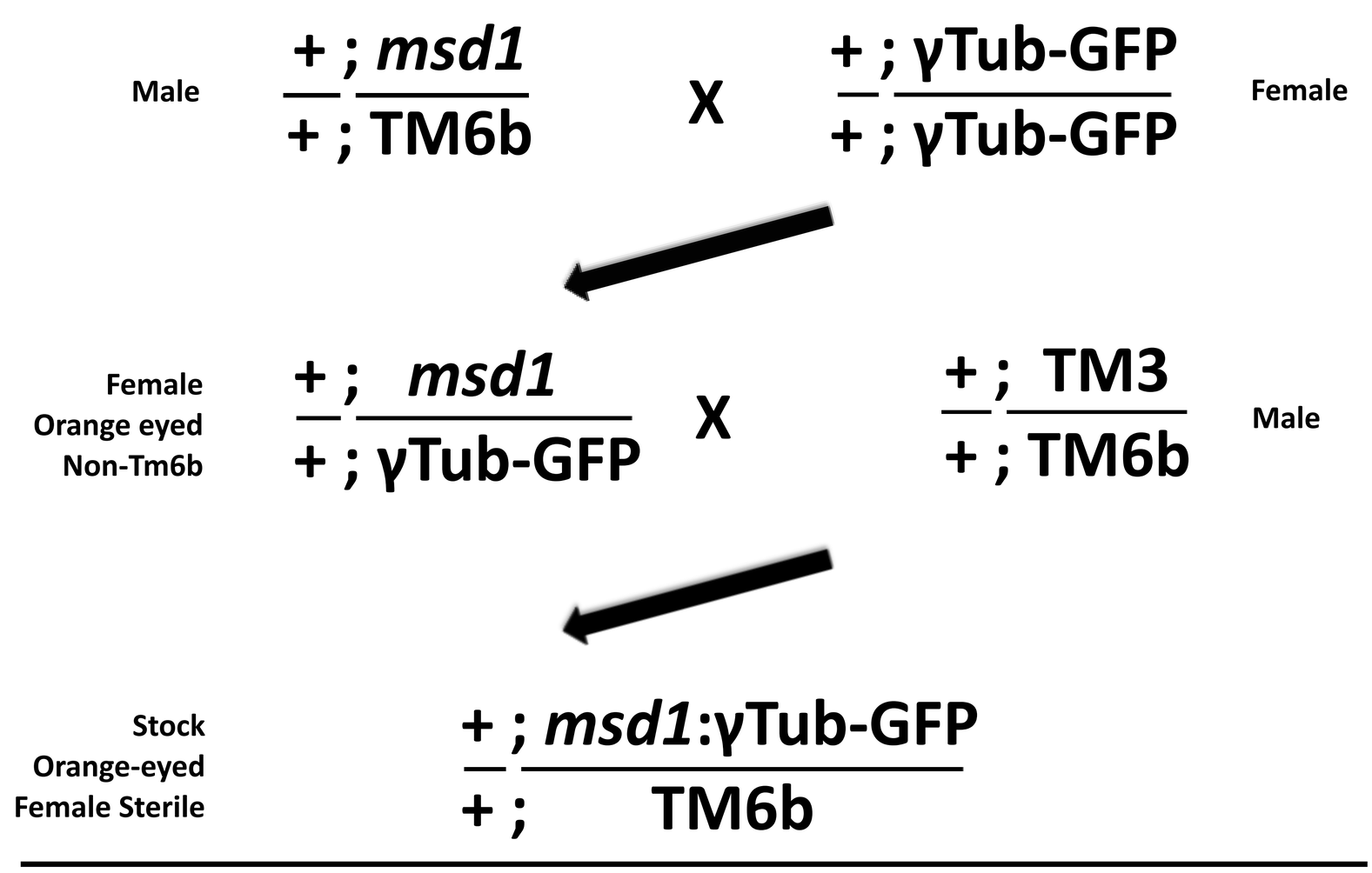


Figure 2-3. Crosses to generate msd1;γTub-GFP chromosome.

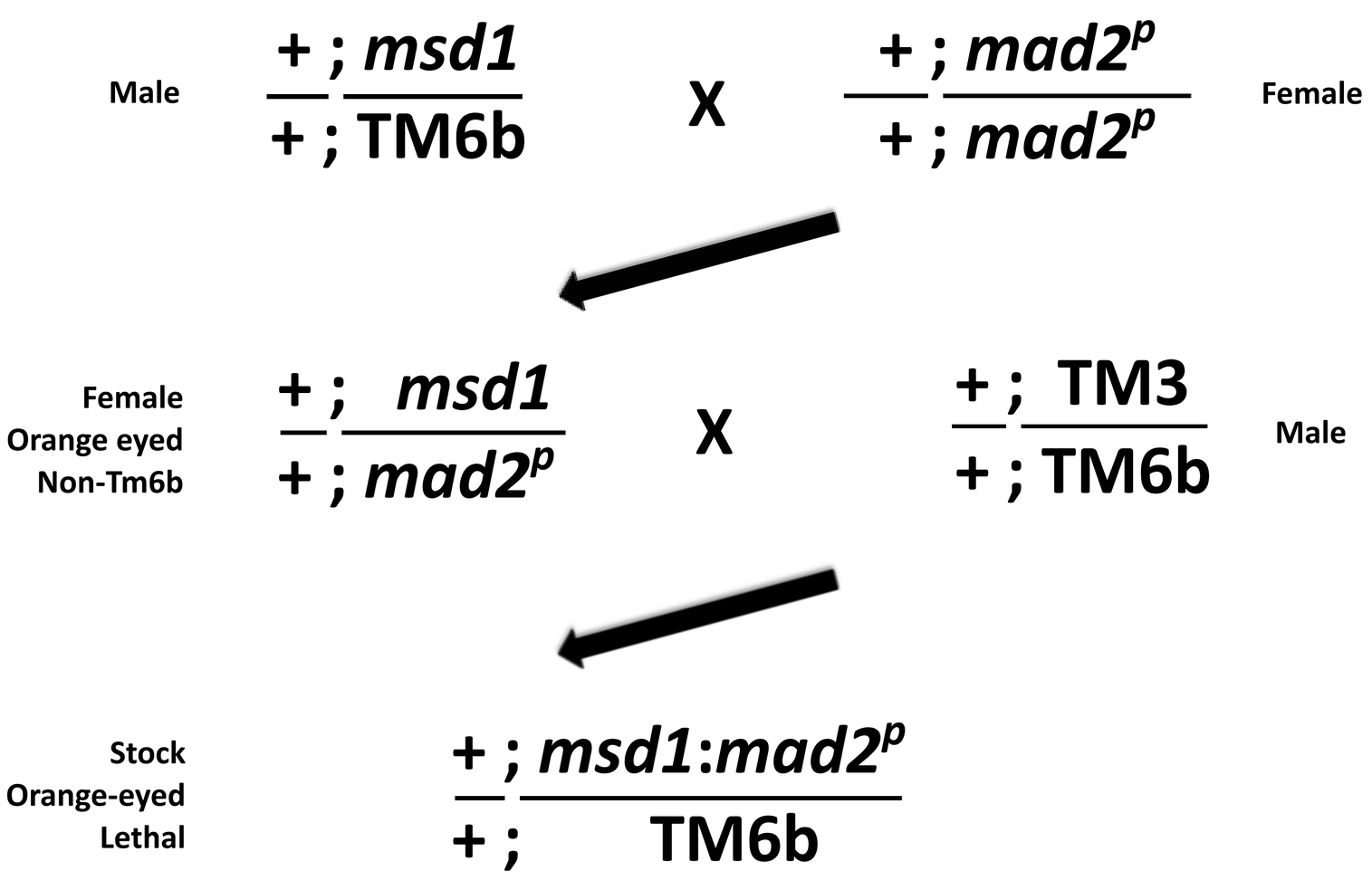


Figure 2-4. Recombination crosses to generate a *msd1;mad2* chromosome.

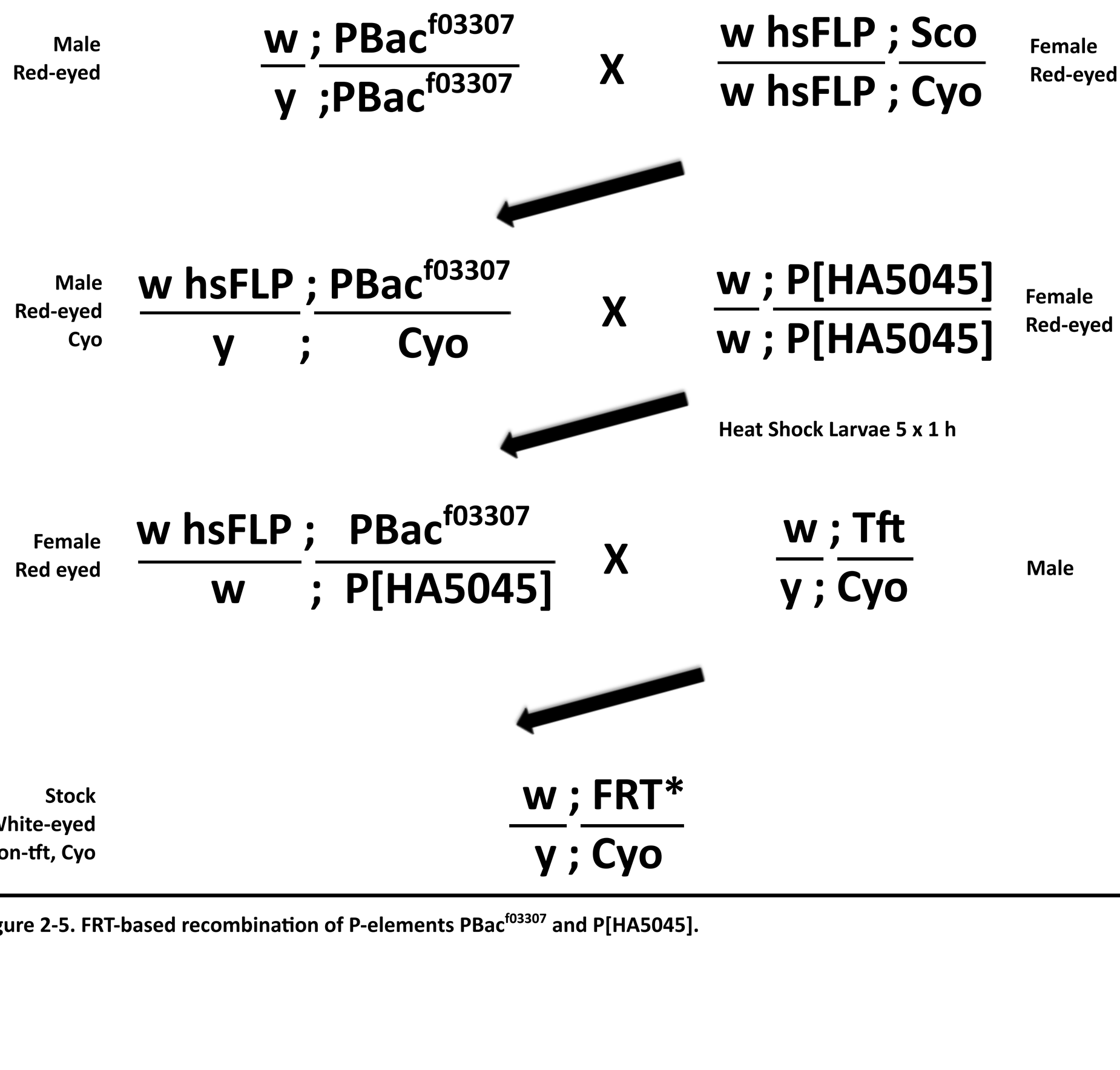


Figure 2-5. FRT-based recombination of P-elements PBac^{f03307} and P[HA5045].

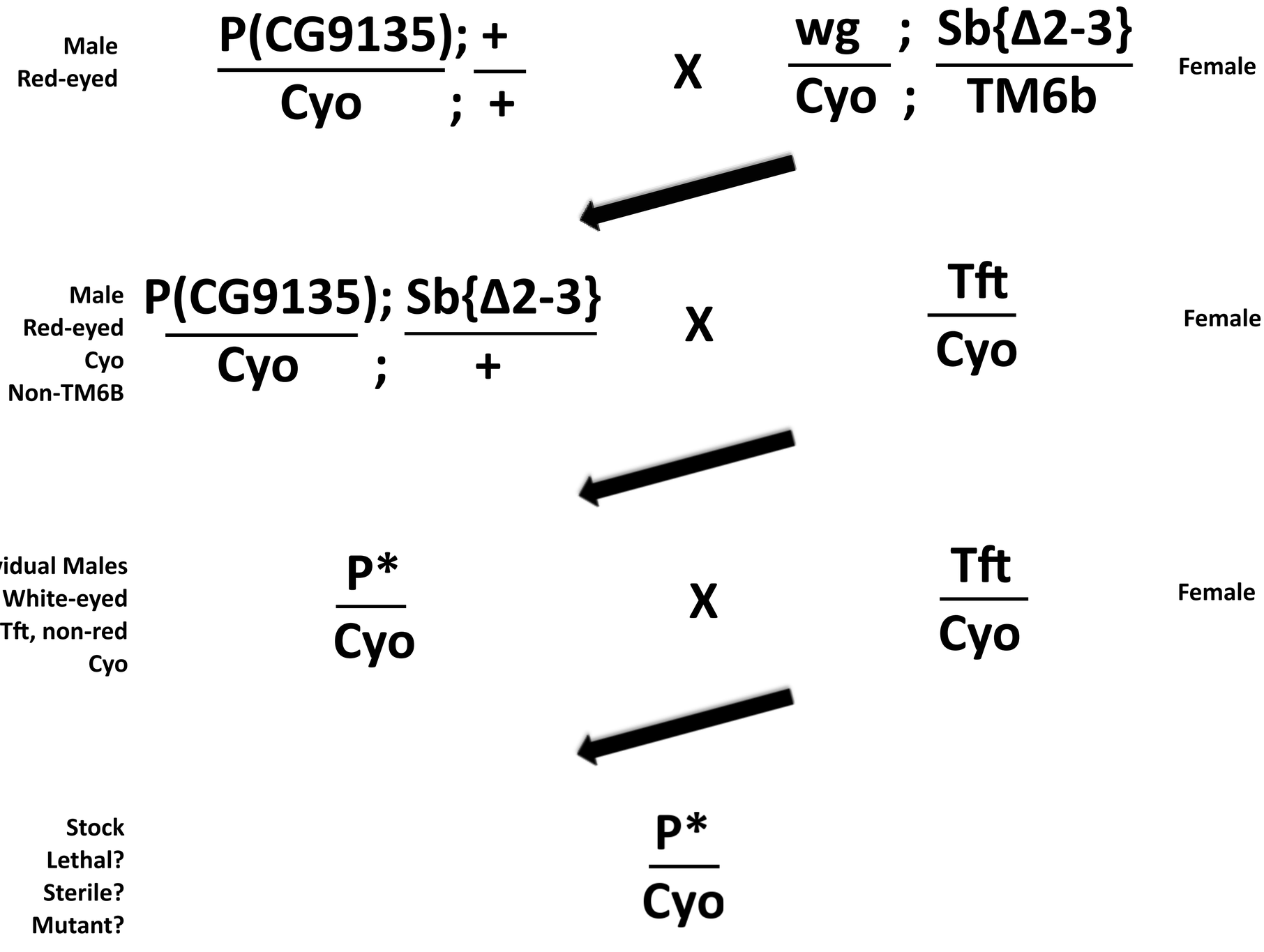


Figure 2-6. Crosses to generate a P-element excision using a Δ2-3 source.

2.3. Molecular Techniques

2.3.1. Isolation of gDNA

Ten 3rd instar larvae were flash frozen in liquid nitrogen and homogenised in 300μl Buffer A (100mM Tris-HCl pH9, 100mM EDTA, 1%SDS). This solution was then incubated at 70°C for 30 minutes. 67.2μl of 5M Potassium Acetate (KoAc) was added before vortexing and incubating for a further 30 minutes on ice. The sample was centrifuged at 13,000rpm for 10 minutes. The pellet was discarded and the process repeated. 150μl of Isopropanol was then added to the aliquoted supernatant to precipitate the gDNA. This precipitate was then vortexed and centrifuged at 13,000rpm for 15 minutes. The pellet was retained and gently floated in 200μl 70% ethanol. This was then centrifuged for a further 5 minutes at 13,000rpm to produce a pellet, which was air-dried and resuspended in 30μl DEPC H_2O.

2.3.2. Isolation of gDNA from Individual Males

Males heterozygous for P-element excisions were isolated and crushed in a 0.6ml microcentrifuge tube in 50μl 'Squishing Buffer' (10mM Tris-HCL pH8.0, 1mM EDTA, 25nM NaCl, 200μg/ml Proteinase K) using a 200μl pipette tip. Tubes were incubated for 30 minutes at 37°C. Tubes were then incubated at 95°C for 3 minutes. 1μl of solution was used in 20μl PCR reactions for molecular diagnosis.

2.3.3. Isolation of mRNA

mRNA was precipitated from 0.01g 0-3h embryos or from ten 3rd instar larvae by homogenising the flash-frozen tissue in 0.5ml Trizol (Invitrogen) and incubating for 5 minutes at room temperature. 200μl of chloroform was added and the tube was incubated on ice for 5 minutes before being centrifuged at 13,000rpm for 15 minutes. The clear, aqueous upper layer was taken and centrifuged for a further 15 minutes. Again, the aqueous upper layer was taken and to it, 500μl Isopropanol was added and incubated at 4°C for 10 minutes. The precipitate was centrifuged for 10 minutes at 13,000rpm, and the resulting pellet was washed with 70% ethanol. A further centrifugation for 5 minutes at 13,000rpm ensured there was a robust pellet, which was air-dried and dissolved in 30μl DEPC H_2O.

2.3.4. Production of cDNA

cDNA was synthesised from mRNA of S2 cell extracts or 0-3h *Drosophila* embryos according to manufacturers' instructions for the Invitrogen Superscript III cDNA synthesis kit.

2.3.5. Production of dsRNA

dsRNA was produced from PCR products using half-enzyme reactions of the MEGAScript T7 Transcription Kit according to manufacturer's instructions, and incubated overnight at 37°C. PCR products encoding the target gene region for knock-down were produced using primers with full length T7 sequences at each 5' end to allow polymerase binding, according to manufacturer's instructions. Reaction products were purified by first adding 1μl 3M Sodium Acetate (NaOAC, pH 5.2) and

30μl 100% Ethanol. The tube was incubated on ice for 5 minutes before being centrifuged for 15 minutes at 13,000rpm. The pellet was washed with 70% Ethanol and the tube was centrifuged for a further 5 minutes at 13,000rpm. The pellet was air-dried and eluted in 10μl DEPC water. 0.5μl was taken to analyse the concentration by agarose gel electrophoresis.

2.3.6. PCR

PCRs were performed using either the Standard Taq system (New England Biolabs) or Pfx blunt end polymerase (Invitrogen) in a Biometra T3 Thermocycler. Primers (Eurofins, MWG Biotech) were kept as 50μM stocks and diluted to 1μM in each reaction. Primers were designed with annealing temperatures of 55-58°C. PCRs were carried out using either cDNA or gDNA from the appropriate tissues as a template. For production of dsRNA, a T7 tag was added to the 5' end of each primer to allow T7 polymerase binding. For Gateway cloning, a CACC tag was added to the 5' primer for directional recombination.

2.3.7. Purification of PCR Products

PCR products were resolved on 1% Agarose (Sigma) gels using a Tris-Borate EDTA (TBE) buffer with 1μg/μl Ethidium Bromide (Sigma). Products were purified from gels using the QiaQuick gel extraction kit (Qiagen) according to manufacturer's instructions. Alternatively, PCR products in solution were column purified using the PCR Purification Kit (Qiagen) according to manufacturer's instructions.

2.3.8. Sequencing

Sequencing of DNA fragments was performed using Big Dye Terminator v3.1 Cycle Sequencing Kit (Applied Biosystems) according to manufacturer's instructions. Sequencing reactions were precipitated by incubating the reaction mixture with 30μl Ethanol, 1μl EDTA and 1μl 3M NaOAc (pH5.2). The tube was centrifuged at 13,000rpm for 15 minutes and the pellet washed briefly with 70% Ethanol. The reaction pellet was then air-dried and sequenced at the Department of Zoology, Oxford. Sequences were analysed using 4Peaks (mekentosj.com).

2.3.9. Cloning GFP Fusion Proteins

Both N-Terminal and C-Terminal fusion proteins of dTD-60 were created first by cloning PCR products of full length dTD-60. These products were ligated into the TOPO/pENTR vector (Invitrogen) in half reactions according to manufacturer's instructions. Directional recombination between the pENTR vectors and the destination vectors pPGW and pPWG (Murphy Lab) was performed. Positive clones were distinguished by restriction digest and by sequencing using primers annealing within the GFP sequence. Recombination reactions using LR sites were performed using the LR Clonase II Kit (Invitrogen) and transformed into TOP10 chemically competent *E.Coli* (Invitrogen) according to manufacturer's instructions. Plasmids from positive clones were purified to 1μg/μl using Midi Prep Kits (Qiagen) according to manufacturer's instructions.

2.3.10. Restriction Digests

Restriction digests were performed to confirm the identity of positive clones. 20μl reactions were performed using approximately 1μg of purified plasmid DNA. Restriction enzymes were used together in the appropriate double digest buffer (New England Biolabs). Reactions were then incubated for one hour at 37°C and products were analysed by agarose gel electrophoresis.

2.4. Biochemistry

2.4.1. SDS PAGE

Protein products were analysed using SDS Polyacrylamide Gel Electrophoresis in the BioRad mini-protean-3 system according to manufacturer's instructions. Protein samples were prepared using 2X Laemmli's Sample Buffer (BioRad) and incubated at 100°C for 10 minutes to denature protein sequences. Samples were loaded on 8, 10 or 12% gels, depending upon the desired molecular weight resolution, and run at 150V for 80 minutes. Gels were subsequently prepared for Western Blotting or stained for total protein using Imperial Protein Stain (Pierce).

2.4.2. Western Blotting

Resolved protein samples from SDS-PAGE were blotted on to nitrocellulose membrane (Amersham) for 1 hour at 250mA. Membranes were then blocked in TBST (Tris-Buffered Saline/ 0.05% Tween) with 5% Skimmed Milk Powder. Blocked membranes were then probed overnight at 4°C with rotation, with the appropriate 1° antibody concentration in blocking solution. Membranes were washed 3 x 15 minutes with TBST before adding secondary antibody (1/5000 in blocking solution) for 2 hours at room temperature. Again, the membrane was washed 3 x 15 minutes in TBST. Antibody was detected using ECL Western Blotting Substrate (Pierce) according to manufacturer's instructions.

2.4.3. MT Spin-down (MTSD)

MTSD experiments were performed on 0.1g of embryos expressing GFP fusion proteins. Embryos were homogenised in 1ml Column Buffer on ice (50mM HEPES pH7.6, 50mM KCl, 1mM EGTA, 1mM $MgCl_2$, 1mM NaF and 0.05% NP-40) containing protease inhibitor cocktail (Roche). The homogenate was then clarified by centrifuging for 2 x 15 minutes at 13,000rpm at 4°C. The supernatant was divided into two - an experimental sample and a control sample. GTP and Dithiothreitol (DTT) were added to a final concentration of 1mM and the tubes were incubated at 25°C for 10 minutes to encourage MT polymerisation. Taxol was then added to the experimental sample to a final concentration of 0.5mM to polymerise MTs and the tube was incubated for a further 10 minutes at 25°C. Both samples were then placed on ice. Both samples were carefully layered onto a 40% sucrose cushion in Column Buffer, before the polymerised MTs were pelleted at 100,000g for 1 hour at 4°C. Samples of both the supernatant and pellet from both control and experimental samples were taken and boiled in Laemmli's Sample Buffer for 10 minutes. Samples were analysed by Western Blotting, probing with an α-GFP monoclonal antibody (Roche).

2.4.4. Coupling of Antibodies to Protein A Beads

The antibody to be coupled was added to Protein A beads at a concentration of 2mg/ml of wet beads and incubated for 1 hour at room temperature with gentle rocking. The beads were washed twice with 10 volumes 0.2M Sodium Borate (pH 9.0). The beads were then resuspended in 10 volumes 0.2M Sodium Borate (pH 9.0) and dimethylpimelimidate (solid) was added to a final concentration of 20mM. The

beads were then incubated for 30 minutes at room temperature with gentle rocking. The reaction was terminated by washing the beads once in 0.2M ethanolamine (pH 8.0) and incubating for 2 hours at room temperature in this solution with gentle mixing. Antibody-coupled beads were then washed 3 x 10 minutes in PBST and the efficiency of coupling was analysed using SDS PAGE.

2.4.5. Antibody Co-Immunoprecipitation

Embryo extracts expressing GFP fusion proteins were prepared by homogenising 0.1g 0-3h embryos in 1ml Column buffer (See section 2.4.3) with protease inhibitors (Roche), before 2 x 13,000rpm centrifugation at 4°C to clarify the homogenate. The sample was divided into two and approximately 8μg of α-GFP primary antibody (Roche) was added to the experimental sample and 8μg of α-β-lac antibody was added to the control sample. Both tubes were incubated at 4°C for 4 hours with rotation. 50μl of Protein G bead slurry (Roche), pre-washed in Column Buffer (3 x 10 minutes) were then added to each tube, and incubated for 3 hours at 4°C with rotation. The beads were then pelleted with gentle centrifugation and a sample taken and boiled in Sample Buffer for 10 minutes. The beads were then washed thoroughly (3 x 10 minutes) in 1ml Column Buffer. Samples of the beads were then boiled in 2 x Sample Buffer for 10 minutes. The samples were then analysed by Western Blot or Mass Spectrometry (University of Exeter).

2.4.6. Antibody Co-Immunoprecipitation with Chromotek α-GFP Beads

0-3h embryo extracts were prepared as described previously and incubated with rotation for 2 hours at room temperature with GFP-Trap A beads (Chromotek) pre-

washed with Column Buffer (3 x 10 minutes). Following incubation, beads were washed in Column Buffer (3 x 10 minutes) before samples were prepared for Mass Spectrometry. Positive hits were identified by elimination of false-positives from previous Co-Immunoprecipitation experiments under identical conditions in the Wakefield lab. MAPs dTD-60 and Msd1 were identified as having a MASCOT score (based on number and size of peptides) greater than 30 in Hughes *et. al,* 2009.

2.4.7. Sucrose Gradients

Msd1-GFP 0-3h embryo extract was prepared by homogenising 0.1g embryos expressing Msd1-GFP in Column Buffer with protease inhibitors (Roche), before 2 x 13,000rpm centrifugation at 4°C to clarify the homogenate. A 6-38% discontinuous sucrose gradient was prepared and allowed to settle over night. 250μl of sample was loaded onto the gradient and centrifuged at 55,000rpm for 4h at 4°C in a Beckman Coulter SW41Ti swinging-bucket centrifuge. The gradient was then divided into 14 fractions and the samples analysed by Western Blotting.

2.5. Cytology

2.5.1. Fixing Embryos

Embryos were collected on Fruit Juice Agar plates and dechorionated in thin bleach for 3 minutes with gentle agitation. All tissues were briefly washed in Dulbecco's PBS (dPBS) before fixation in 1:1 Methanol : Heptane in a 1.6ml eppendorf tube. Fixed embryos were washed twice in 100% methanol before being rehydrated in dPBS for antibody staining.

For embryos fixed in formaldehyde, embryos were first transferred to a 1.6ml eppendorf tube containing 1:1 Formaldehyde (37%) : Heptane for 30 minutes before replacing the formaldehyde with methanol and continuing with the aforementioned fixation protocol. Embryos were stored at -20°C in Methanol.

2.5.2. Culturing *Drosophila* S2 Cells

Drosophila S2 cells were cultured at 25°C in 25ml Canted, Vented Cap Flasks (BD) in Schneider's S2 Cell medium (Lonza) with 10% FBS and 1% Penicillin/Streptomycin (Gibco). Cell density was kept between 5 x 10^5 and 5 x 10^6/ml, measured using a haemacytometer. Cells were passaged approximately 1/5 when necessary.

2.5.3. Transient Transfection of S2 Cells

Approximately 1 x 10^6 cells were allowed to settle in sterile 6 well culture dishes for 24 hours in Schneider's S2 cell medium containing 10 FBS and 0.5%

Penicillin/Streptomycin. Growth medium was replaced and 1μg of plasmid DNA was transfected using Effectene transfection reagent (Qiagen) according to manufacturers instructions.

2.5.4. S2 Cell RNAi

Approximately 1 x 10^6 cells were allowed to settle in sterile 6 well culture dishes for at least 3 hours. Growth medium was replaced by Serum Free medium for 30 minutes. Approximately 10μg of the appropriate purified dsRNA (as measured by comparison with standards using gel electrophoresis) was allowed to form complexes with Cellfectin transfection reagent (Invitrogen) in 1ml Serum-Free, antibiotic-free medium according to manufacturer's instructions. The transfection complexes were added to the cells. Cells were incubated for 1 hour at room temperature before adding 1ml of Serum-Free Medium and 1ml 30% FBS medium, both containing 1% Penicillin/Streptomycin, to each well to make a final concentration of 10% FBS. Cells were then incubated for 2-5 days at 25°C as appropriate. Cells were then harvested by pipetting gently to dislodge and aliquot adherent cells.

2.5.5. Fixing S2 Cells

S2 cells were uniformly fixed in -20°C methanol. Approximately 1 x 10^6 cells were allowed to settle for 3 hours on Concanavlin A (Sigma) coated 22x22mm coverslips on the base of sterile 6 well culture dishes. Cells were briefly washed in 2ml PBS. The dPBS was removed and 3ml methanol (-20°C) was pipetted directly on top of the cells to fix. The cells were then incubated on dry ice for 20 minutes before being

removed and equilibrated to room temperature for a further 20 minutes. The methanol in each well was then replaced for 10 minutes with 2ml dPBS before adding blocking solution for antibody staining.

2.5.6. Antibody Staining of Fixed Tissues

Tissues were incubated for 30 minutes in Blocking Solution (dPBST/3% BSA (Sigma)) with gentle oscillation. 1° antibodies were then added in Blocking Solution and the samples were incubated at 4°C overnight, with embryos being rotated and treated with 2.5mg/ml RNase A. Samples were washed 3 x 10 minutes in dPBST before the appropriate 2° antibody was added in Blocking Solution for 2 hours at room temperature with gentle oscillation. Tissues were washed 3 x 15 minutes, with Propidium Iodide (Sigma) being added to the second embryo wash at 1μg/ml to visualise DNA. Samples were then prepared for mounting:

Embryos were added to 25μl of 85% Glycerol (Sigma) on a 22x22mm coverslip by pipetting. Embryos were spread across the coverslip before being mounted on a glass slide.

Fixed and stained S2 cells were removed from the final wash and dried on tissue paper. 4μl VectaShield Mounting Media with DAPI (VectaLabs) was added to each coverslip. Coverslips were mounted on glass slides.

2.5.7. Imaging Fixed S2 Cells

S2 cells were imaged using an Eclipse TE2000 (Nikon) inverted fluorescence microscope using a 60X oil immersion lens. Images were taken on IPLab v3.1 software (BD Biosciences).

2.5.8. Imaging Live S2 Cells

S2 cells expressing GFP-fusion proteins were allowed to settle for 2h on 20mm glass-bottomed dishes (Matek) coated with Concanavlin A. Time-lapse spinning disc confocal microscopy was performed with an Ultraview RS3 (PerkinElmer), and images collected with Volocity image acquisition software (PerkinElmer).

2.5.9. FRAP in S2 Cells

S2 cells stably expressing eGFP-α-Tubulin were allowed to settle for 2h on 20mm glass-bottomed dishes (Matek) coated with Concanavlin A. A region of the prospective central spindle was photobleached during anaphase A. After photobleaching, images were collected at 5 second time intervals in a single Z-plane using a 5 Live Duoscan confocal microscope (Zeiss). Time-lapse movies were normalised to maximum intensity to account for photobleaching and measured using ImageJ FRAP plug in (NIH). FRAP curves were plotted using GraphPad (GraphPad Software Inc.), and an F-ratio was obtained as a measure of the difference in Sums of Squares between the control and experimental models. The F-ratio was then tested for significance using the F-test.

2.5.10. Imaging Fixed Embryos

Fixed and stained embryos were visualised using a Radiance 2000 Confocal Microscope (BioRad) using a 40X oil immersion lens. Images were then processed using Lasersharp 2000 software (Zeiss).

2.5.11. Imaging Live Embryos

Time-lapse fluorescence microscopy was performed on 1-3h embryos expressing the appropriate GFP fusion protein. Embryos were dechorionated by hand using forceps and double-sided tape under a dissecting microscope. Dechorionated embryos were immobilised to the surface of a 22x22mm coverslip coated with a line of heptane glue, and covered to prevent desiccation with Voltalef halocarbon oil (Sigma). The coverslip was then inverted and viewed on the confocal microscope. Time series typically consisted of one image taken every 10 seconds with a Kalman averaging 2. Movies were then visualised in ImageJ (NIH), and multi-channel images were analysed and pseudo-coloured in GNU Image Manipulation Program (GIMP).

3. Results

3.1. Msd1 and the Augmin Complex

Preliminary studies of *msd1* had been carried out prior to the onset of this project. First, the identification of Msd1 as a MAP that has a role in mitotic spindle assembly was the result of a previous screen conducted by the Wakefield lab (Hughes *et. al,* 2008). Second, cloning of Msd1-fusion proteins and determination of protein localisation in embryos was carried out by A.Wainman.

3.1.1. Msd1 is a MAP

msd1 was identified in an S2 cell RNAi screen following isolation of *Drosophila* mitotic MAPs (Hughes *et. al,* 2008). To confirm MT binding, a MT-spin-down assay was performed using 0-3h embryo extract (Figure 3-1). Msd1-GFP co-sedimented with Tubulin in the presence of Taxol (+Taxol, P). In the absence of Taxol, Msd1-GFP was present with unpolymerised Tubulin in the supernatant (-Taxol, S). Thus, Msd1-GFP binds to polymerised MTs embryo extracts – a result that is consistent with the localisation of Msd1-GFP to spindle MTs throughout mitosis (Wainman *et. al,* 2009).

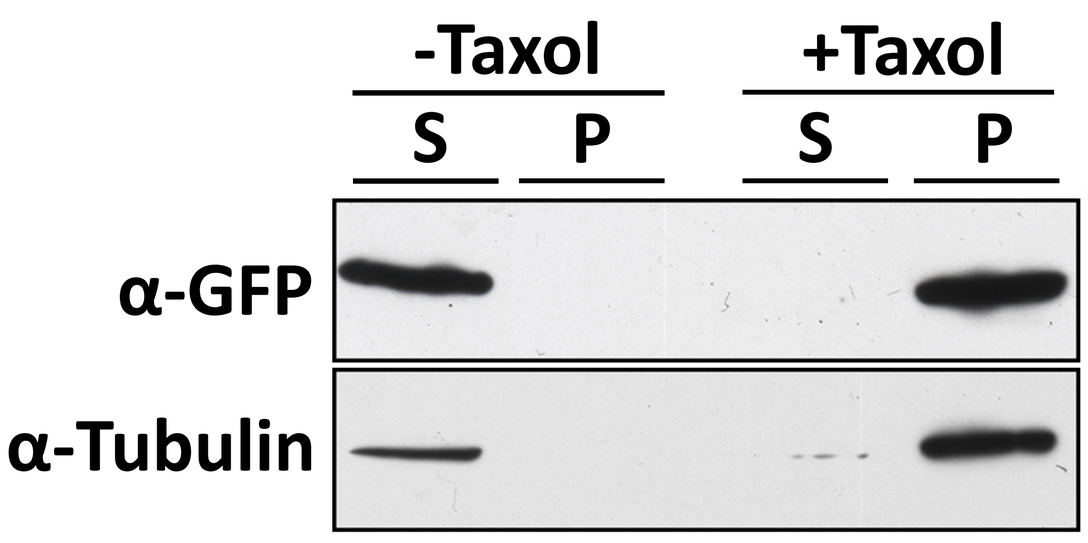


Figure 3-1. Msd1 is a MAP.
0-3h extracts of embryos expressing Msd1-GFP were incubated in both the presence and absence of Taxol and spun at 100,000g for 45' through a sucrose cushion. Msd1-GFP and α-Tubulin are present in the supernatant (S) in the absence of taxol. When MTs are polymerised with Taxol, Msd1-GFP and α-Tubulin are found in the pellet (P). Msd1 is a MAP.

3.1.2. *msd1* RNAi Significantly Reduces Mitotic Spindle Density

RNAi of *msd1* induces mitotic spindle defects in S2 cells (Hughes *et. al,* 2008). Mitotic spindle density was measured in S2 cells treated with dsRNA for 2 days (Figure 3-2). In cells treated with *msd1* dsRNA (Figure 3-2B) a number of spindle MTs were present but the density of MTs in the metaphase spindle appeared reduced compared with control treatments (Figure 3-2A). Spindle morphology was elongated, and astral MTs appeared longer in *msd1* knock-down cells compared with control-treated cells.

Measurement of the intensity of α-Tubulin staining within the spindle and at centrosomes revealed a significant reduction in spindle MT density relative to centrosome MT density (spindle/centrosome ratio hereafter) in *msd1* knock-down cells compared with control treatments (Figure 3-3; spindle/centrosome = 1.00±0.06 SEM vs. 1.53±0.07 SEM, $p<0.001$).

This phenotype is the result of two possible scenarios; centrosomal MT density might increase in the absence of Msd1, thus reducing the relative density of spindle MTs; or MT density is reduced within the spindle relative to the centrosome. The latter explanation is preferred because Msd1 localises to spindle MTs.

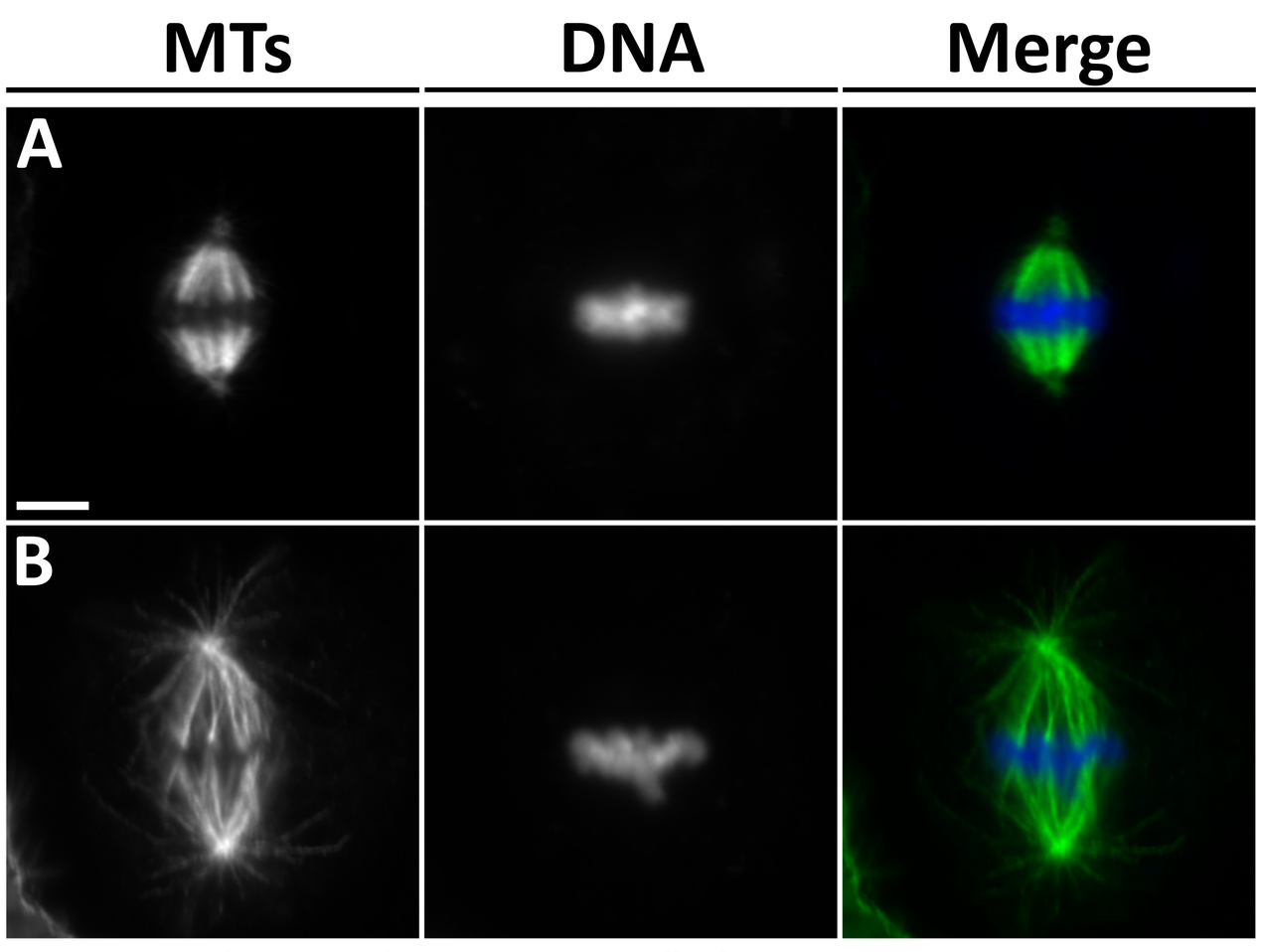


Figure 3-2 *msd1* RNAi reduces mitotic spindle density.
S2 cells were treated for 2d, fixed in methanol and stained for α-Tubulin (Green) and DNA (Blue). (A) Metaphase cell treated with *β-lac* dsRNA shows a robust bipolar spindle. (B) Metaphase cell treated with *msd1* dsRNA has an elongated spindle with less dense MTs and longer astral MTs. Scale bar = 5 µm.

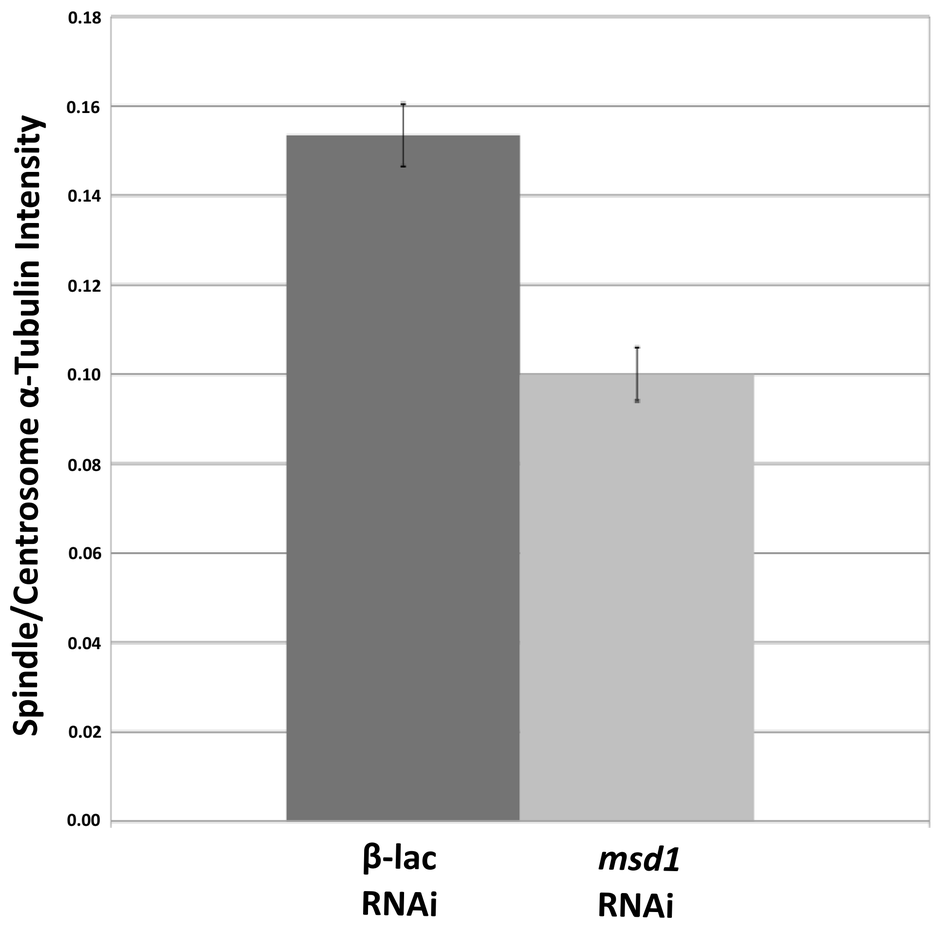


Figure 3-3. *msd1* RNAi reduces spindle/centrosome α-Tubulin intensity.

Average α-Tubulin pixel intensity for S2 cell half-spindles and centrosomes was measured in ImageJ, and spindle/centrosome ratio calculated. Spindle/centrosome intensity of α-Tubulin was significantly reduced in *msd1* RNAi (1.53±0.07 SEM, n=15) compared with control cells (1.00±0.06 SEM n=15). P<0.001.

3.1.3. Duration of *msd1* RNAi Exposes a Phenotypic Progression

Disruption of MT dynamics can affect the stability of the spindle, resulting in collapse into monopolar spindles (Hughes *et. al,* 2008). S2 cells were fixed and stained 2 days and 3 days after treatment with *msd1* dsRNA (Figure 3-4; Table 4). After 2 days, the majority of *msd1* RNAi cells were bipolar (14.3% bipolar normal, 72.3% bipolar abnormal, 14.3% monopolar) and exhibited reduced mitotic spindle density. After 3 days the number of monopolar spindles was increased (33.9% bipolar normal, 29.5% bipolar abnormal, 36.6% monopolar). 'Bipolar abnormal' cells were scored as any cell that appeared grossly defective for any reason, but remained bipolar. Control treatments showed no such effect - the majority of spindles were bipolar and normal, as determined by visual examination of morphology, irrespective of treatment duration (2 days 68.4%, 3 days 72.4%). Therefore, the *msd1* knock-down phenotype progresses over time. A lack of spindle density might result in collapse of metaphase spindles into monopolar spindles – an effect that would be evident via visualisation of MT dynamics in live S2 cells.

	Bipolar Normal	**Bipolar Abnormal**	**Monopolar**
β-lac 2d	68.4	23.7	7.9
β-lac 3d	72.4	19.5	8.0
msd1 2d	14.3	72.3	14.3
msd1 3d	33.9	29.5	36.6

Table 4. *msd1* Phenotype Progression

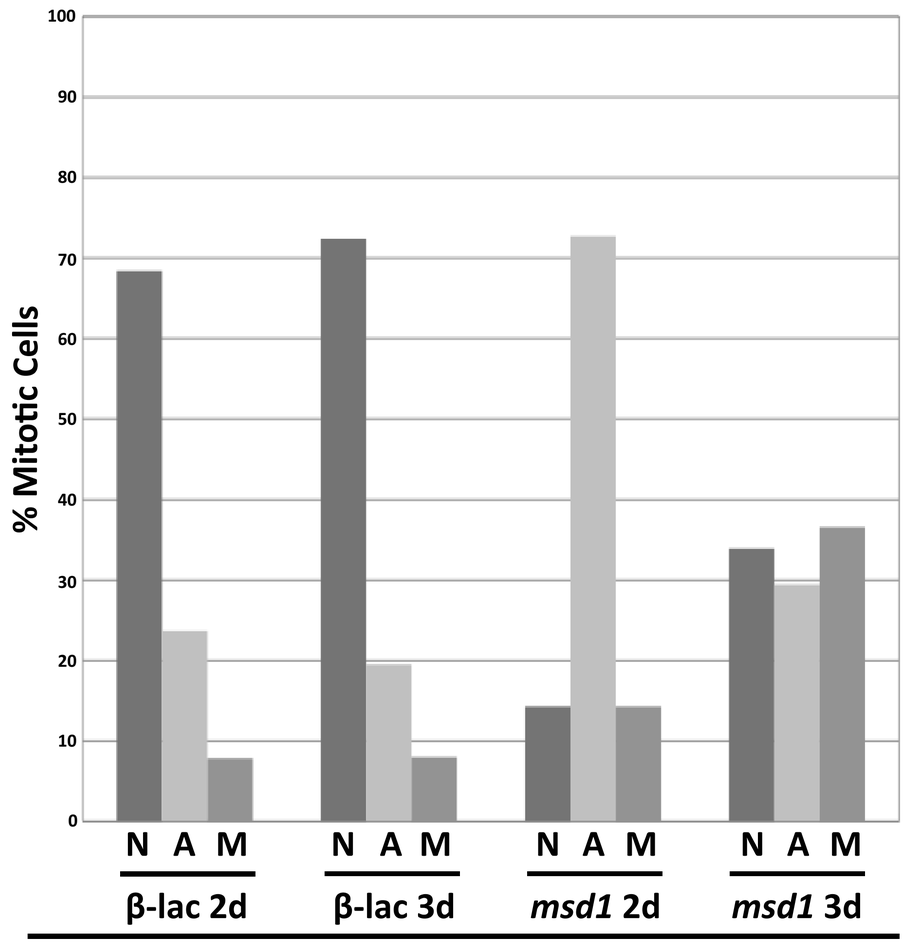


Figure 3-4. Duration of *msd1* RNAi causes different phenotypes.

S2 cell spindles were scored as normal (N), abnormal with long, less dense spindles (A) and monopolar (M) following dsRNA treatment. Duration of *β-lac* treatment had no effect on spindle classification (2d; N=68.4%, A=23.7%, M=7.9%; 3d N=72.4%, A=19.5%, M=8.0%). While 2d *msd1* dsRNA treatment increased the number of abnormal spindles (N=14.3%, A=72.3%, M=14.3%), the number of monopolar spindles increased after 3d *msd1* dsRNA treatment (N=33.9%, A=29.5%, M=36.6%).

3.1.4. *msd1* RNAi Eliminates γ-Tubulin Staining from Spindle MTs, Independently of the Centrosome

A reduction in MT density within the spindle might be caused by diminished MT nucleation. In the absence of functional centrosomes, EB1-GFP punctae originate from existing MTs within the spindle, suggesting that new MTs form from a site distinct from the chromatin, even when centrosomes are not present (Goshima *et. al,* 2006). 5 *msd* genes (*msd1-5*) were identified with identical phenotypes, and thus it was hypothesised that they shared the same function (Hughes *et. al,* 2008). Msd2,3 and 4 were subsequently shown to be required for γ-Tubulin localisation to spindle MTs (Goshima *et. al,* 2008), and therefore it was hypothesised that Msd1 shared this role. The intensity of γ-Tubulin was measured on the spindle in S2 cells treated with *msd1* dsRNA (Figure 3-5). γ-Tubulin staining was present at centrosomes and on spindle MTs in control treated cells (Figure 3-5A). In *msd1* RNAi cells, spindle localisation of γ-Tubulin appeared reduced, without eliminating the centrosomal localisation (Figure 3-5B). Spindle/centrosome γ-Tubulin intensity was significantly reduced in *msd1* RNAi cells compared with control treatments (Figure 3-6; spindle/centrosome = 0.05 vs. 0.14 $p<0.001$). Therefore, Msd1 is required to localise γ-Tubulin specifically to spindle MTs, independently of the centrosomal localisation of γ-Tubulin.

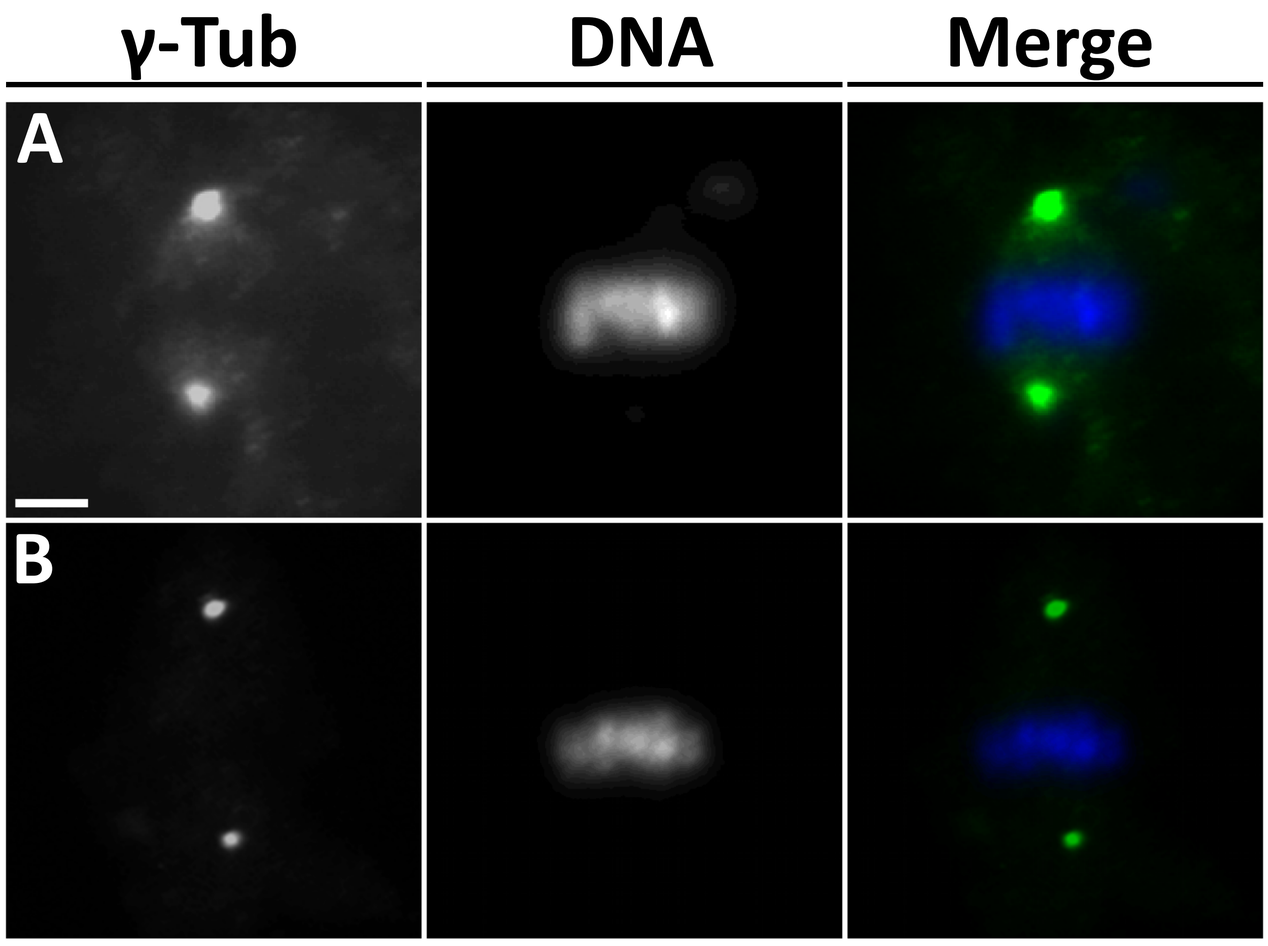


Figure 3-5. Msd1 is required to localise γ-Tubulin specifically to the spindle.
S2 cells were treated for 2d with dsRNA, fixed in methanol and stained for γ-Tubulin (Green) and DNA (Blue). (A) Control metaphase cell treated with *β-lac* dsRNA shows γ-Tubulin staining brightly on the centrosomes and also on spindle MTs. (B) Metaphase cell treated with *msd1* dsRNA retains centrosomal γ-Tubulin staining, but staining is absent from the spindle. Scale bar = 5µm.

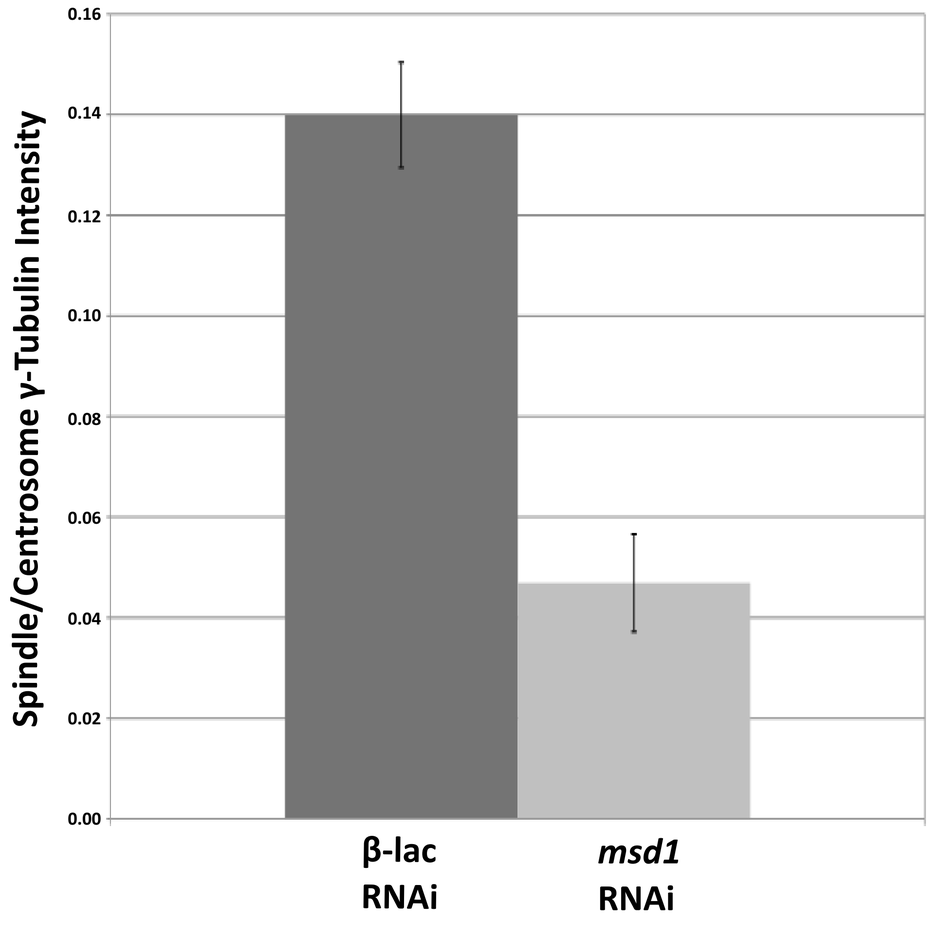


Figure 3-6. *msd1* RNAi significantly reduces spindle/ centrosome γ-Tubulin intensity.

Average γ-Tubulin pixel intensity for S2 cell half-spindles and centrosomes was measured in ImageJ, and spindle/ centrosome ratio calculated. Spindle/centrosome intensity is significantly lower in *msd1* RNAi cells (0.14± SEM=0.01; n=30) than in β-lac RNAi cells (0.05± SEM=0.01; n=27). $P < 0.001$.

3.1.5. Msd1 is Required for the Localisation of Dgt6 to the Spindle

Dgt6 is a member of the conserved Augmin complex, required for the localisation of γ-Tubulin to spindle MTs, and thus amplification of spindle MTs (Goshima *et. al,* 2008). Therefore, a role for Msd1 in Dgt6 localisation was investigated. In fixed S2 cells treated with dsRNA for 2 days (Figure 3-7), Dgt6 localised to spindle MTs in untreated S2 cells (Figure 3-7A). *msd1* RNAi reduced Dgt6 staining from the spindle (Figure 3-7B). While this demonstrates a co-dependent localisation of subunits in the complex, the stability of the complex in the absence of individual subunits is unclear, but might provide insight into the mechanisms by which Augmin is regulated.

3.1.6. Msd1 Co-Fractionates with the Augmin Complex

Five Augmin subunits (Dgt2, 3, 4, 5 and 6) identified by Goshima and co-workers are associated in a complex in S2 cells (Goshima *et. al,* 2008). The above experiments suggest that Msd1 behaves similarly to Augmin subunits. To test the hypothesis that Msd1 is in fact a novel Augmin component, a sucrose gradient was carried out using Msd1-GFP embryo extract to determine whether Msd1 associates with the Augmin complex (Figure 3-8). Extracts of embryos expressing Msd1-GFP were fractionated in a sucrose gradient. Msd1-GFP co-fractionated with Dgt5, Dgt6, Wac and γ-Tubulin, while control proteins did not (eIF4a). Therefore, Augmin subunits associate in the same biochemical fraction in embryo extracts - evidence that is consistent with the hypothesis that Msd1 is a component of the Augmin complex.

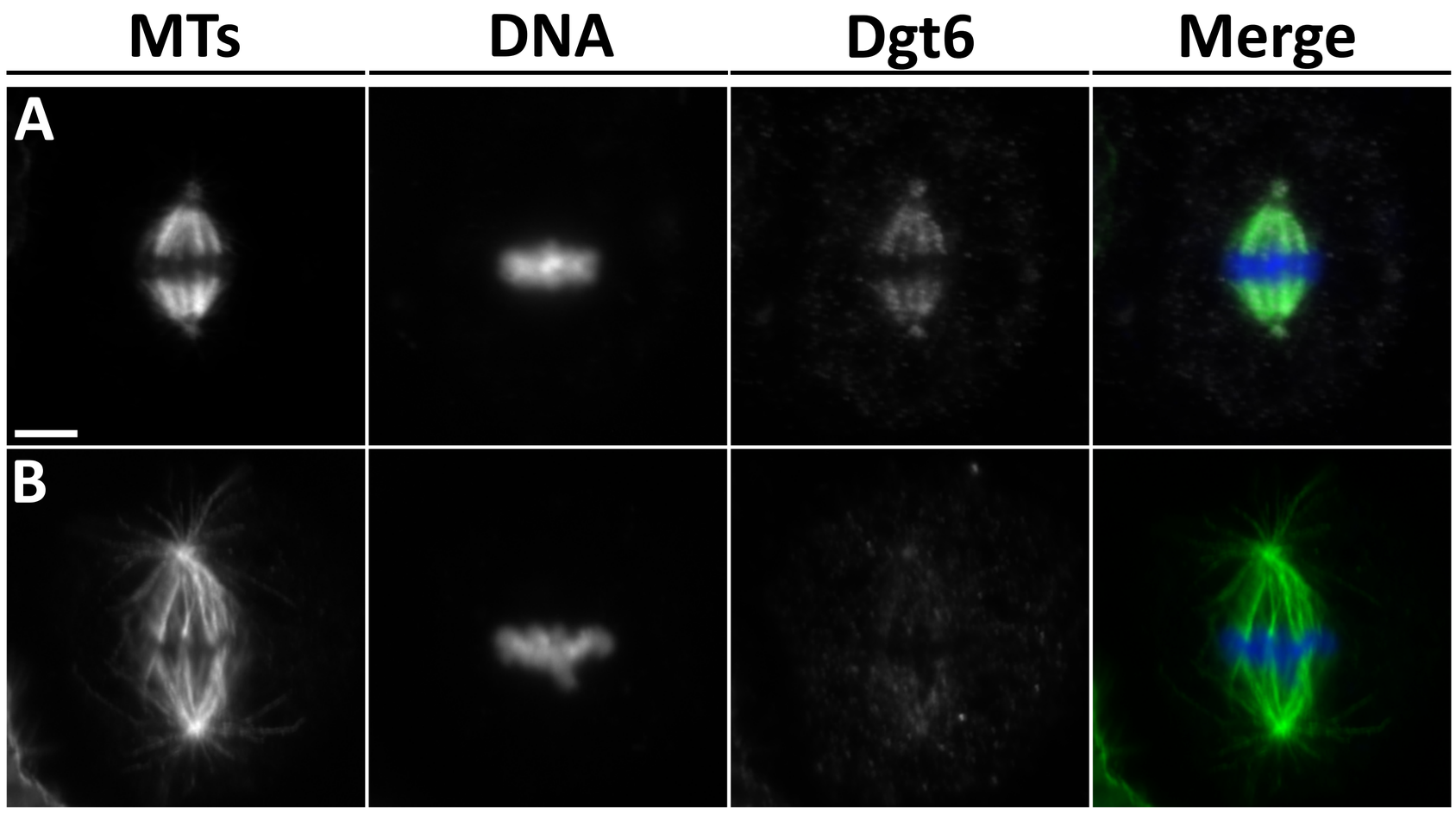


Figure 3-7. Msd1 is required for the localisation of Augmin subunit Dgt6 to Spindle MTs.
S2 cells were treated for 2d with dsRNA, fixed in methanol and stained for α-Tubulin (Green), DNA (Blue) and Dgt6 (Red). (A) Metaphase cell treated with *β-lac* dsRNA has dense spindle MTs and short astral MTs. Dgt6 localises to all spindle MTs and centrosomes. (B) Metaphase cell treated with *msd1* dsRNA has a low density of spindle MTs, an elongated spindle and long astral MTs. Dgt6 staining is absent from MTs and centrosomes. Scale bar = 5 μm.

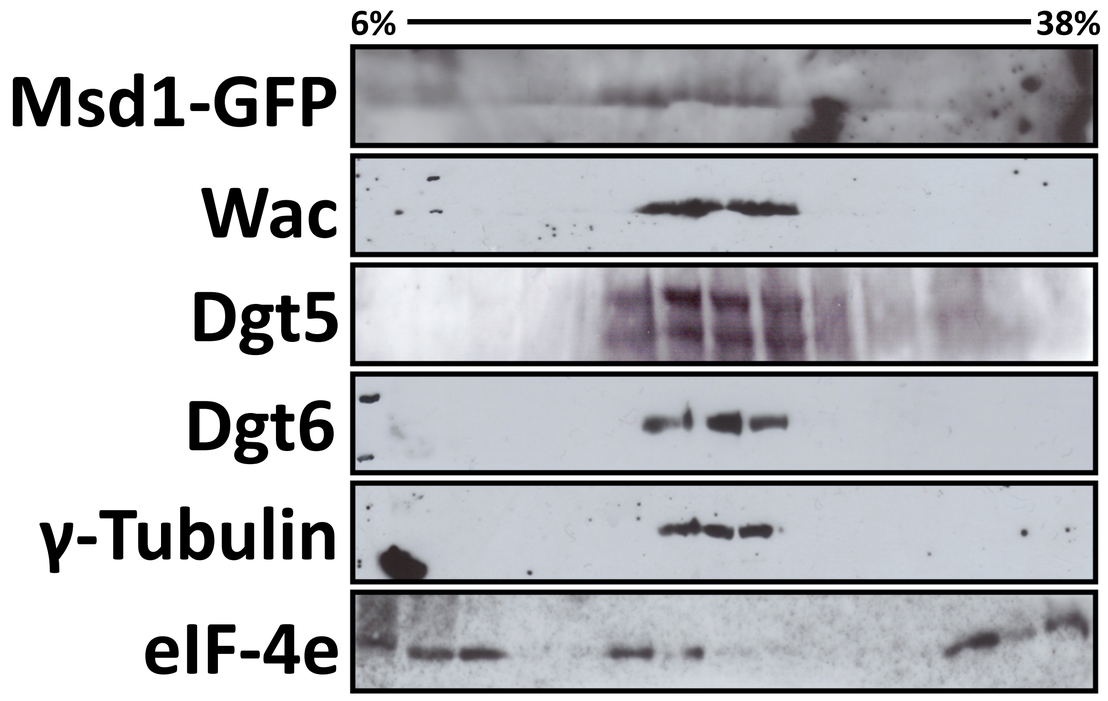


Figure 3-8. Msd1 co-fractionates with the Augmin complex.
0-3h embryo extract expressing Msd1-GFP was loaded onto a 6-38% Sucrose gradient and centrifuged for 4h at 40,000g. The column was separated into fractions and Western blotting was used to identify co-fractionating proteins. Msd1-GFP co-fractionated with Wac, Dgt5, Dgt6 and γ-Tubulin, but did not co-fractionate with eIF-43, a translation initiation factor.

3.1.7. Msd1 Co-Precipitates with the Augmin Complex

To investigate a physical interaction between Msd1-GFP and Augmin components, Msd1-GFP was immunoprecipitated from embryo extracts. Msd1-GFP co-immunoprecipitated with all subunits of the Augmin complex tested (Figure 3-9) while a control protein (PNUT; A MAP with no reported role in MT generation) did not associate with Msd1-GFP. A control antibody (β-Lac) did not immunoprecipitate any proteins tested. Interestingly, Dgt4 appears to be the only Augmin subunit that is fully depleted from the extract. Furthermore, γ-Tubulin did not co-immunoprecipitate with Msd1-GFP. Thus, Msd1 physically interacts with the Augmin complex.

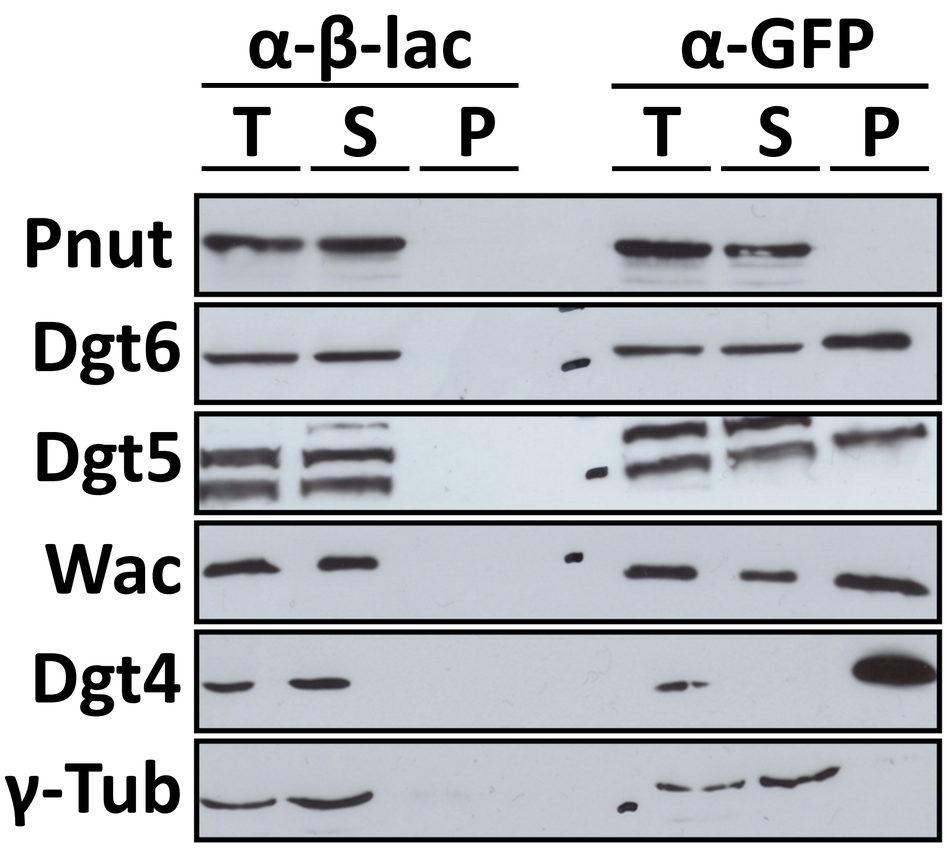


Figure 3-9. Msd1 co-precipitates with the Augmin complex.
0-3h extracts of embryos (Total, T) expressing Msd1-GFP were incubated with α-β-lac (control) and α-GFP antibodies for 2h. All proteins were present only in the supernatant in control samples (α-β-lac, S). All Augmin subunits tested (Dgt4,5,6, Wac) were present in the pellet with Msd1-GFP (α-GFP, P), whereas γ-Tubulin was not. Control antibodies (Pnut) did not co-precipitate with α-GFP (α-GFP, P).

3.1.8. Large Scale Co-Immunoprecipitation Shows Msd1 Interactors via Mass-Spectrometry

Because co-immunoprecipitation experiments show only interactions between candidate target proteins, Msd1-GFP was immunoprecipitated on a large-scale and the subsequent pellet was analysed by Mass-Spectrometry. The resultant peptide profile revealed an interaction between Msd1-GFP and every other subunit of the Augmin complex so far identified (Table 5; Goshima *et. al,* 2008).

Msd1 appears to exist in an 8-subunit hetero-octomeric complex. While few other interactors were found by two independent runs, both Actin and Myosin appeared to be enriched in the pellet.

Interactor	Symbol	Comments	MS Score
Dim gamma-tubulin 2	Dgt2	Augmin Subunit	29.10
Dim gamma-tubulin 3	Dgt3	Augmin Subunit	35.60
Dim gamma-tubulin 4	Dgt4	Augmin Subunit	27.90
Dim gamma-tubulin 5	Dgt5	Augmin Subunit	34.00
Dim gamma-tubulin 6	Dgt6	Augmin Subunit	43.60
Wee-augmin component	Wac	Augmin Subunit	40.70
Mitotic spindle density 5	Msd5	Augmin Subunit	36.60
Mitotic spindle density 1	Msd1	Augmin Subunit	25.10
Actin	Act	Cytoskeleton, Cytokinesis	47.90
Non-muscle myosin II Heavy chain	MHC1	Cytokinesis	48.50
Myosin Heavy Chain	MHC	Actin-Myosin Interaction	31.60
Myosin light chain cytoplasmic	Mlc-c	Actin-Myosin Interaction	29.50
Myosin alkali light chain I	Mlc1	Actin-Myosin Interaction	33.70
Tropomyosin 1	Tm1	Actin-Myosin Interaction	30.80
Calmodulin	CaM	Myosin-Binding	27.70
Barrier to autointegration factor	Baf	Nuclear Envelope, Chromatin	24.60

Table 5. Msd1-GFP Interactors.

3.1.9. Discussion

Several pieces of evidence accumulated during this study confirm Msd1 as a member of the conserved Augmin complex (Goshima *et. al,* 2008). First, these results establish that Msd1 is a MAP that is required for the stability of the mitotic spindle – observations that are consistent with the screen in which Msd1 was identified (Hughes *et. al,* 2008).

The knock-down phenotype of *msd1* indicates a comparable role in spindle formation to the Augmin complex. Msd1 is required to localise γ-Tubulin to existing spindle MTs, independently of γ-Tubulin localisation at the centrosome. In the absence of Msd1, γ-Tubulin was significantly reduced on the spindle relative to the centrosomes, resulting in a significant reduction in mitotic spindle density during metaphase. The absence of γ-Tubulin on the spindle is likely to be the cause of this phenotype – a hypothesis that was confirmed by measurement of the rate at which EB1-GFP comets originated from spindle MTs. Here, a significant reduction in MT nucleation rate was observed (Wainman *et. al,* 2009). The resulting phenotype is increasingly severe over time because of a progression from an unstable bipolar spindle to a monopolar spindle.

Msd1 is required for the localisation of Dgt6 to spindle MTs. Previous studies have demonstrated that knock-down of any component of the Augmin complex results in mislocalisation of all other subunits tested (Goshima *et. al,* 2008). In addition to this evidence, Msd1 was shown to co-fractionate with, and co-precipitate all

characterised subunits of the Augmin complex tested. Thus, Msd1 is a *bonafide* component of the Augmin complex.

Interestingly, co-immunoprecipitation of Msd1 from embryo extracts resulted in a marked immunodepletion of Dgt4 from the total extract, raising the prospect that the stoichiometry of Augmin is not necessarily 1:1, and that rate-limiting factors could have a role in regulation of spindle formation. *In vitro* studies of complex formation might further elucidate this hypothesis.

Furthermore, Mass Spectrometry of Msd1 interactors revealed an enrichment of Actin and Myosin II peptides. HAUS6/Dgt6 has a role in the completion of cytokinesis in HeLa cells (Uehara *et. al,* 2009), and it is possible that by interacting with other cytoskeletal components, Augmin can modulate structures such as the contractile ring in cytokinesis – a mechanism that is investigated further in Chapter 3.2 of this thesis.

While it is clear that Msd1 regulates γ-Tubulin localisation during spindle assembly, the mechanism by which Augmin operates is not known in detail. *In vitro* studies using a reconstituted complex could establish if Augmin is capable of nucleating MTs in the absence of existing MTs. Moreover, ultrastructural analysis, or super-resolution microscopy of Augmin-nucleated MTs might provide insight into the periodicity and branching of new MTs forming upon existing MTs. Finally, further insight into the regulation of Augmin during mitosis is necessary. Plk1-dependent phosphorylation of Dgt6/FAM29A is required for DGrip71WD/NEDD1 localisation to

the spindle (Zhu *et. al,* 2009). Spatio-temporal regulation by major mitotic kinases is thus likely to have a role in spindle assembly via Augmin. Temporal isolation of the Augmin complex at discrete cell cycle stages and subsequent analysis by Mass Spectrometry would enable identification of regulation of Augmin subunits by kinases.

3.2. Msd1 and *Drosophila* Development

No study described so far has sought to identify the importance of any Augmin subunit in the somatic divisions of a multicellular organism. The following section describes a characterisation of the role of Msd1 in *Drosophila* development. A hypomorphic mutant allele of *msd1* was generated by A.Wainman prior to the onset of this study. Furthermore, the Msd1-GFP fusion protein used here was generated prior to the onset of this study, and shown to localise to all spindle MTs and centrosomes throughout mitosis (Wainman *et. al,* 2009).

3.2.1. *msd1*^{ex51} is a Hypomorphic Allele Causing Maternal Effect Lethality

msd1^{ex51} is a hypomorphic allele generated by imprecise excision of element EY11673 in the 5'UTR of *CG13915* (Figure 3-10; A.Wainman). The deletion generated is internal to the P-element, but disrupts expression levels of Msd1 (Figure 3-10A). RT-PCR with control primers showed equal amounts of template RNA extracted from wild-type and *msd1*^{ex51} 3rd instar larvae. Primers specific to *msd1* demonstrated a reduction in expression in *msd1*^{ex51} mutants (Figure 3-10B). Thus, *msd1*^{ex51} is a hypomorphic allele.

95% of embryos laid by homozygous *msd1*^{ex51} mothers fail to hatch, whereas male adults are fertile (See section 3.2.4). Thus, *msd1*^{ex51} causes maternal effect lethality.

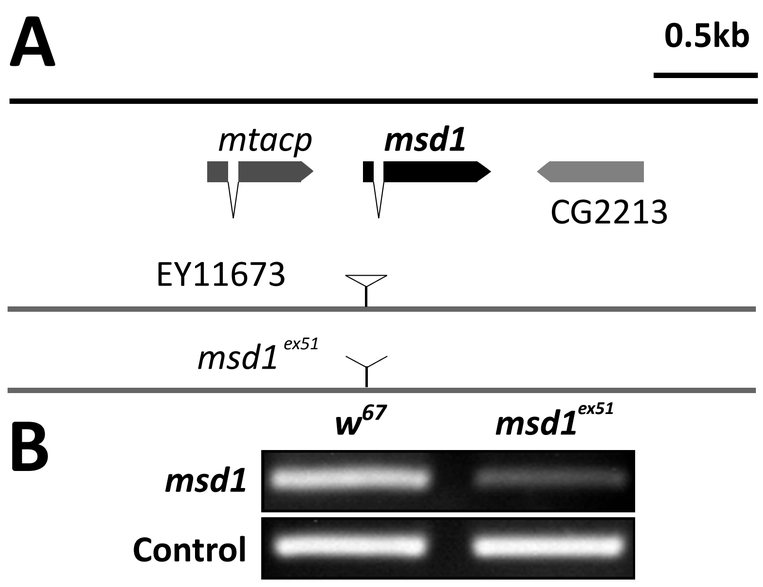


Figure 3-10. *msd1*^{ex51} is a hypomorphic allele that is maternal-effect lethal.
(A) *msd1*^{ex51} is an allele generated by imprecise excision of the P-element in line EY11673 in the 5'UTR of CG*13914* (A.Wainman). The aberration is caused by a deletion internal to the P-element, giving white eyes. (B) RT-PCR of third instar larvae. Control primers amplified equal amounts of cDNA, whereas *msd1* primers amplify considerably less cDNA in the mutant relative to *w*^{67} flies.

3.2.2. *msd1*^{ex51} Meiotic Spindles Appear Normal

A null mutation in the small Augmin component *wac* is maternal-effect lethal. Bipolar meiotic spindle formation in *wac* mutant embryos is not severely disrupted, suggesting it is largely driven by MTs nucleated from chromatin in *Drosophila.* However, no *wac* embryos have been observed to progress past meiosis II, and are thus arrested at this stage (Meireles *et. al,* 2009).

To investigate the effect of *msd1*^{ex51} on meiotic spindle formation, 0-30 minute embryos were fixed and stained for α-Tubulin and DNA (Figure 3-11). *msd1*^{ex51} meiotic spindles (Figure 3-11B) did not appear morphologically abnormal compared with *w*^{67} meiotic spindles (Figure 3-11A). Spindles were bipolar, and showed no obvious defects in chromosome congression. However, spindles did appear reduced in MT density – consistent with observations in mitotic cells.

3.2.3. *msd1*^{ex51} Phenotype is Intensified Over Deficiency

To elucidate the nature of the *msd1*^{ex51} hypomorphic allele, flies with a known deletion at this locus were crossed into the *msd1*^{ex51} background. 1-4h embryos were fixed and stained for DNA, and used to investigate relative rates of development. (Figure 3-12; Table 6). Wild-type 1-4h embryos showed a largely even distribution of developmental stages, reflecting normal development through pre-cortical and cortical divisions towards cellularisation. Some embryos laid by *msd1*^{ex51} homozygous mothers (*msd1*^{ex51} embryos hereafter) developed to cycles 10-14. However, the proportion that reaches cycles 10-14 is significantly reduced. Embryos laid by

mothers of the genotype *msd1*^{ex51}/*Df(3L)Bab-PG* (*msd1*^{ex51}/Df embryos hereafter), failed to reach cycles 10-14 100% of the time. This reflects the relative levels of Msd1 expression between *msd1*^{ex51}/*msd1*^{ex51} and *msd1*^{ex51}/Df. It is unclear whether *msd1*^{ex51}/Df embryos arrest in meiosis, but *msd1*^{ex51} embryos are likely to have a sufficient complement of maternal Msd1 to support limited syncytial development.

	Pre-Cortical %	**Cortical %**	**>10 Cycles %**
w^{67}	41.9	29.9	28.2
msd1^{ex51}/*msd1*^{ex51}	59.8	33.7	6.5
msd1^{ex51}/*Df*	100	0	0

Table 6. *msd1*^{ex51} hatch rates.

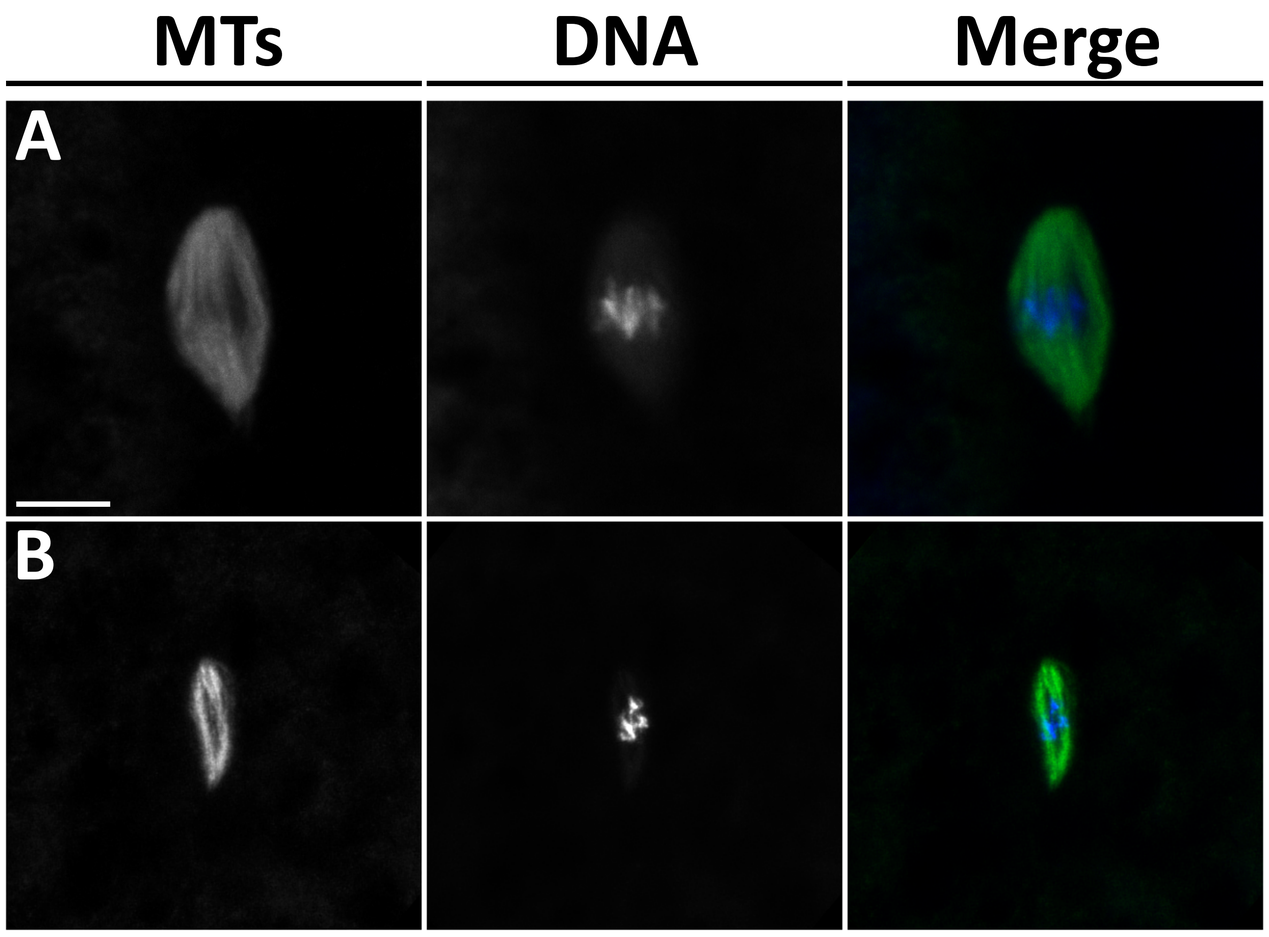


Figure 3-11. Spindle bipolarity is not disrupted in *msd1*^{ex51} meiotic spindles.
0-30' embryos were dechorionated, fixed in methanol and stained for α-Tubulin and DNA. Confocal microscopy was used to take 5µm Z-stacks. (A) *w*^{67} metaphase meiotic spindle is anastral and bipolar with chromosomes congressed on the metaphase plate. (B) *msd1*^{ex51} meiotic metaphase spindle shows no defects in spindle bipolarity or chromosome congression. Meiotic spindle density appears reduced. Scale bar = 5µm

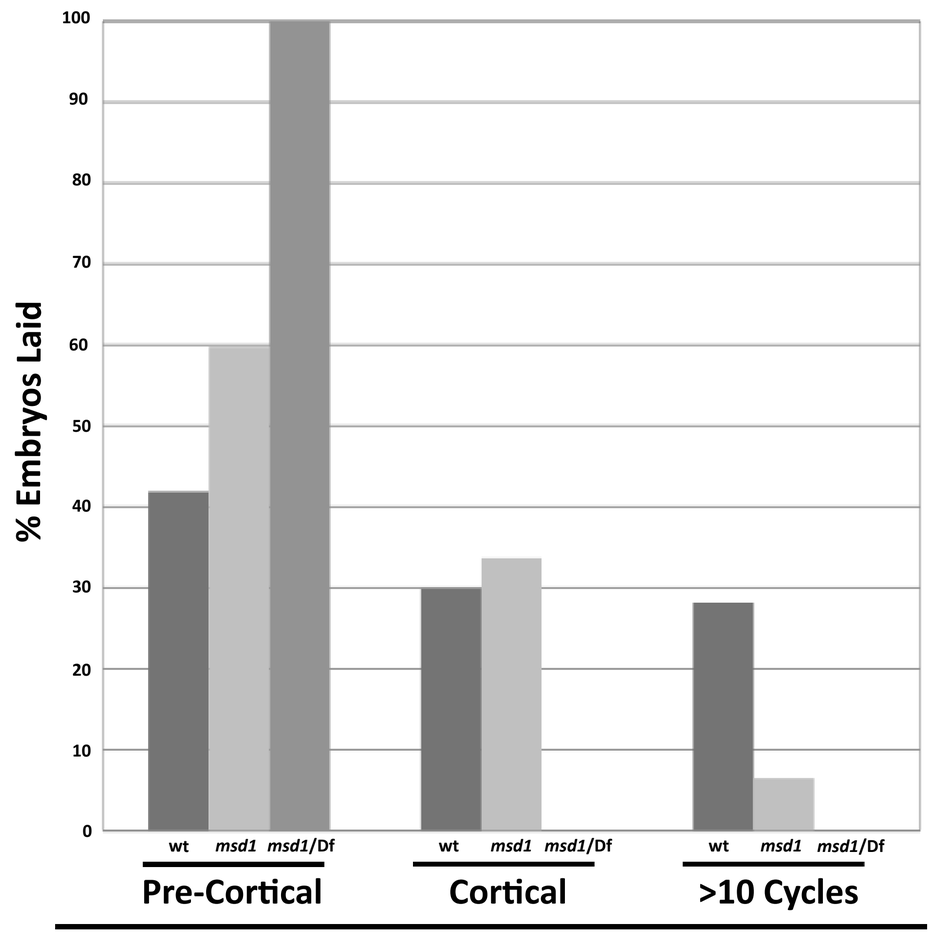


Figure 3-12. *msd1*^{ex51} developmental failure is intensified over deficiency.

0-4h embryos of the following genotypes were fixed, stained for DNA and classified by their developmental stage. Nuclei in wt embryos exhibit an even distribution of stages (41.9% Pre-cortical, 29.9% Cortical, 28.2% >10 Cycles). Some *msd1*^{ex51} embryos survive to cortical cycles (59.8% Pre-cortical, 33.7% Cortical, 6.5% >10 Cycles). *msd1(ex51)*/Df embryos never survive to cortical cycles (100% Pre-cortical, 0% Cortical, 0% >10 Cycles).

.

3.2.4. *msd1*^{ex51} is Rescued by Msd1-GFP in Embryos

To examine whether the maternal effect lethality of *msd1*^{ex51} is due to decreased Msd1 expression, *msd1*^{ex51} was rescued by over-expression of Msd1-GFP under the control of the mat-α-TubGAL4 promoter (Figure 3-13). While 79.5% of *w*^{67} embryos hatched after 24 hours, only 5.2% of *msd1*^{ex51} embryos hatched (P<-0.001), and no *msd1*^{ex51}/Df embryos hatched (P<0.001). Hatch rates similar to wild-type were observed in *msd1*^{ex51} embryos rescued by the addition of Msd1-GFP driven by the mat-α-TubGAL4 driver (86.2%; P>0.05), but the transgene alone (without driver) could not (0%; P<0.001). Thus, the maternal-effect lethality of *msd1*^{ex51} is caused by a reduction in Msd1 expression. Furthermore, the hatch rate discrepancy between *msd1*^{ex51} and *msd1*^{ex51}/Df embryos is consistent with previous observations that the hypomorphic allele can support syncytial divisions.

3.2.5. *msd1*^{ex51} Phenotype is Consistent with S2 Cells

To investigate whether the *msd1*^{ex51} phenotype in the developing fruit fly was comparable to that observed in S2 cells, 0-3h embryos were fixed and stained for α-Tubulin and DNA (Figure 3-14). Immunofluorescence analysis revealed that of the embryos that progressed to cortical nuclear divisions, *msd1*^{ex51} embryos (Figure 3-14B) exhibited longer, less dense spindles than those in *w*^{67}embryos (Figure 3-14A) at equivalent stages. This is consistent with the phenotype observed in S2 cells, and suggests that the primary role of Msd1 in the organism is similar to that in S2 cells. Live analysis of MT and DNA dynamics will reveal mechanism by which the majority of *msd1*^{ex51} embryos fail to reach cellularisation (see Section 3.2.6).

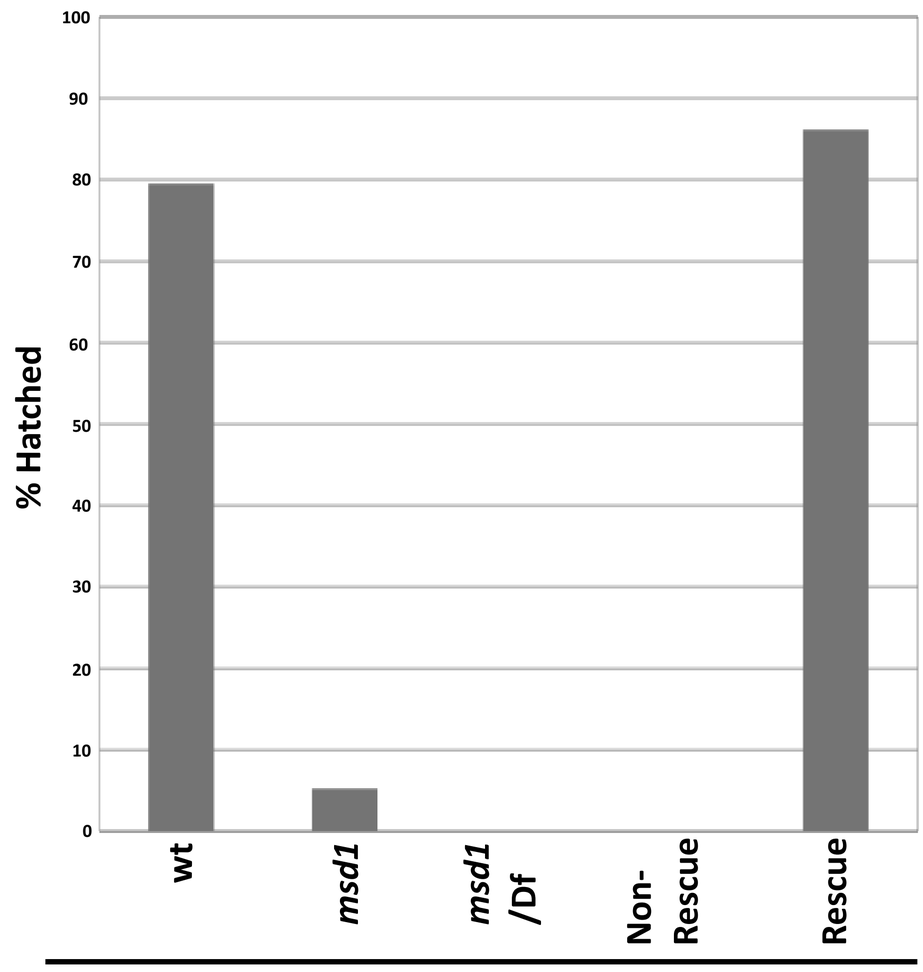


Figure 3-13. *msd1*^{ex51} embryos are rescued by Msd1-GFP. Hatch rates were counted after 24h for embryos laid by flies flies of the following genotypes; *msd1*^{ex51} embryos hatch significantly less (5.2%) than *w*^{67} (79.5%. P<0.001). No *msd1*/Df or non-rescue (Msd1-GFP transgene, without driver) embryos hatched (0% P<0.001). Msd1-GFP driven by the maternal-α-Tubulin promoter rescued the *msd1* phenotype to *w*^{67} levels (86%. P>0.05).

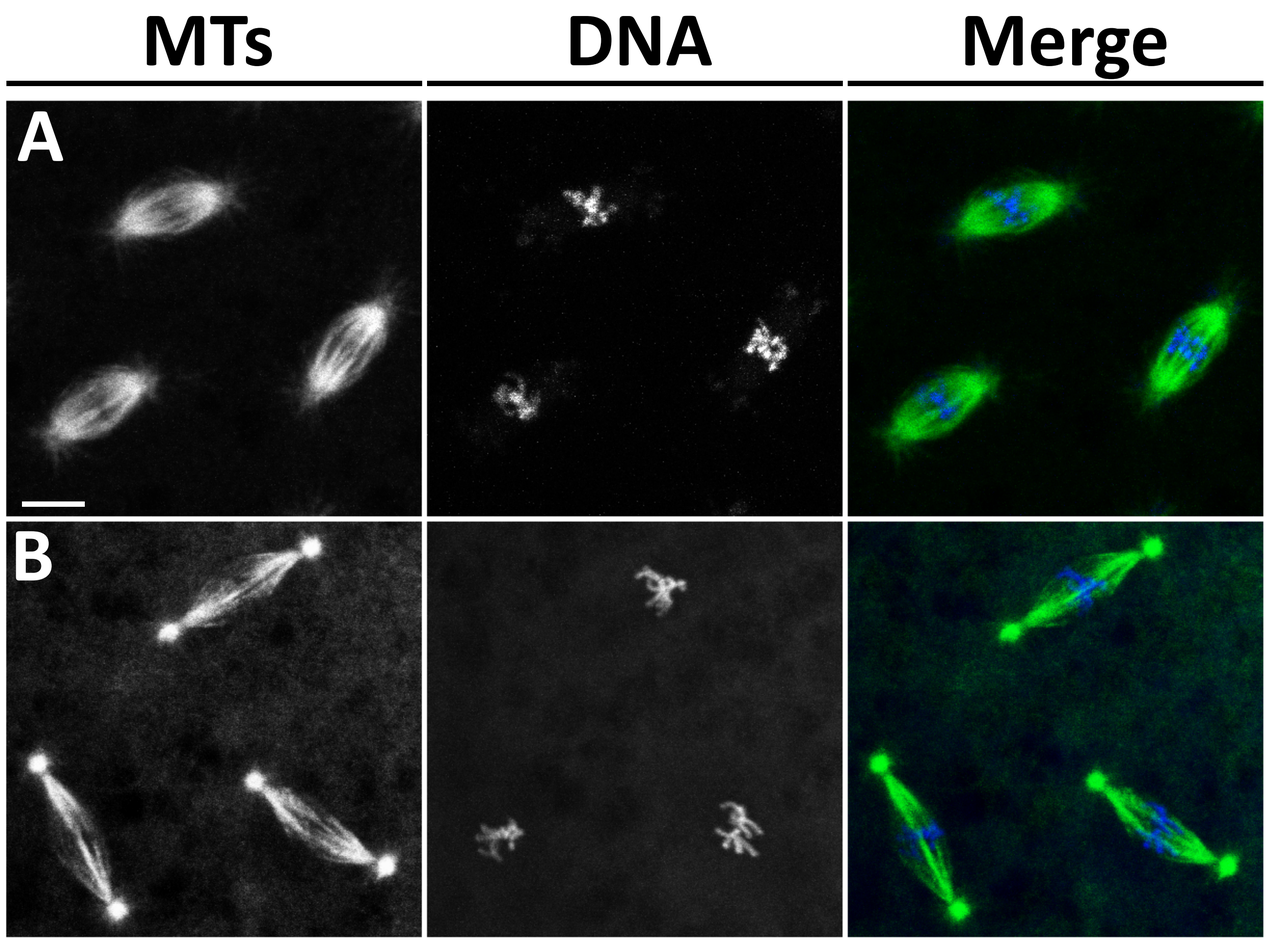


Figure 3-14. *msd1*^{ex51} embryos show a phenotype comparable to S2 cells.
0-3h embryos were dechorionated, fixed in methanol and stained for α-Tubulin and DNA. Confocal microscopy was used to take 5µm Z-stacks. (A) *w*^{67} metaphase showing barrel-shaped spindles with chromosomes aligned. (B) Metaphase in an *msd1*^{ex51} embryo shows elongated spindles that are less dense. No obvious defects in chromosome congression or spindle bipolarity were observed. Scale bar = 5µm.

3.2.6. *msd1*^{ex51} has a Significantly Reduced Mitotic Spindle Density in Early Embryos Expressing α-Tubulin-GFP

Visualising the dynamics of spindle assembly in the absence of Msd1 will provide further insight into the maternal effect lethality observed in embryos. α-Tubulin-GFP under the poly-ubiquitin promoter was crossed into the *msd1*^{ex51} background to visualise MTs (Figure 3-15; Movies 1A; 1B). Time-lapse microscopy in wild-type embryos showed MTs emanating predominantly from the centrosomes following NEB, before synchronously forming barrel shaped spindles in metaphase (Figure 3-15A). Similarly, in the *msd1*^{ex51} background, MTs predominantly emanated from the centrosomes, but failed to form a robust, barrel-shaped spindle, instead forming elongated spindles that appeared bent and disorganised relative to neighbouring spindles (Figure 3-15B). Monopolar spindles were not observed, however.

The spindle/centrosome α-Tubulin-GFP intensity was significantly reduced in *msd1*^{ex51} relative to wild-type embryos (Figure 3-16; spindle/centrosome = 0.72±0.05SEM vs. 0.88±0.03SEM $p<0.05$). Thus, the mechanism of action of Msd1 is consistent between S2 cells and embryos.

The *msd1*^{ex51} phenotype in embryos revealed further aspects not evident in fixed S2 cells. First, the density of MTs at the central spindle appeared reduced in *msd1*^{ex51} relative to controls. Although the central spindle is not associated with a cleavage furrow in *Drosophila* embryos, this robust structure does not persist for as long in *msd1*^{ex51} embryonic cycles.

Second, although cortical contractions occurred in an organised manner during syncytial mitoses, movement of nuclei in *msd1*^{ex51} mutant embryos appeared disorganised, and neighbouring spindles regularly interfered with each other.

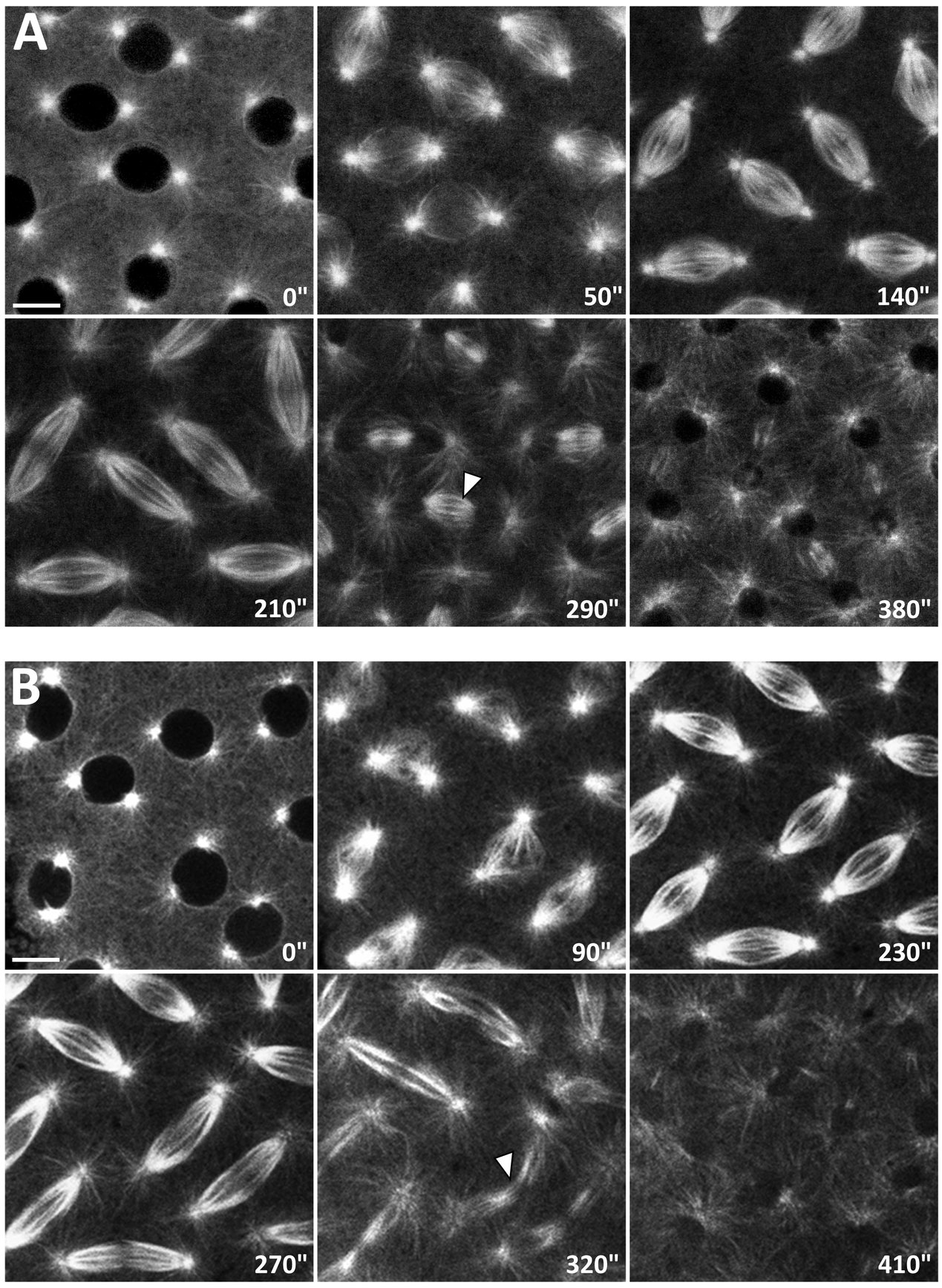


Figure 3-15. α-Tubulin-GFP shows a phenotype consistent with Augmin in *msd1*^{ex51} embryos.

1-2h embryos expressing α-Tubulin-GFP to visualise MTs were dechorionated and mounted on coverslips with heptane glue. Time-lapse confocal microscopy was used to take a 5µm Z-stack every 10". (A) In wt embryos, barrel-shaped spindles form at metaphase (140") before spindles elongate during anaphase (210") and a dense spindle mid-body forms in telophase (290"). (B) In *msd1*^{ex51} embryos, metaphase is delayed and spindles are more elongated with large asters (230"). In anaphase, some elongated spindles bend (270"). MTs at the mid-zone (arrows) appear less dense. Scale bar = 5µm.

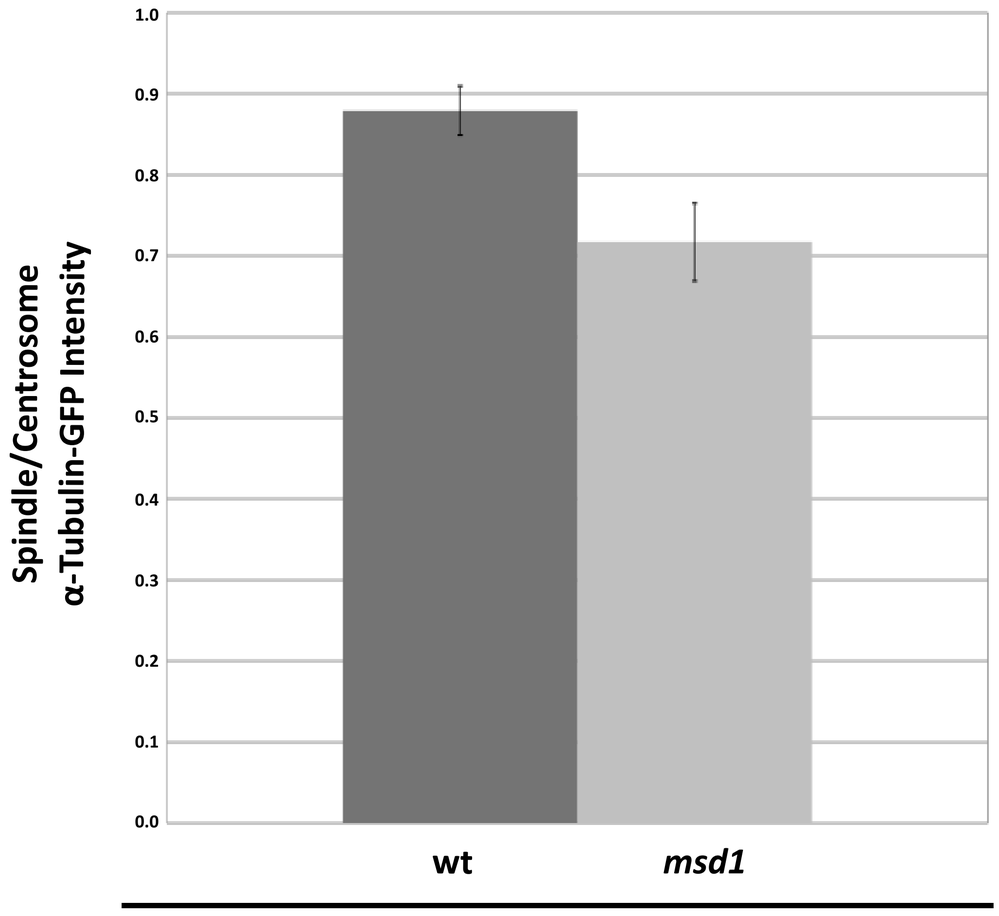


Figure 3-16. *msd1*^{ex51} embryos have a significantly reduced spindle/centrosome α-Tubulin intensity.
Average α-Tubulin-GFP pixel intensity for embryo half-spindles and centrosomes was measured in ImageJ, and spindle/centrosome ratio calculated. Average of multiple nuclei per embryo = 1 data point. In *msd1*^{ex51} embryos, the spindle/centrosome ratio is significantly reduced (0.72±0.05 SEM, n=10) compared with wt embryos (0.88 ±0.03 SEM, n=5). P<0.05.

3.2.7. *msd1*^{ex51} Embryos Are Delayed in Metaphase Progression

msd1^{ex51} 3rd instar larval neuroblasts exhibit a significant increase in metaphase-anaphase ratio (Wainman *et. al,* 2009). Thus, in the absence of the Augmin complex, spindle assembly is delayed, and might contribute to the phenotype observed. Analysis of time-lapse images of α-Tubulin-GFP in embryos in their 9th cycle, revealed that NEB-Metaphase time (NEB = 1st frame of α-Tubulin-GFP fluorescence in the nuclear space; Metaphase = 1 frame prior to anaphase onset) is significantly increased in *msd1*^{ex51} embryos relative to wild-type embryos (Figure 3-17; 296 seconds ±11.1 SEM vs. 186.6 seconds ±7.6 SEM, $p<0.001$).

To investigate this further, *msd1*^{ex51} was crossed into a checkpoint-deficient *mad2* null background (Buffin *et. al,* 2007). While the *mad2* mutant alone is viable and fertile, *msd1*^{ex51};*mad2* double mutants are lethal, suggesting that in the absence of a functional SAC, *msd1*^{ex51} (and therefore Augmin-templated MTs) are required for *Drosophila* development. The delay in metaphase progression observed when Msd1 was absent is presumably due to SAC activation – a mechanism that is essential to prevent major mitotic defects such as aneuploidy that would otherwise occur in the *msd1*^{ex51} background.

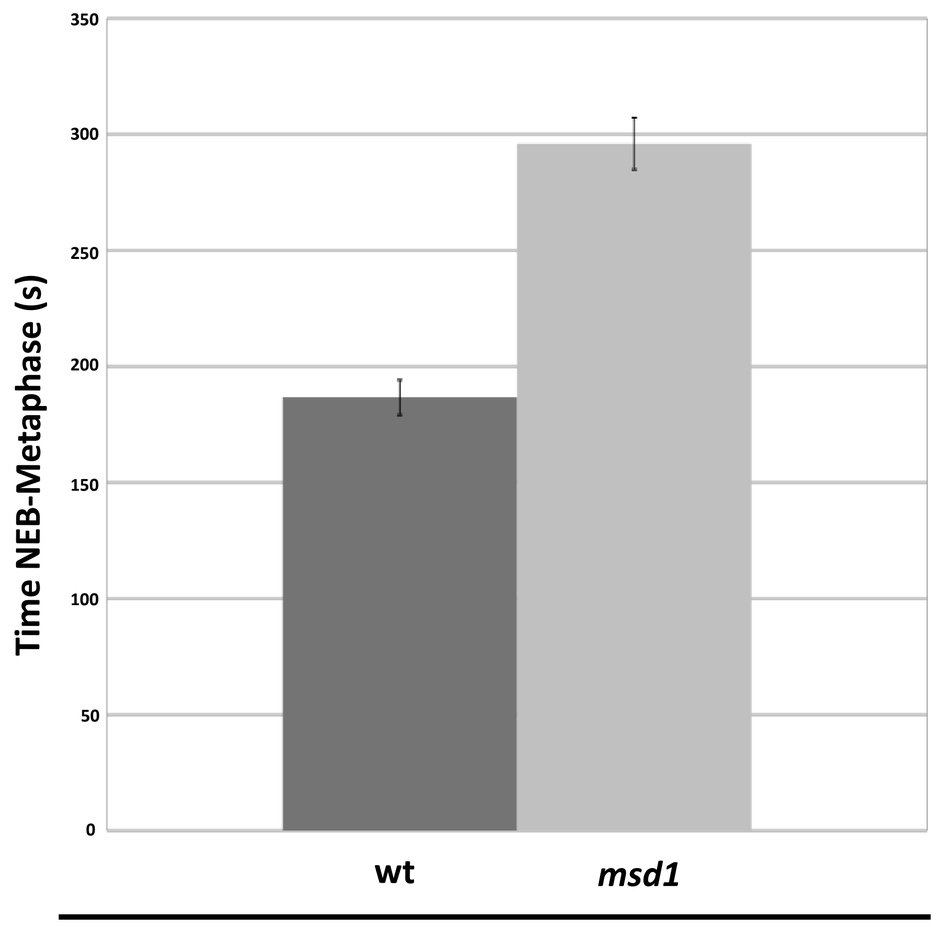


Figure 3-17. *msd1*^{ex51} embryos are delayed in metaphase progression.

Time between NEB-metaphase was measured using time-lapse movies of embryos expressing α-Tubulin-GFP. NEB was scored as the first frame following MT invasion into the nuclear space. Metaphase was scored as being a single frame prior to anaphase onset. *msd1*^{ex51} embryos are significantly delayed (296"±11.1 SEM, n=10) compared with wt embryos (186.6"±7.6 SEM, n=6). P<0.001.

3.2.8. *msd1*^{ex51} Nuclei Have Errors in Chromosome Congression and Aneuploidy

Histone H2A-GFP (His-GFP hereafter) was crossed into the *msd1*^{ex51} background under the control of the mat-α-TubGAL4 promoter (Figure 3-18; Movies 2A; 2B). Time-lapse microscopy of wild-type embryos expressing His-GFP showed the 4 *Drosophila* chromosomes attaching to the spindle as it formed and aligning on the metaphase plate, before being segregated during anaphase (Figure 3-18A). In contrast, *msd1*^{ex51} nuclei showed asynchrony in nuclear divisions. Defects in chromosome alignment resulted in lagging chromosomes during anaphase, ultimately generating grossly aneuploid nuclei. These nuclei fail in subsequent divisions (Figure 3-18B). The severity of this phenotype is likely to be exacerbated by the lack of a robust SAC in syncytial mitoses, rendering the embryo incapable of correcting aberrant chromosome attachments before anaphase in the absence of Msd1.

3.2.9. *msd1*^{ex51} has a Significantly Reduced Spindle/Centrosome Ratio of γ-Tubulin-GFP in Early Embryos

Msd1 is required to localise γ-Tubulin specifically to the spindle in fixed S2 cells. However, the dynamics of γ-Tubulin in the absence of Msd1 remained unclear, first because no live analysis had been carried out, plus variations between fixing procedures and antibody affinities can complicate these interpretations. γ-Tubulin-GFP (a gift from S.Endow; Hallen *et. al,* 2008) under the *ncd* promoter was recombined with the *msd1*^{ex51} allele to visualise γ-Tubulin dynamics (Figure 3-19; Movies 3A; 3B). Time-lapse microscopy of wild-type embryos (Figure 3-19A) showed

high γ-Tubulin-GFP intensity at the centrosome throughout the cell cycle, and a distinct localisation to spindle MTs shortly after NEB. γ-Tubulin-GFP persisted on spindle MTs throughout spindle formation, and was present at the central spindle as it formed in anaphase. In the *msd1*^{ex51} background, γ-Tubulin-GFP fluorescence was at the centrosome throughout the cell cycle, but appeared to be absent from spindle MTs following NEB (Figure 3-19B). Furthermore, γ-Tubulin-GFP was absent from the central spindle during anaphase in *msd1*^{ex51} embryos.

Measurement of the spindle/centrosome ratio of γ-Tubulin-GFP intensity at metaphase revealed a significant decrease in *msd1*^{ex51} embryos compared with wild-type embryos (Figure 3-20; spindle/centrosome = 0.04±0.02SEM vs. 0.21±0.05SEM $p<0.01$). Therefore Msd1, as in S2 cells, is required for the localisation of γ-Tubulin to MTs during spindle formation, and in anaphase in syncytial development.

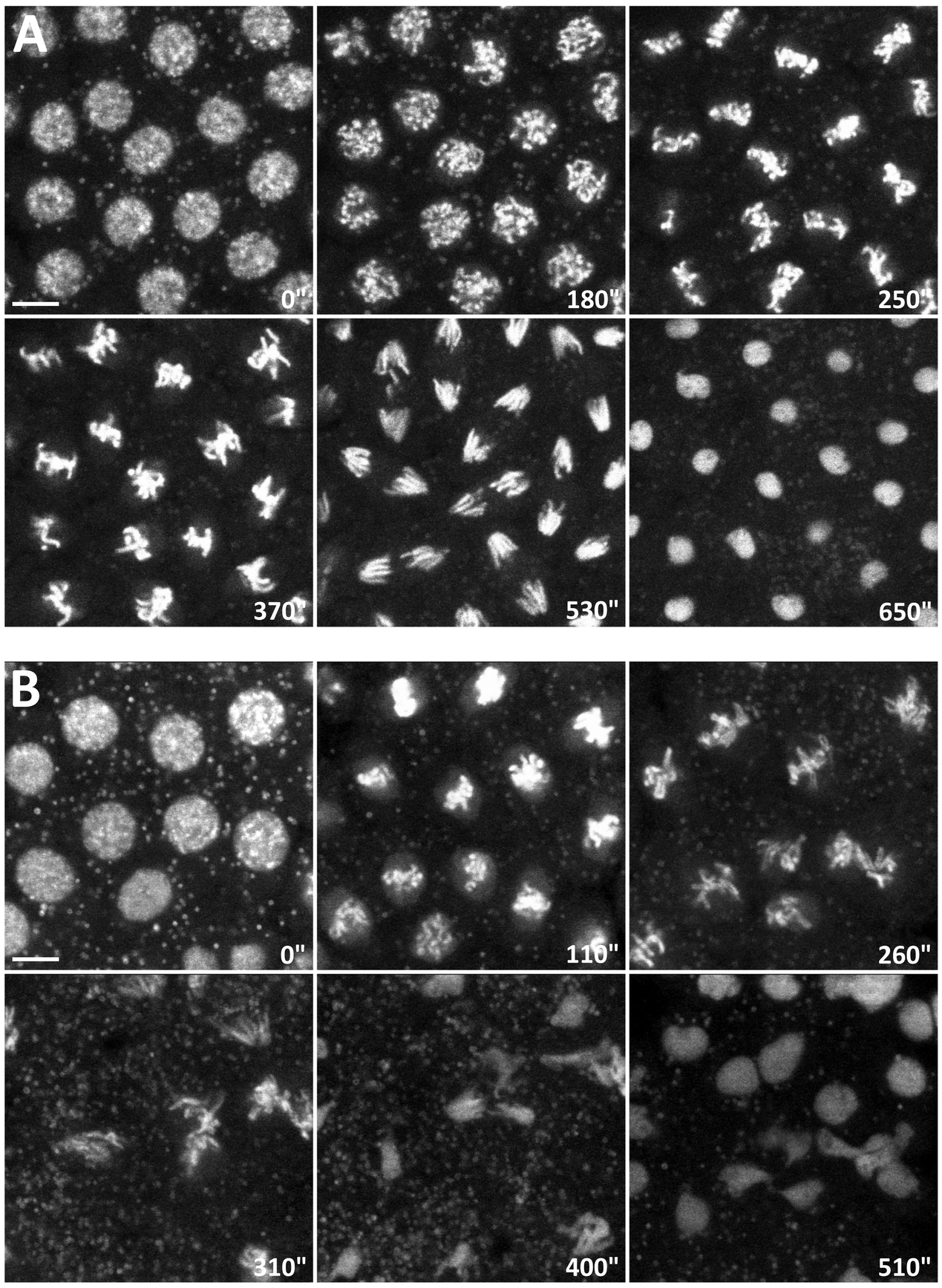


Figure 3-18. *msd1*^{ex51} embryos show errors in chromosome congression and aneuploidy.

1-2h embryos expressing Histone-GFP to visualise DNA were dechorionated and mounted on coverslips with heptane glue. Time-lapse confocal microscopy was used to take a 5µm Z-stack every 10". (A) In wt embryos, condensed chromosomes congress normally on the metaphase plate (250"), before being distributed equally and synchronously into daughter nuclei (650"). (B) In *msd1*^{ex51} embryos, condensed chromosomes congress on the metaphase plate, but nuclei are aneuploid (260'). Anaphase is asynchonous between nuclei (400") and results in lagging chromosomes and failure to fully segregate chromatin during telophase (510"). Scale bar = 5µm.

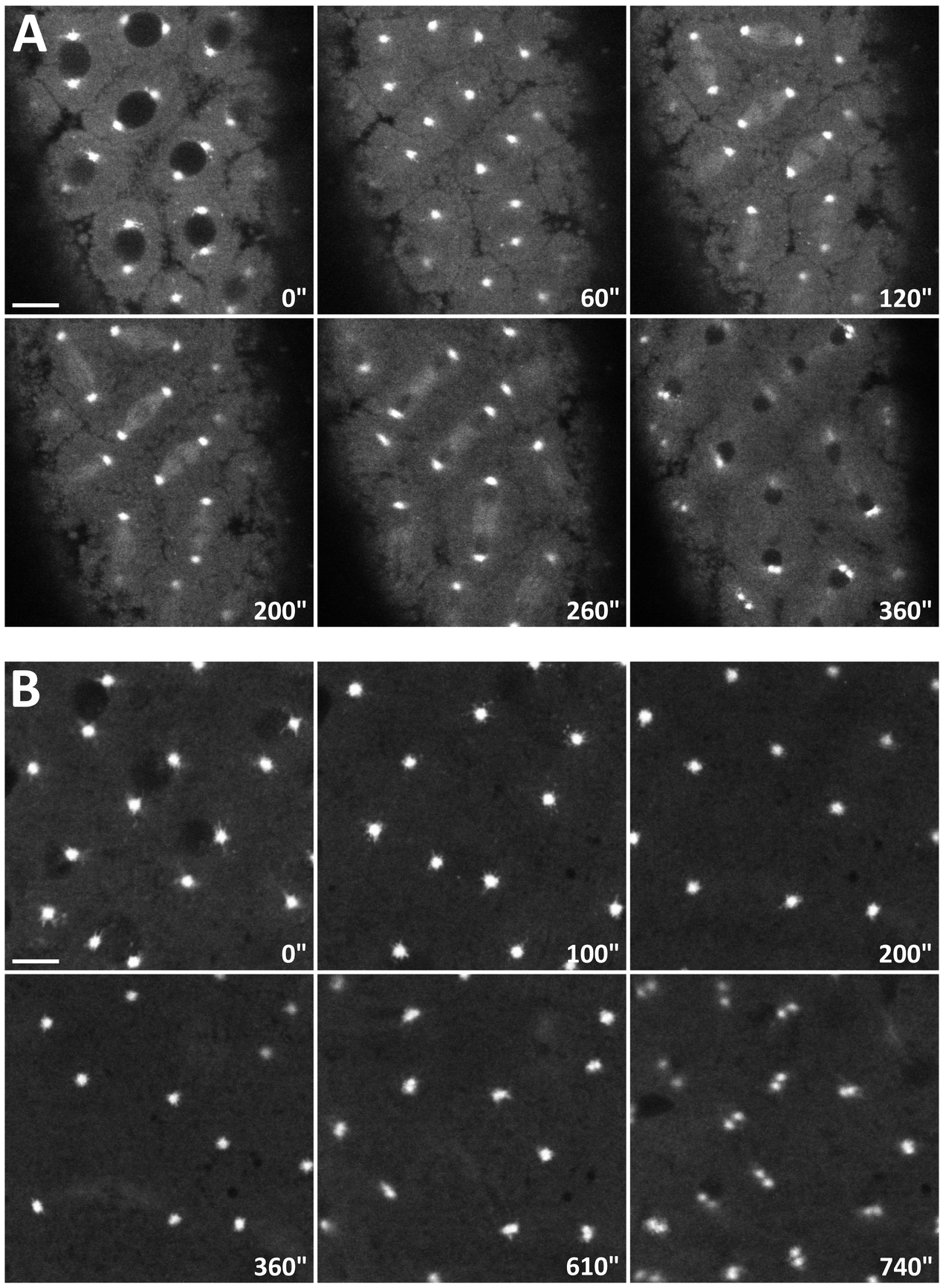


Figure 3-19. γ-Tubulin-GFP is absent from spindles in *msd1*^{ex51} embryos.
1.2h embryos expressing γ-Tubulin-GFP were dechorionated and mounted on coverslips with heptane glue. Time-lapse confocal microscopy was used to take 5µm Z-stacks every 10". (A) In wt embryos, γ-Tubulin localises to centrosomes throughout the cell cycle, and to spindle MTs shortly after NEB through to metaphase (120"). In anaphase, γ-Tubulin localises to the spindle midzone (260"). (B) In *msd1*^{ex51} embryos, γ-Tubulin localises to the centrosomes, but is absent from both spindle MTs in metaphase (200") and the spindle midzone in anaphase/ telophase (610"). Scale bar = 5µm.

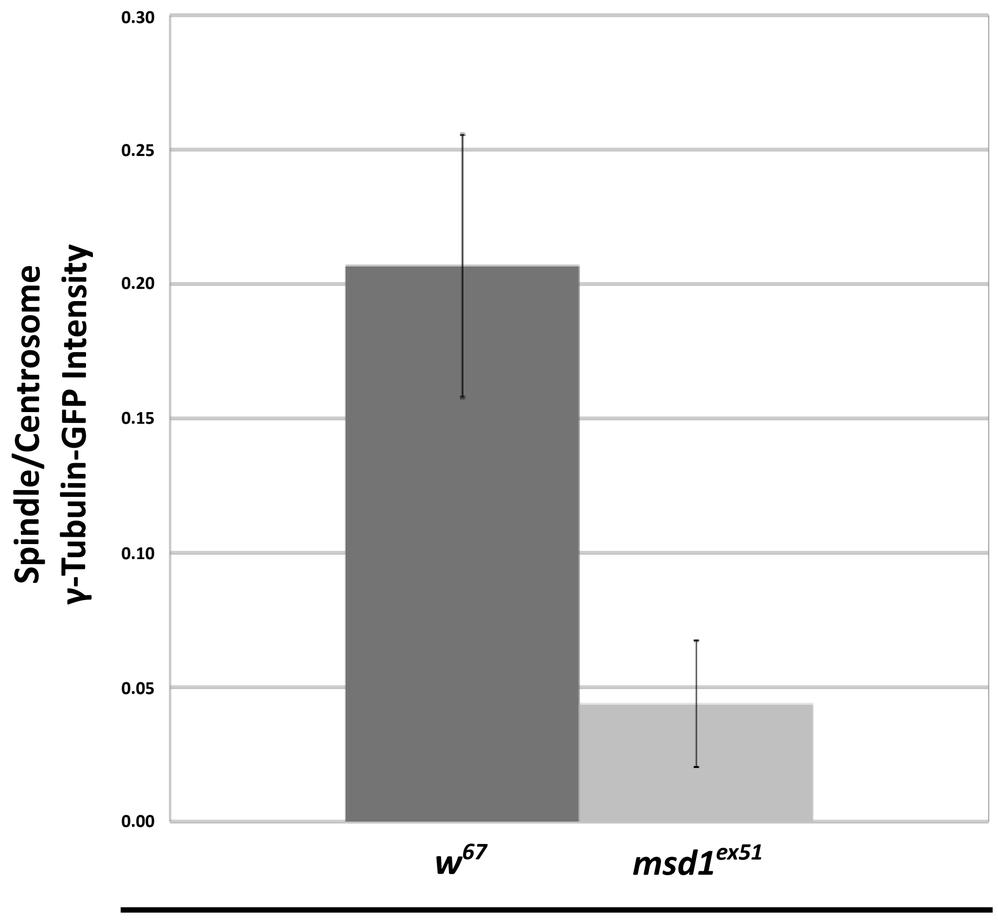


Figure 3-20. *msd1*^{ex51} embryos have significantly reduced spindle/centrosome γ-Tubulin-GFP intensity.
Average γ-Tubulin-GFP pixel intensity for embryo half-spindles and centrosomes was measured in ImageJ, and spindle/centrosome ratio calculated. Average of multiple nuclei per embryo = 1 data point. In *msd1*^{ex51} embryos, the spindle/centrosome ratio is significantly reduced (0.04±0.02 SEM, n=6) compared with wt embryos (0.21 ±0.05 SEM, n=4). P<0.01.

3.2.10. Live Analysis of Moesin-GFP Reveals No Clear Defects in Actin Organisation in *msd1*^{ex51} embryos

Msd1-GFP co-immunoprecipitated Actin and Myosin subunits, and *msd1*^{ex51} embryos exhibit grossly disorganised nuclear positioning in the syncytial blastoderm. To investigate whether this phenotype is an effect of Actin dysfunction, a GFP fusion protein containing the C-terminal F-Actin binding domain of Moesin was used to visualise Actin localisation (a gift from J. Bloor; Dutta *et. al,* 2002). Moesin-GFP (Moe-GFP hereafter) was crossed into the *msd1*^{ex51} background under the control of the mat-α-TubGAL4 promoter (Figure 3-21; Movies 4A; 4B).

Time-lapse microscopy of Moe-GFP in wild-type embryos showed cortical Actin caps forming around nuclei and expanding throughout interphase. Immediately before mitosis, actin caps expanded and eventually abutted each other. During mitosis, the caps disintegrated, and Actin outlined each nucleus. At anaphase, Actin partially invaginated at the cleavage furrow, before again capping the reformed nuclei (Figure 3-21A). In *msd1*^{ex51} embryos, Actin caps were present, and expanded during interphase. Actin caps did not completely abut each other in *msd1*^{ex51} embryos – possibly due to a high rate of nuclear fall-out in these embryos. Nuclei exhibited gross cortical contractions, as observed with α-Tubulin-GFP, but Moe-GFP localisation is unperturbed at the cleavage furrow during anaphase (Figure 3-21B).

Thus, the functional significance of the relationship between Actin dynamics and the *msd1*^{ex51} phenotype is unclear, since Actin localisation is comparable during both interphase and mitosis in wild-type and *msd1*^{ex51} embryos.

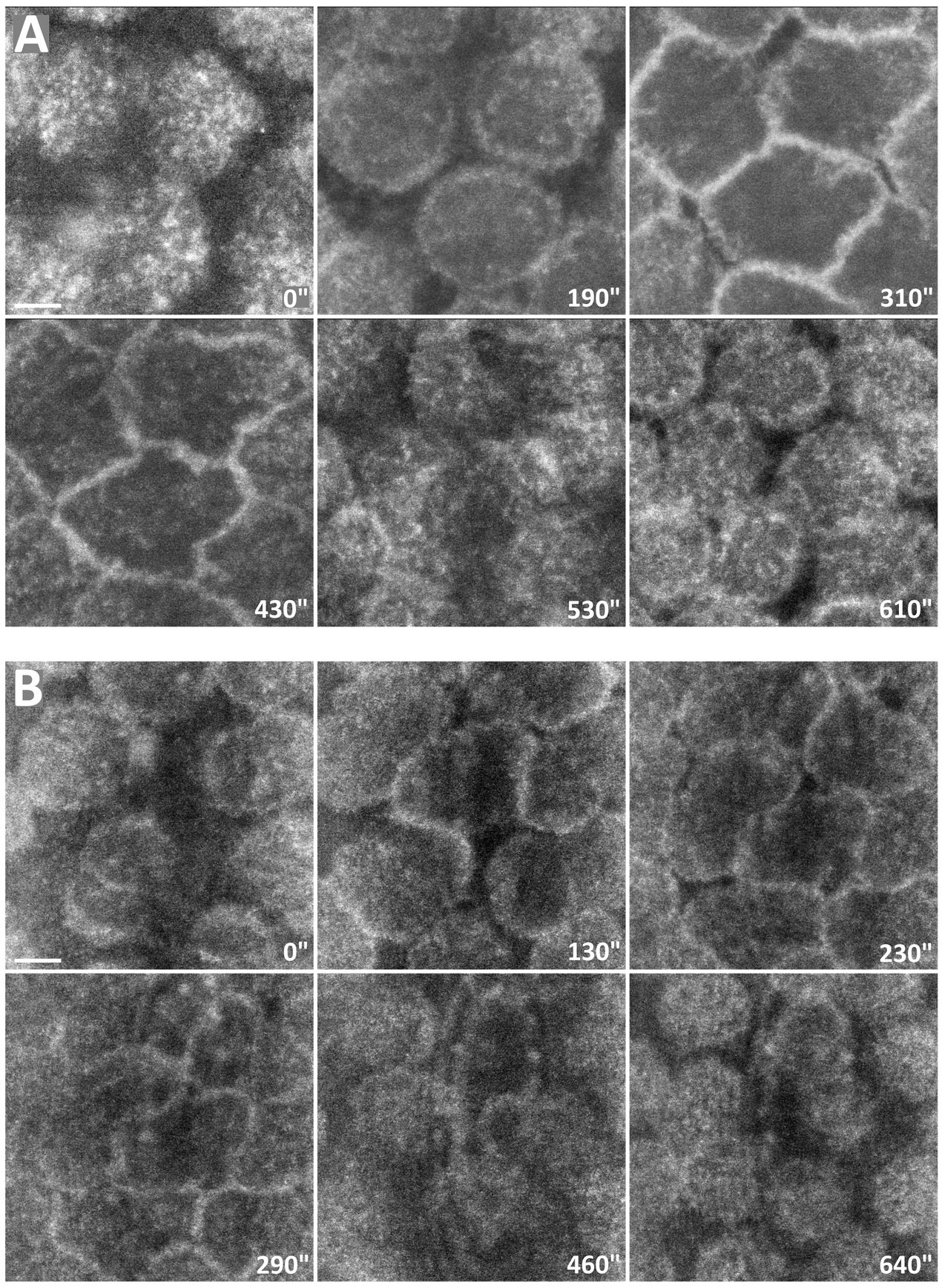


Figure 3-21. *msd1*^{ex51} embryos have no clear defects in Actin dynamics..
1-2h embryos expressing Moe-GFP to visualise Actin dynamics were dechorionated and mounted on coverslips with heptane glue. Time-lapse confocal microscopy was used to take 5µm Z-stacks every 10". (A) In wt embryos, Actin caps expand around nuclei during interphase (0") and outline the nuclei during metaphase (190"). The pseudo-cleavage furrow is evident in anaphase (430") and Actin caps reform and expand in the following interphase (530", 610"). (B) *msd1*^{ex51} embryos show no obvious defects in Actin organisation. Actin caps are not disrupted in interphase (0", 460", 640") and pseudo-cleavage furrows form around nuclei in mitosis (130", 230"). Errant cortical contraction of nuclei is evident, as observed with α-Tubulin-GFP. Scale Bar = 5µm.

3.2.11. Discussion

The *msd1*^{ex51} allele is crucial for understanding the role of Msd1 in the development of a multicellular organism. The population of MTs generated by Augmin in the spindle is integral to the development of the fly.

Initial characterisation of the *msd1*^{ex51} phenotype revealed that *msd1*^{ex51} is a hypomorphic allele that is required for the development of embryos from homozygous mutant mothers. This maternal-effect lethality was intensified over deficiency – while some homozygous-laid embryos develop through many mitotic cycles, and occasionally hatch, embryos laid by *msd1*^{ex51}/Df mothers never progressed past female meiosis. *msd1*^{ex51} is rescued by the addition of Msd1-GFP, showing that the mutant phenotype is due to a lack of Msd1 protein. Thus, *Drosophila* development is sensitive to the embryonic levels of Msd1, and in the absence of Msd1, early embryonic development is unsustainable.

In a parallel study, the relative contribution of Msd1 to mitotic spindle formation was elucidated by eliminating the centrosomal contribution of MTs in spindle formation in the *msd1*^{ex51} background (Wainman *et. al,* 2009). Individually, both *msd1*^{ex51} and *cnn*^{hk} are viable – phenotypes that expose redundancy in pathways that generate MTs for spindle assembly. In combination, *cnn*^{hk}*;msd1*^{ex51} double mutants are lethal at the pupal stage, showing that further redundant MT generation mechanisms cannot sustain *Drosophila* development in the absence of MTs from both centrosomes and Augmin (Wainman *et. al,* 2009).

The hypomorphic *msd1*^{ex51} allele therefore provided an ideal experimental tool for phenotypic analysis in the developing embryo. Many aspects of the *msd1*^{ex51} phenotype are identical to that observed in S2 cells; γ-Tubulin intensity is significantly reduced on spindle MTs relative to the centrosome, resulting in a reduced mitotic spindle density.

msd1^{ex51} meiotic spindles look morphologically normal, which might be explained by the presence of residual Msd1 protein in the early embryo that is sufficient to drive meiotic progression. Null mutants of Augmin subunit *wac* exhibit bipolar meiotic spindles, suggesting that these spindles rely to an extent on the Ran.GTP-directed pathway for MT organisation (Meireles *et. al,* 2009).

A striking characteristic of the *msd1*^{ex51} phenotype is the major NEB-anaphase delay in embryos. The cause of this is likely to be due to aberrant attachment of kMTs to the kinetochores, or a lack of tension. While an increase in mitotic index had been shown previously, this delay had not been shown in live cells (Goshima *et. al,* 2008). Analysis of Histone-GFP in the mutant background revealed gross mis-segregation defects that were a likely cause of embryonic lethality.

Msd1 might be responsible for γ-Tubulin localisation at the prospective central spindle to nucleate new MTs. Further work visualising new MT formation and MT turnover at the central spindle in the absence of Msd1 will elucidate this mechanism (see Section 3.3).

Large cortical movements of nuclei within the blastoderm were an intriguing aspect of the embryonic *msd1*^{ex51} phenotype. This observation, coupled with evidence that Msd1 interacts with Actin/Myosin II, raised the possibility that Msd1 had a role in cytoskeletal dynamics within the blastoderm. Analysis of this phenotype using Moesin-GFP as a marker for Actin did not, however, reveal any clear disruption of Actin caps in embryos. Thus while it is clear that organisation of nuclei within the blastoderm is disrupted, this phenotype does not appear to be dependent upon the Actin cytoskeleton.

Further studies of the role of Augmin in *Drosophila* development will be important. Studies similar to the *cnn*^{hk}*;msd1*^{ex51} double mutant are likely to reveal other genes, whose absence generates synthetic lethality in an Augmin background. Therefore, it might be possible to elucidate the extent of mechanistic redundancy that exists in building a mitotic spindle to sustain normal multicellular development.

3.3. Mitotic Spindle Dynamics After Metaphase

A number of observations indicated that Msd1 might have a role in MT generation during anaphase and the formation of the central spindle. First, Msd1-GFP and γ-Tubulin both localise to the prospective central spindle during anaphase (See Section 3.2). Second, time-lapse movies of α-Tubulin-GFP in *msd1*^{ex51} embryos show defects in central spindle organisation. Finally, cleavage furrow regression is observed in human cells in the absence of HAUS6/Dgt6 (Uehara *et. al,* 2009). Until now, the role of Augmin components during anaphase has not been investigated.

3.3.1. The Central Spindle is Disrupted in *msd1*^{ex51} Early Embryos

Observation of α-Tubulin-GFP in *msd1*^{ex51} embryos shows that in contrast to wild-type, the MTs that form the central spindle do not persist through anaphase (Figure 3-22). While this result suggests a role for Msd1 in central spindle formation, *Drosophila* embryos are not a suitable system for this study due to the absence of cytokinesis in these cells. Thus, S2 cells were used to further study the role of MT-templated MT nucleation during anaphase and telophase.

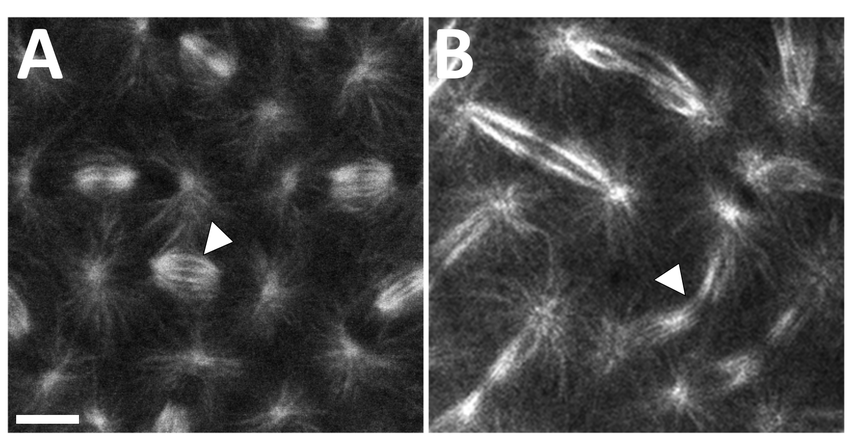


Figure 3-22. The Central Spindle is disrupted in *msd1*^{ex51} embryos.

1-2h embryos expressing α-Tubulin-GFP to visualise MTs were dechorionated and mounted on coverslips with heptane glue. Time-lapse confocal microscopy was used to take a 5µm Z-stack every 10". (A) wt embryo in anaphase assembles a robust MT structure between separated chromosomes. (B) *msd1*^{ex51} forms a central spindle (arrows) that is less robust, and persists for a shorter period. Scale bar = 5µm.

3.3.2. *msd1* RNAi Causes Central Spindle Defects in Live S2 Cells Expressing α-Tubulin-GFP

Time-lapse microscopy of S2 cells stably expressing α-Tubulin-GFP was carried out to investigate MT dynamics in anaphase and telophase (Figure 3-23; Movies 5A; 5B). Control-treated cells exhibit robust MT generation and bundling during central spindle assembly in anaphase, leading to completion of cytokinesis (Figure 3-23A). Cells treated with *msd1* dsRNA, however, are defective in MT bundling during anaphase. While existing interpolar MTs are present, MT generation appears to be impaired, thus affecting central spindle assembly (Figure 3-23B).

Despite this lack of bundling, cytokinesis defects are not evident in populations of Msd1-deficient S2 cells.

3.3.3. *msd1* RNAi Affects EB1-GFP Localisation at the Central Spindle in Anaphase

To further investigate the contribution of Augmin to MT generation in central spindle formation, S2 cells transiently expressing the MT plus-end binding protein EB1-GFP were treated with dsRNA. Control-treated cells appeared to exhibit continuous plus-end generation from MTs during anaphase (Movie 6A), whereas comets originating from existing MTs in cells treated with *msd1* dsRNA appeared reduced (Movie 6B). Due to mild over-expression of transiently transfected EB1-GFP, in combination with cytoskeletal rearrangement during anaphase, the analysis software previously used in Wainman *et. al,* (2009) cannot currently be applied to these time-lapse movies

without extensive development. Clearly, further analysis is essential to directly confirm a role for Augmin-generated MTs during anaphase.

3.3.4. *msd1* RNAi Reduces Turnover of MTs During Central Spindle Formation

It appears that Augmin-dependent nucleation of new MTs occurs during central spindle assembly, though the relative contribution of new MTs to the central spindle is unclear. Fluorescence Recovery After Photobleaching (FRAP) was used to establish the rate of Tubulin-subunit replacement at the central spindle during anaphase. S2 cells stably expressing α-Tubulin-GFP were treated with dsRNA and MTs at the prospective central spindle were photobleached (Figure 3-24). The half-life of recovery was significantly lower in *msd1* dsRNA treated cells (Figure 3-25; 26.24 seconds) compared with control cells (47.62 seconds, $F=23.40$, $p<0.0001$). Conversely, the fluorescence plateau at the central spindle was dramatically higher in control-treated cells (71.65%) compared with *msd1* knock-down cells (52.52%, $F=129.0$, $p<0.0001$). Because cells lacking Msd1 have a lower fluorescence plateau, it is clear that Msd1 contributes to central spindle formation.

Kymographs of fluorescence intensity at the central spindle exposed an interesting role for Msd1 (Figure 3-26). Following photobleaching, fluorescence across both control-treated and *msd1* knock-down samples returned. However, in control-treated cells, a population of MTs originates within the central spindle at a position equidistant from the poles, and distinct from polar MT populations. This fluorescence then begins to expand poleward (Figure 3-26A). In *msd1* RNAi cells, this

MT population is absent, suggesting that Msd1 is required to generate a specific population of new MTs from within the central spindle (Figure 3-26B).

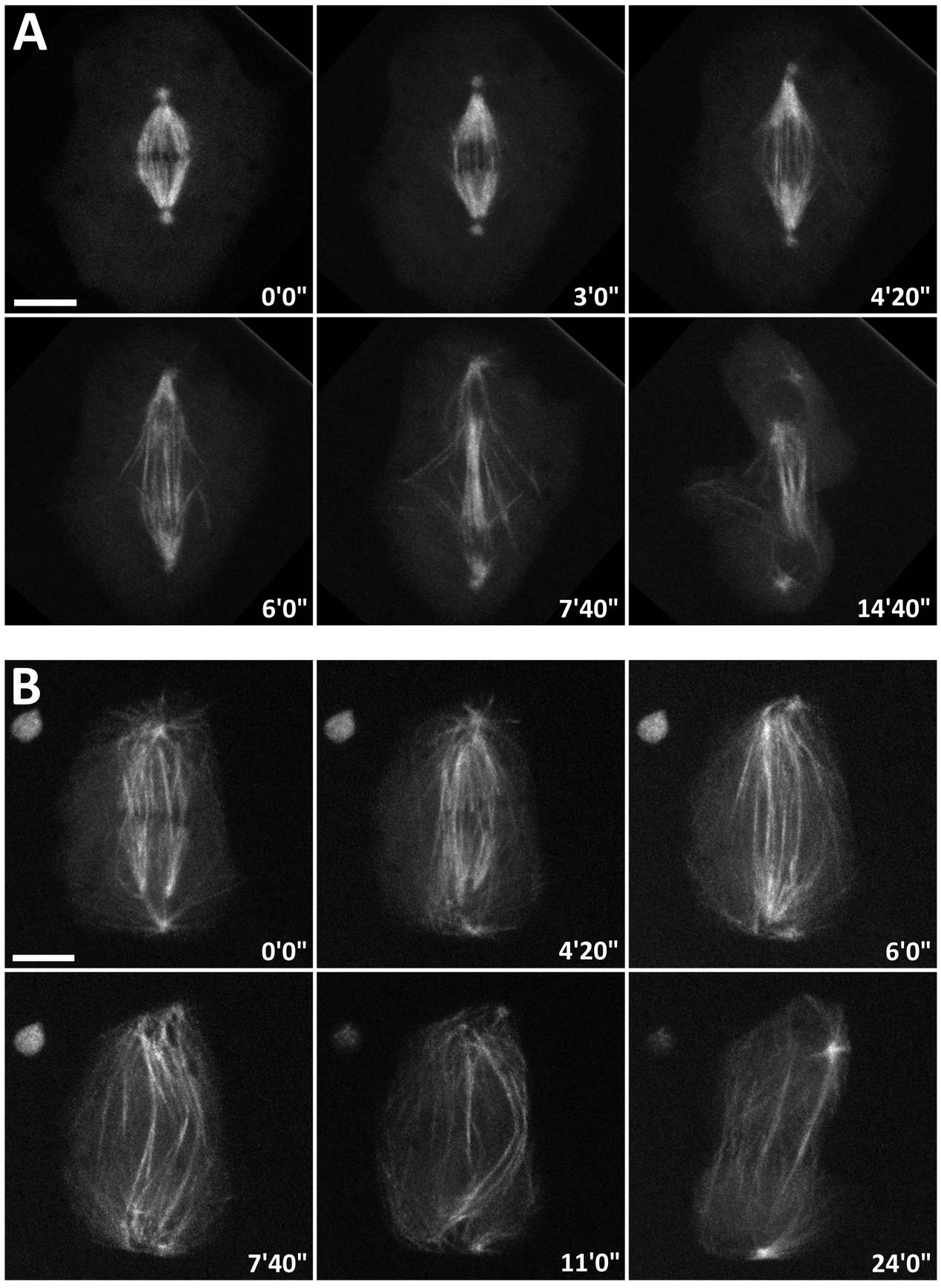


Figure 3-23. *msd1* knock-down causes anaphase defects in live S2 cells.
S2 cells stably expressing α-Tubulin-GFP were treated with dsRNA for 2d and plated on ConA-coated coverslips for 2h before imaging. Time-lapse spinning-disc confocal microscopy was used to take 10µm Z-stacks every 20". (A) Control-treated S2 cell shows the spindle elongating in anaphase A (3'0") before MT bundling drives central spindle formation (6'0") and cleavage furrow ingression telophase (14'40"). (B) Cell treated with *msd1* dsRNA. MT density is reduced (0'0") resulting in sparse interpolar MTs during anaphase (6'0"). MTs fail to bundle during central spindle formation and α-Tubulin-GFP intensity is reduced relative to controls (7'40"). Cleavage furrow ingression is delayed (24'0"). Scale bar = 5µm.

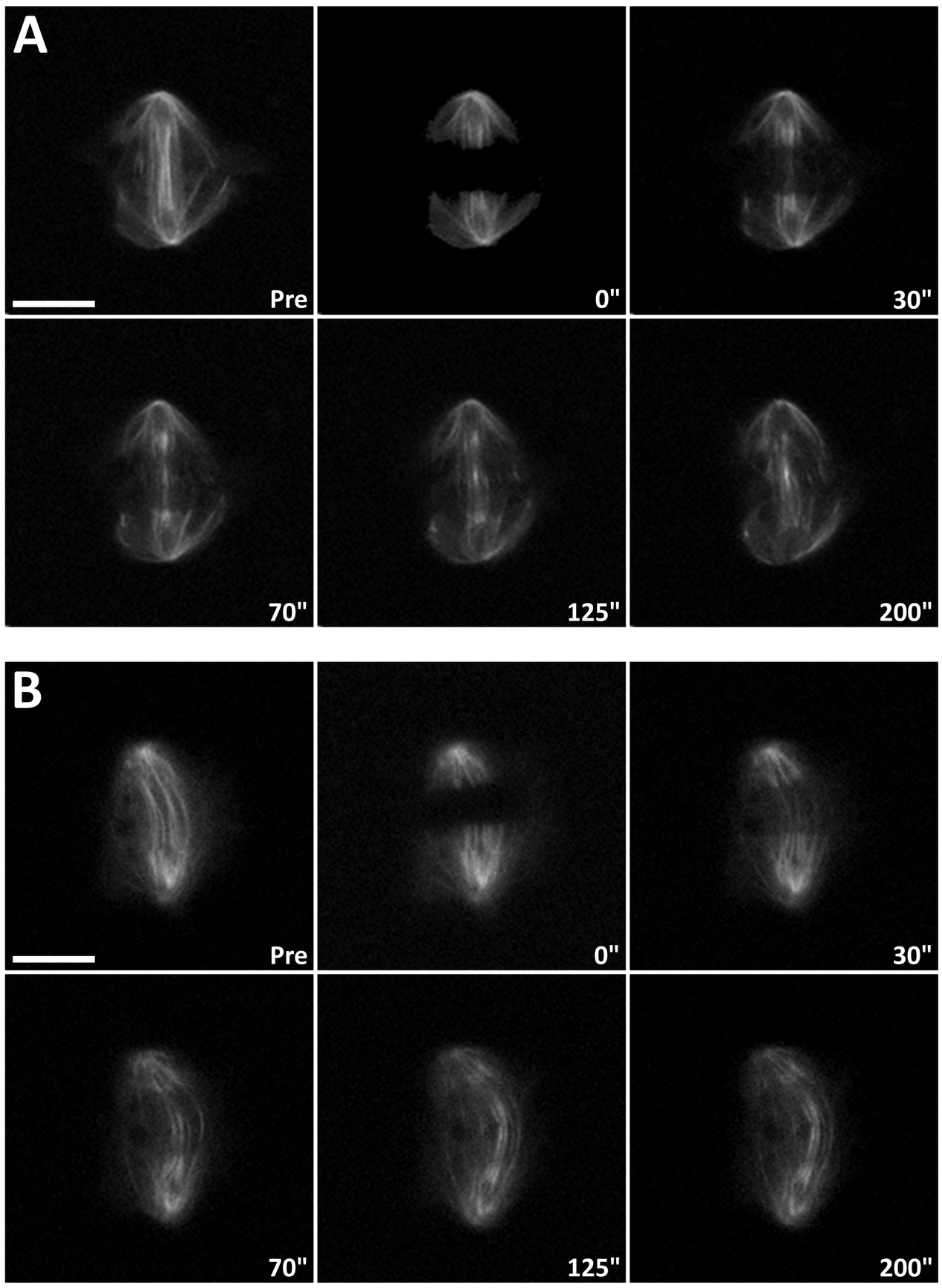


Figure 3-24. Fluorescence recovery is diminished as a result of of *msd1* knock-down in S2 cells.

S2 cells stably expressing α-Tubulin-GFP were treated for 2d with dsRNA and plated on ConA-coated coverslips for 2h before imaging. Cells were treated with with 2 FRAP pulses before being imaged with time-lapse in a single plane every 5". (A) Control-treated anaphase cell (Pre) was photobleached (0") in the prospective central spindle region and analysed for fluorescence recovery. Fluorescence recovery is evident within 30" and continues to increase until 200" where the central spindle is clearly visible. (B) Cells treated with *msd1* dsRNA show fluorescence recovery within 30" but intensity does not return to comparable levels within 200". Scale bar = 5µm.

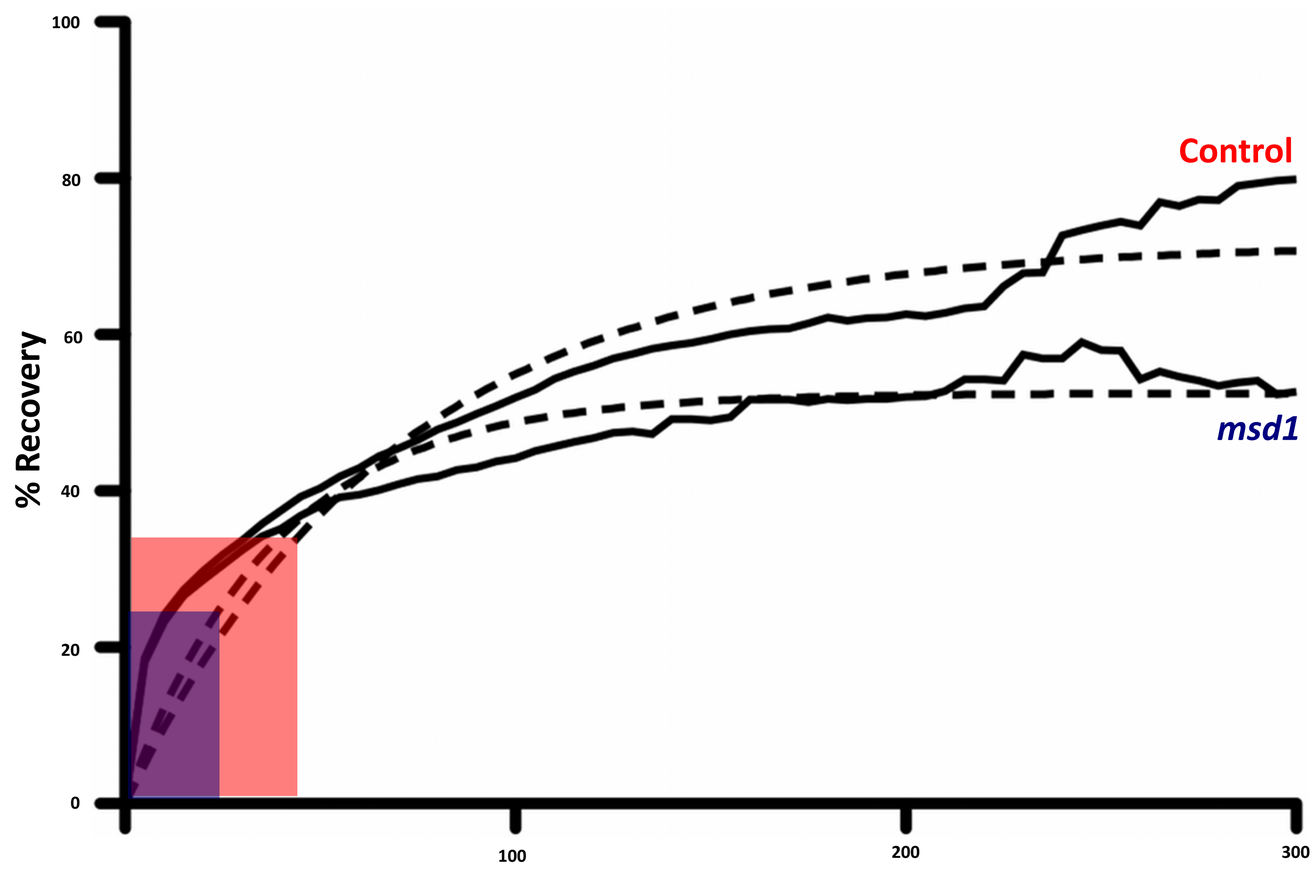


Figure 3-25. Fluorescence recovery of α-Tubulin-GFP is diminished at the central spindle in the absence of Msd1.

Average fluorescence intensity of α-Tubulin-GFP was measured at the central spindle over time following photobleaching. Post-bleach intensities were forced to zero and relative α-Tubulin-GFP intensities were plotted. Half-time of recovery is significantly reduced in *msd1* RNAi cells (26.24") relative to control treated cells (47.62", F=23,40, P<0.0001). The fluorescence plateau is significantly lower in *msd1* RNAi cells (52.52%) relative to control-treated cells (71.65%, F=129.0, P<0.0001).

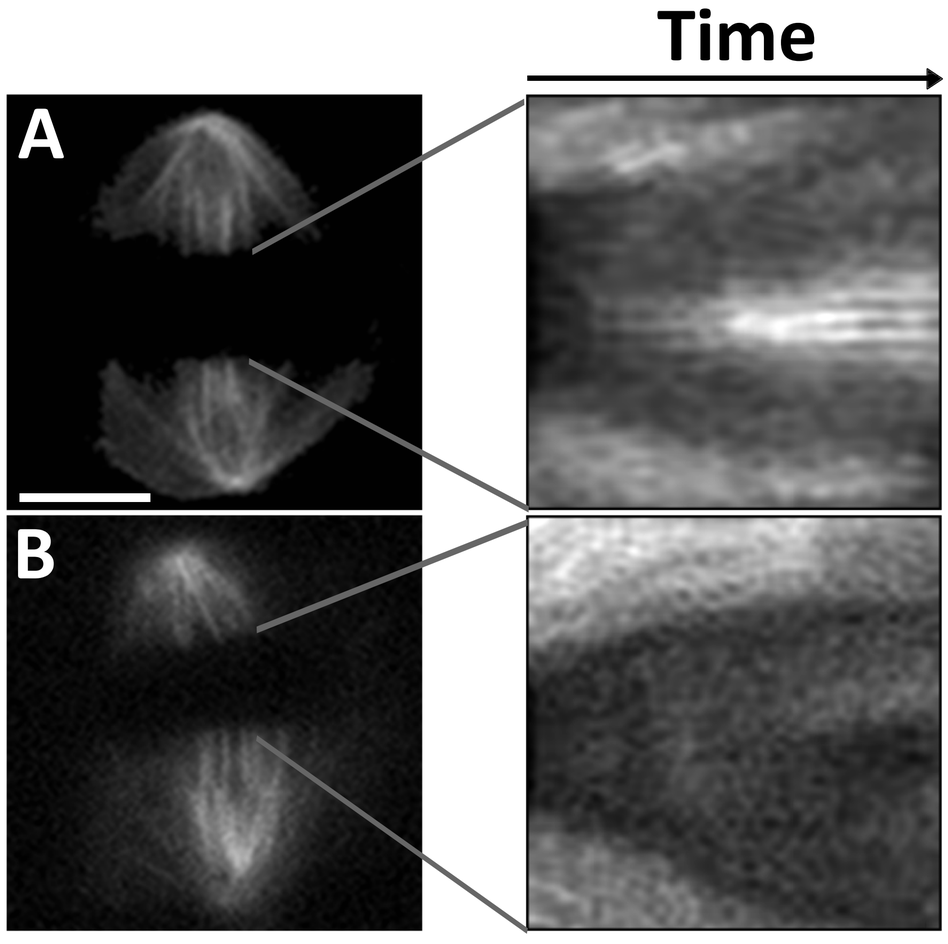


Figure 3-26. Kymographs show that Msd1 is required for a specific population of MTs within the central spindle.
Kymographs of α-Tubulin-GFP fluorescence intensity at the central spindle following photobleaching were generated. (A) In control-treated cells, fluorescence returned over time from a distinct region. Fluorescence appeared to return from a region in the centre of the central spindle, and grew towards the poles. (B) In *msd1* dsRNA treated cells, this central population of MTs appears to be absent. Scale Bar = 5µm.

3.3.5. Discussion

The observation that *msd1*^{ex51} embryos have defects in central spindle formation led to the possibility that MT-templated MT nucleation is required for the assembly of this structure during anaphase. Time-lapse microscopy of S2 cells lacking Msd1 clearly shows that MT generation and bundling is affected in these cells. Curiously, however, this contribution of new MTs is not necessary for cytokinesis in *Drosophila* S2 cells, as it is in humans (Uehara *et. al,* 2009, Lawo *et. al,* 2009). The possible reasons for this discrepancy are numerous. First, the role of HAUS in human cells might be mechanistically distinct from that in *Drosophila*. It is already clear that HAUS has a role in maintaining centrosome integrity (Lawo *et. al,* 2009) – an effect not observed in *Drosophila*. It is possible that while cytokinesis is viable in the absence of MT-templated MT nucleation, further disruption of centrosome function renders the cell incapable of cleavage. Thus, dissection of these major functions of HAUS is necessary. Second, different populations of MTs are dominant depending upon the cell type.

Cells transiently expressing EB1-GFP provide preliminary evidence of comets arising from within the mitotic spindle during central spindle assembly in anaphase. This effect has not been demonstrated previously, and it would be interesting to use tracking software to measure not only the origin, but also the direction and speed at which these novel comets move. Moreover, it would be interesting to investigate further the relationship between these comets and Msd1. In the absence of Msd1, both the number of comet origins, and the speed of their movement appeared

reduced. Partitioning the anaphase spindle into discrete sections to analyse these comets would help to elucidate whether Augmin dependent nucleation is localised during central spindle assembly.

While this work was in progress, a study has indeed shown a role for Augmin-generated MT nucleation during anaphase (Uehara *et. al,* 2010). MT regrowth during anaphase is severely diminished in the absence of HAUS subunits in human cells. This process is required for cytokinesis in these cells, and acts in concert with other MT-generating mechanisms such as HURP (Uehara *et. al,* 2010). From the results shown above, it is clear that Augmin has a similar role during anaphase. Augmin is not required for cytokinesis, in either *Drosophila* S2 cells or spermatocytes, however, further emphasising the discrepancy between the relative roles of redundant mechanisms in different cell types.

A new population of MTs at the central spindle would facilitate MT bundling by motors and central spindle assembly and stability. The lower half-life of fluorescence recovery observed in the absence of Msd1 might be explained by the lower plateau itself. Because total recovery is reduced, the level fluorescence recovery required to measure the half-life is comparably reduced.

Cytokinesis in S2 cells is clearly robust, and central spindle formation appears to rely upon numerous mechanisms. While cytokinesis can proceed in the absence of Msd1, it would be interesting to investigate other mechanisms that might cause 'synthetic lethality' of the central spindle when Augmin-generated MTs are not present. This

would elucidate the degree of mechanistic redundancy during central spindle assembly.

Furthermore, analysis in different cell types, most notably in *Drosophila* spermatocytes might provide insight here. Wac appears to be responsible for a distinct inner population of central spindle MTs in spermatocytes, despite being dispensable for cytokinesis. However, in a *wac;spd-2* double mutant, central spindle formation is severely perturbed (M. Giansanti, personal communication).

3.4. Characterisation of dTD-60

hTD-60 is a putative component of the CPC that is required for prometaphase-metaphase progression in human cells (Mollinari *et. al,* 2003). hTD-60 is an RCC1 family member – RCC1 itself is a Guanine Nucleotide Exchange Factor (GEF) for the small GTPase Ran (Bischoff *et. al,* 1991) that localises to the nucleus, binds to DNA and is required for chromosome condensation during mitosis (Ohtsubo *et. al,* 1989). *CG9135* was previously predicted to be the *Drosophila* homologue of hTD-60, but has remained uncharacterised. Prior to this project, a Rabbit polyclonal antibody to full-length *CG9135* (dTD-60 hereafter) was generated, and a preliminary RNAi characterisation was performed. The object of the following section is to first determine whether *dTD-60* is functionally homologous to *hTD-60*, and to gain insight into other functions of dTD-60 protein.

3.4.1. CG9135 Shows Homology to hTD-60

The *Drosophila* protein CG9135 shares 61% protein sequence similarity, 43% identity and is the protein with the highest homology to hTD-60, (Figure 3-27). CG9135 was identified via 4 peptides in a MT spin-down assay with a combined Mass Spectrometry score of 117 (Hughes *et. al,* 2008). Furthermore, CG9135 was previously postulated to be the *Drosophila* homologue of hTD-60 (Mollinari *et. al,* 2003).



Figure 3-27. CG9135 shows homology to human TD-60.
Amino acid sequences of *CG9135* and hTD-60 were aligned using a pairwise BLAST. *CG9135* shares 61% sequence similarity and 43% identity with hTD-60. BLAST score = 417.

3.4.2. dTD-60 Localisation Differs from hTD-60

hTD-60 was first identified by JH Antiserum to localise to inner centromeres from G2 until the metaphase-anaphase transition, where it is dynamically relocalised to the spindle mid-zone (Mollinari *et. al,* 2003). To investigate whether this localisation was conserved in *Drosophila,* S2 cells were fixed and stained for α-Tubulin and dTD-60 using a polyclonal α-dTD-60 antibody generated against full-length dTD-60 in Rabbit during an undergraduate project prior to this study. This antibody was affinity purified and its specificity tested by Western Blotting (Figure 3-30; T.Duncan 2007). The localisation observed was distinct from hTD-60 localisation in HeLa cells. In metaphase, α-dTD-60 antibody localised to chromatin, as opposed to specifically at the inner centromeres (Figure 3-28A). Subsequently, dTD-60 did not localise to the spindle mid-zone in anaphase, but associated with the mid-body during late telophase (Figure 3-28B).

3.4.3. GFP-dTD-60 Localises Dynamically in the Early Embryo

To further investigate the localisation of dTD-60 in *Drosophila,* flies possessing an N-terminal GFP-fusion protein under the control of the UASp promoter were generated and crossed to the mat-α-TubGAL4 driver for expression in the early embryo (Figure 3-29; Movie 7). GFP-dTD-60 was nuclear during interphase. Upon chromosome condensation, GFP-dTD-60 localised to chromatin, and weak fluorescence was also observed on the spindle and centrosomes during metaphase. In anaphase, GFP-dTD-60 localisation persisted on chromatin, and no clear fluorescence was observed at the spindle mid-zone at any point.

The localisation of GFP-dTD-60 to chromatin is consistent with that observed in S2 cells. Because syncytial nuclei exist in a shared cytoplasm, they do not undergo cytokinesis. Thus the late telophase localisation observed in S2 cells is unlikely to occur in embryos. While dTD-60 localisation is distinct from that in human cells, this does not discount a possible role for dTD-60 in mitosis, given the dynamic localisation of GFP-dTD-60 throughout the cell cycle.

The localisation of dTD-60 differs from hTD-60, and might reflect a divergent role between the two proteins in different organisms.

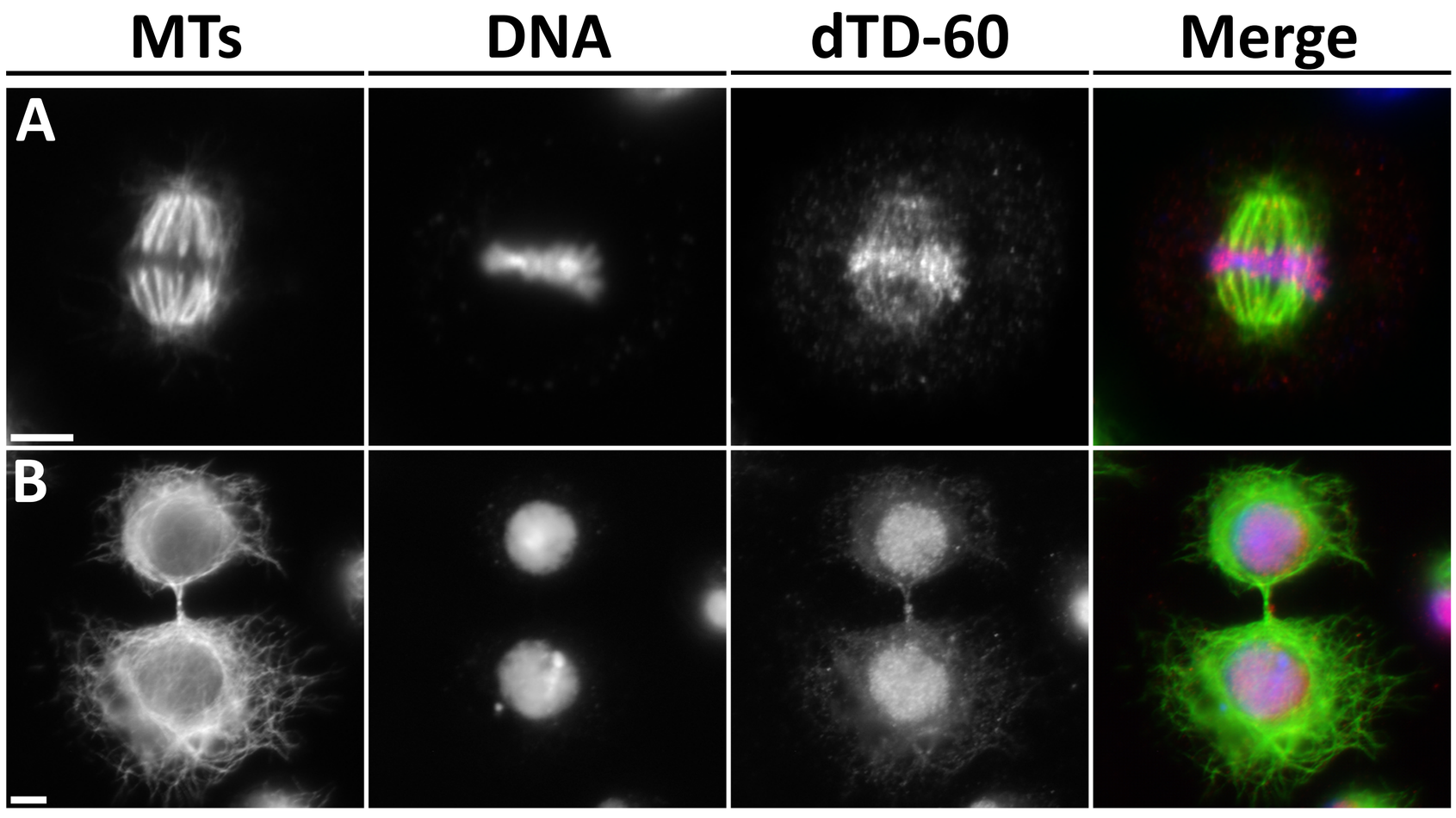


Figure 3-28. dTD-60 localises to chromatin and the spindle in metaphase, and the mid-body in late telophase.

S2 cells were fixed in methanol and stained for α-Tubulin (Green), DNA (Blue) and α-dTD-60 (Red). (A) Metaphase cell showing dTD-60 localising brightly to the chromatin and also faintly on the spindle. (B) In late telophase, dTD-60 localises to nuclei and faintly at the mid-body. Scale bars = 5µm.

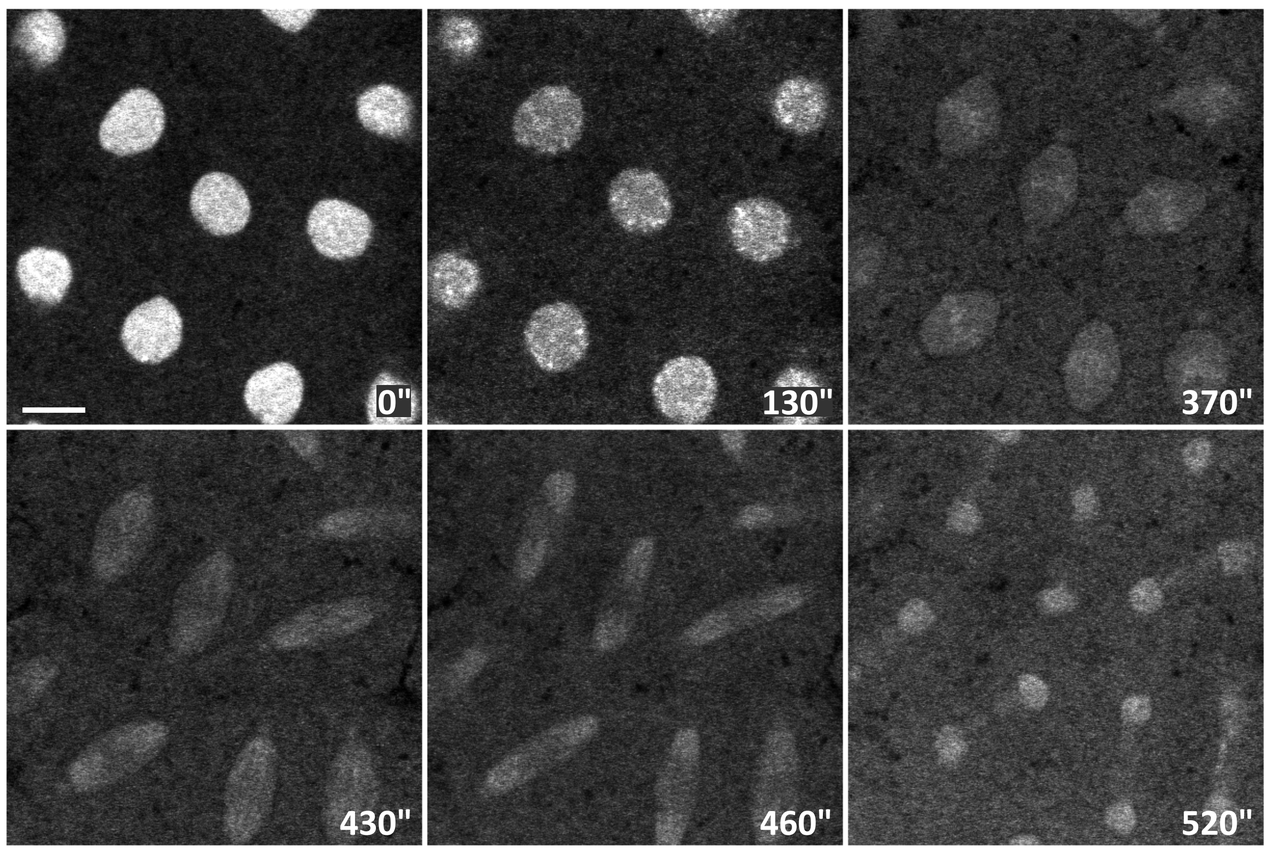


Figure 3-29. dTD-60-GFP localises dynamically in the early embryo.
1-2h embryos expressing dTD-60-GFP were dechorionated and mounted on coverslips with heptane glue. Time-lapse confocal microscopy was used to take 5µm Z stacks every 10". dTD-60-GFP is nuclear in interphase (0"). After NEB, dTD-60-GFP localises to chromatin (130") and is visible on both chromatin and the spindle at metaphase (370"). dTD-60-GFP remains on chromatin and faintly on MTs during anaphase (430,460"). During telophase, dTD-60-GFP is nuclear but does not clearly localise to the central spindle (520").

3.4.4. *dTD-60* RNAi Shows No Clear Phenotype

hTD-60 knock-down by siRNA in HeLa cells prevents prometaphase-metaphase progression, caused by disorganised spindles compared to controls (Mollinari *et. al,* 2003). To investigate the function of dTD-60 in *Drosophila,* S2 cells were treated with dsRNA specific to an exon within *dTD-60* (See Section 2.1). Levels of dTD-60 protein were almost undetectable after 5 days as determined by Western Blotting. Neither multiple treatments, nor a 7-day treatment period, discernibly decreased protein levels further, although the levels of dTD-60 may have been only marginally lower than is detectable by this antibody via Western Blot (Figure 3-30). Nonetheless, prometaphase arrest was not observed in *dTD-60* RNAi cells, since no difference in mitotic index was observed between control-treated, and *dTD-60* RNAi cells (Figure 3-31; 4.4% ±0.4SEM vs. 3.8% ±0.4SEM, $p<0.05$). α-dTD-60 staining was absent from spindles, but appeared to have no effect on bipolar spindle formation (Figure 3-32).

Thus, neither the localisation of dTD-60, nor the RNAi phenotype of *dTD-60* in *Drosophila* is consistent with observations in human cells.

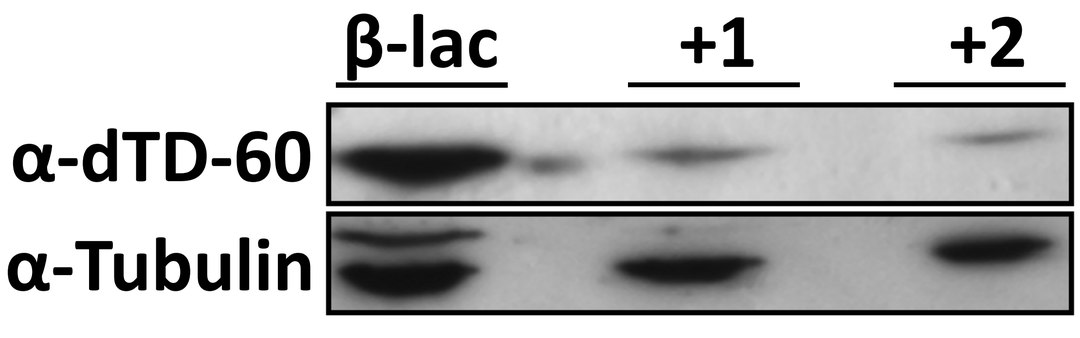


Figure 3-30. *dTD-60* RNAi reduces dTD-60 protein levels.
Western blotting was used to determine protein levels in S2 cells treated with dsRNA. Following 5d treatment with *dTD-60* dsRNA, dTD-60 protein levels were greatly reduced relative to controls (α-dTD-60). No difference in the extent of knock-down was observed between 1 and 2 additions (+1, +2). α-Tubulin levels remained constant in all treatments (α-Tubulin).

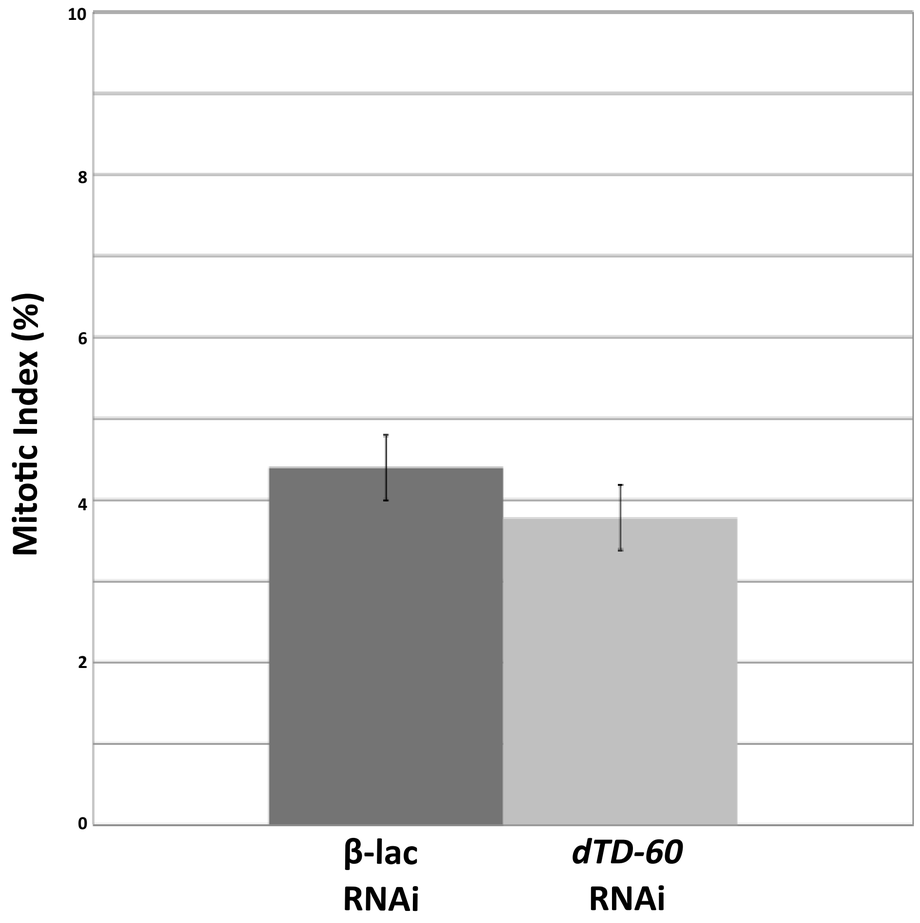


Figure 3-31. *dTD-60* RNAi has no effect on mitotic index. Mitotic index was score as the percentage of cells in mitosis. No significant difference in mitotic index was found between *β-lac* (4.4%±0.4 SEM) and dTD-60 dsRNA treatments (3.8%±0.4 SEM). t-test P>0.05.

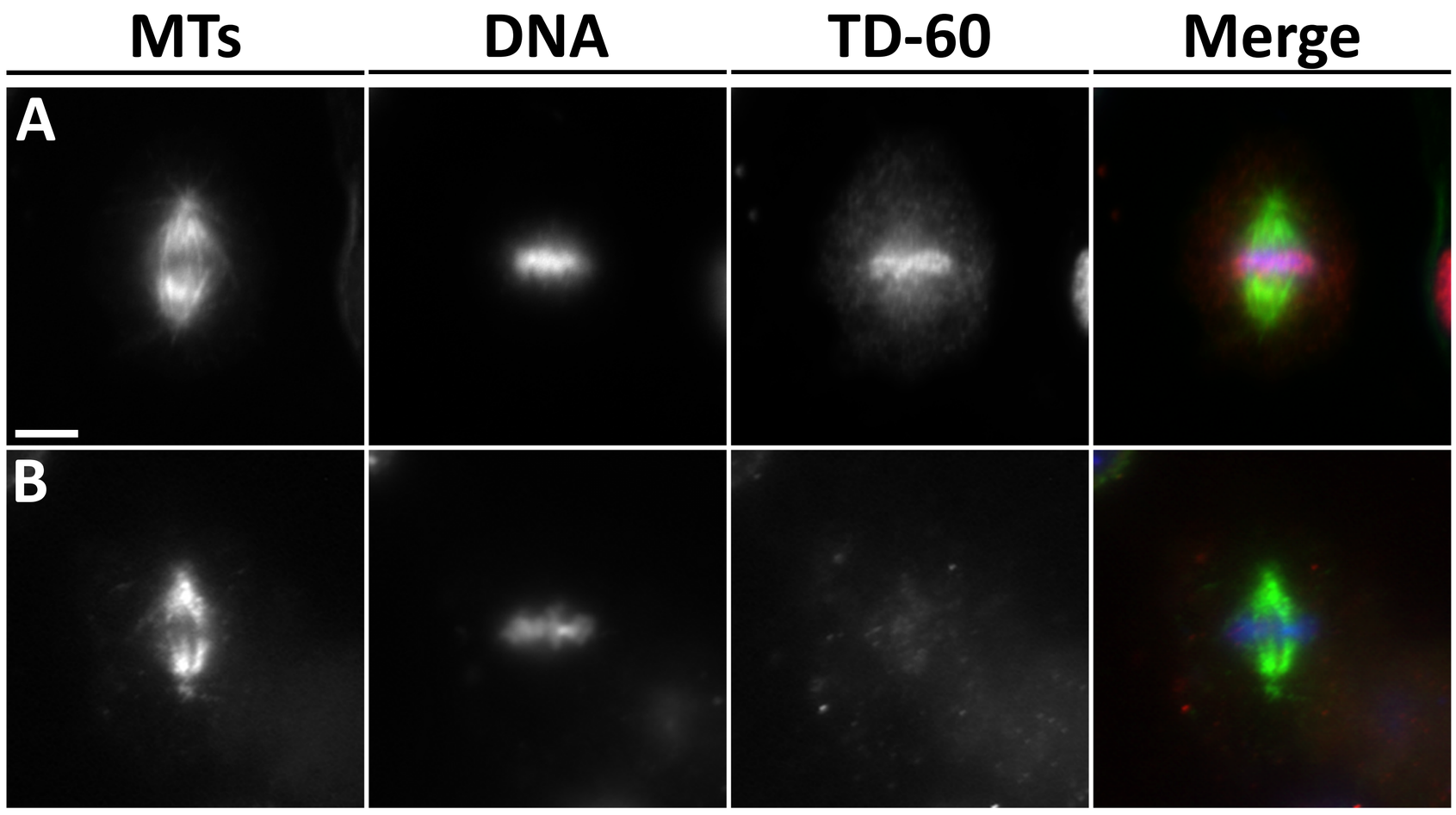


Figure 3-32. *dTD-60* RNAi shows no clear phenotype.
S2 cells were treated for 5d with dsRNA, fixed in methanol and stained for DNA (Blue), α-Tubulin (Green) and dTD-60 (Red). (A) Metaphase cell treated with *β-lac* dsRNA showing a robust bipolar spindle, with chromosomes aligned. dTD-60 localised clearly to the chromatin and faintly to the spindle. (B) Metaphase cell treated with *dTD-60* dsRNA shows no morphological spindle defects in the absence of dTD-60 localisation. Scale bar = 5µm.

3.4.5. *dTD-60* RNAi Does Not Disrupt INCENP Localisation

hTD-60 is required for the recruitment of the CPC to the inner centromere during prophase in HeLa cells (Mollinari *et. al,* 2003). To investigate this interaction in *Drosophila,* S2 cells treated with *dTD-60* dsRNA were fixed and stained for α-Tubulin and the chromosomal passenger protein INCENP (Figure 3-33). In both control-treated (Figure 3-33A), and *dTD-60* knock-down cells (Figure 3-33B), INCENP consistently localised to the inner centromere during prophase-metaphase. This is perhaps unsurprising, given that dTD-60 does not localise specifically to the inner centromere in S2 cells.

hTD-60 is required for the recruitment of the CPC to the central spindle during late anaphase/telophase in HeLa cells (Mollinari *et. al,* 2003). To further investigate the role of dTD-60 in this process, S2 cells were treated for 5 days with *dTD-60* dsRNA, fixed in methanol and stained for α-Tubulin and INCENP (Figure 3-34). INCENP localisation was unperturbed during anaphase in both control-treated (Figure 3-34A) and *dTD-60* RNAi cells (Figure 3-34B), localising distinctly to the central spindle. Thus, dTD-60 is not required for the localisation of the CPC during anaphase – an observation that is distinct from HeLa cells.

3.4.6. Double Knock-Down of *dTD-60* and its Orthologue, *bj1,* Shows No Clear Phenotype

The closest orthologue of dTD-60 is *rcc1*/*bj1*, a Guanine-Nucleotide exchange factor (GEF) for the GTPase Ran (BLAST Score 51.6). RCC1/BJ1 localises to chromatin during mitosis in *Drosophila*, although the null mutant phenotype shows no gross cell cycle defects (Shi *et. al,* 2004). To investigate a possible functional redundancy between dTD-60 and BJ1, a double knock-down experiment was performed. S2 cells were treated for 5 days with dsRNA, fixed in methanol and stained for α-Tubulin and DNA (Figure 3-35). Single knock-down of *bj1* showed no mitotic defects relative to control-treated cells (Figure 3-35A). Furthermore, cells treated with both *dTD-60* and *bj1* dsRNA exhibited no morphological defects (Figure 3-35B). These results suggest that the two orthologous proteins, dTD-60 and BJ1, do not have redundant functions during mitosis, since no additive effect on spindle morphology was found upon knock-down of both genes simultaneously. However, since knock-down was not measured with antibody staining, the extent of knock-down of each protein in a given cell was unable to be determined.

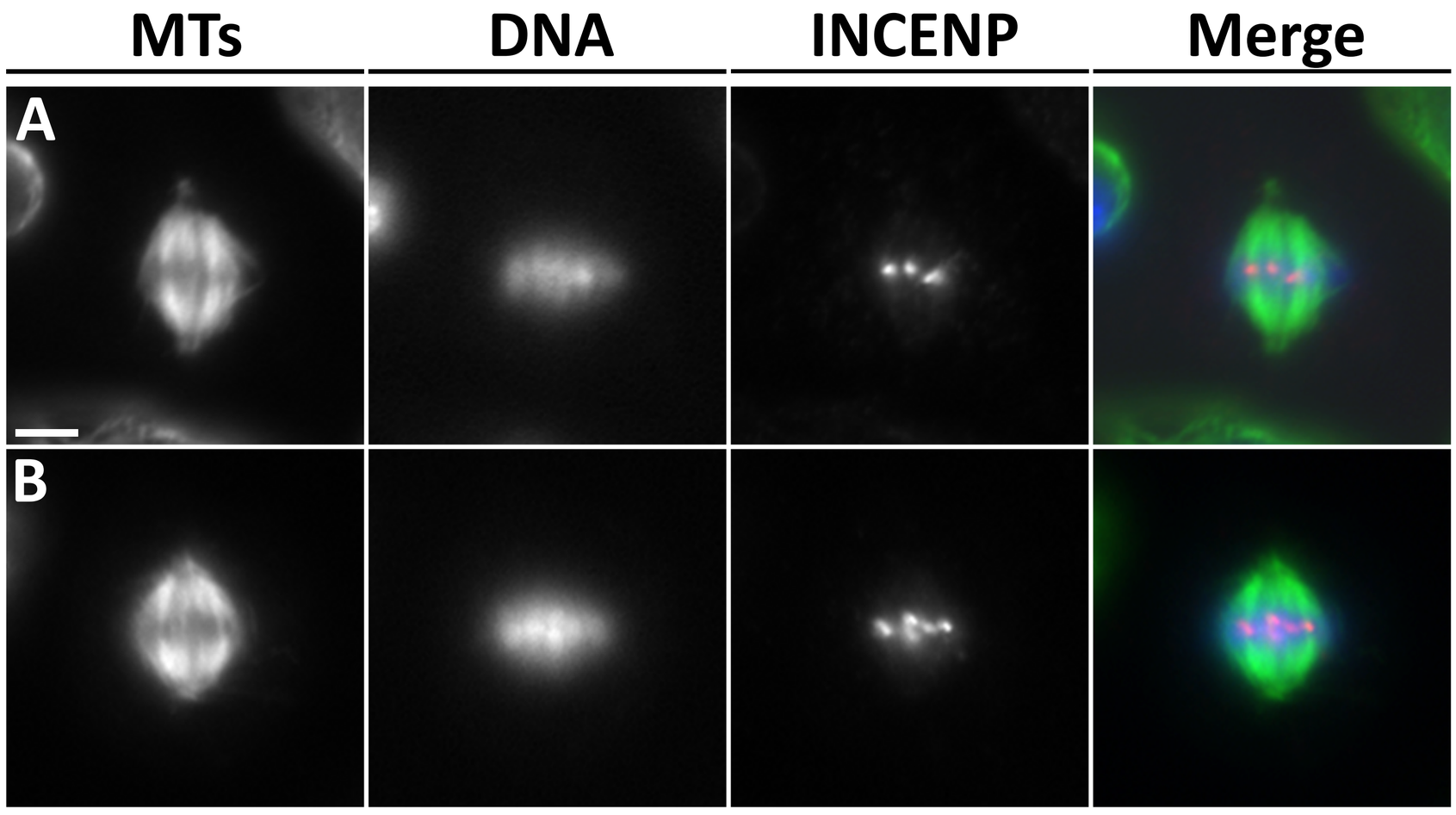


Figure 3-33. *dTD-60* RNAi does not disrupt INCENP localisation in metaphase.
S2 cells were treated for 5d with dsRNA, fixed in methanol and stained for α-Tubulin, DNA and α-INCENP. (A) Control-treated metaphase cell shows a punctate localisation of INCENP to kinetochores. (B) Metaphase cell treated with *dTD-60* dsRNA shows no disruption of INCENP localisation to kinethochores. Scale bar = 5µm.

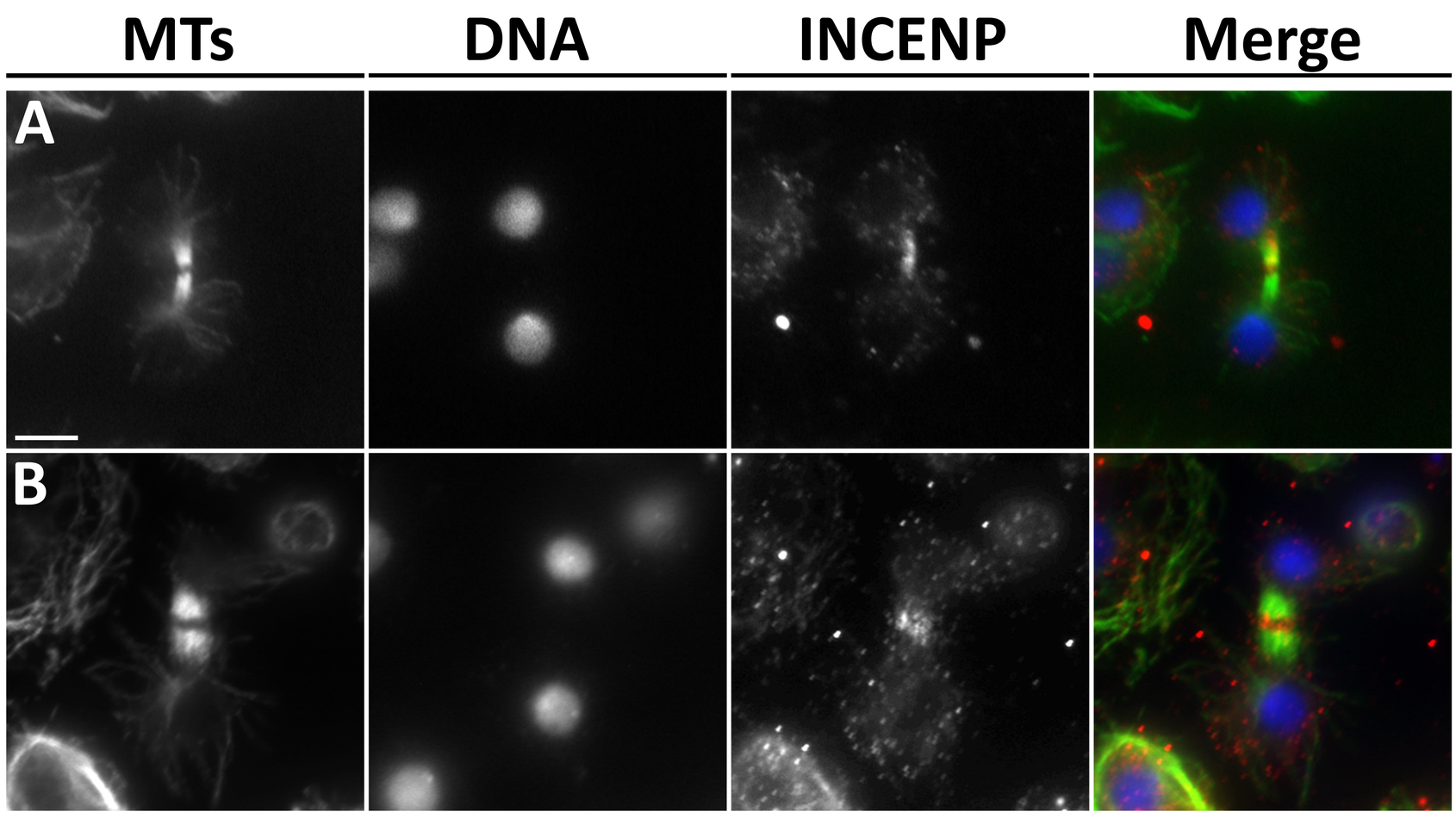


Figure 3-34. *dTD-60* RNAi does not disrupt INCENP localisation in telophase.
S2 cells were treated for 5d, fixed in methanol and stained for α-Tubulin (Green), DNA (Blue) and INCENP (Red). (A) Telophase cell treated with *β-lac* dsRNA shows INCENP localising to MTs at the mid-body. (B) Telophase cell treated with *dTD-60* dsRNA does not show a cytokinesis phenotype, and INCENP localisation to the mid-body is indistinguishable from control cells in all cells observed. Scale bar = 5µm.

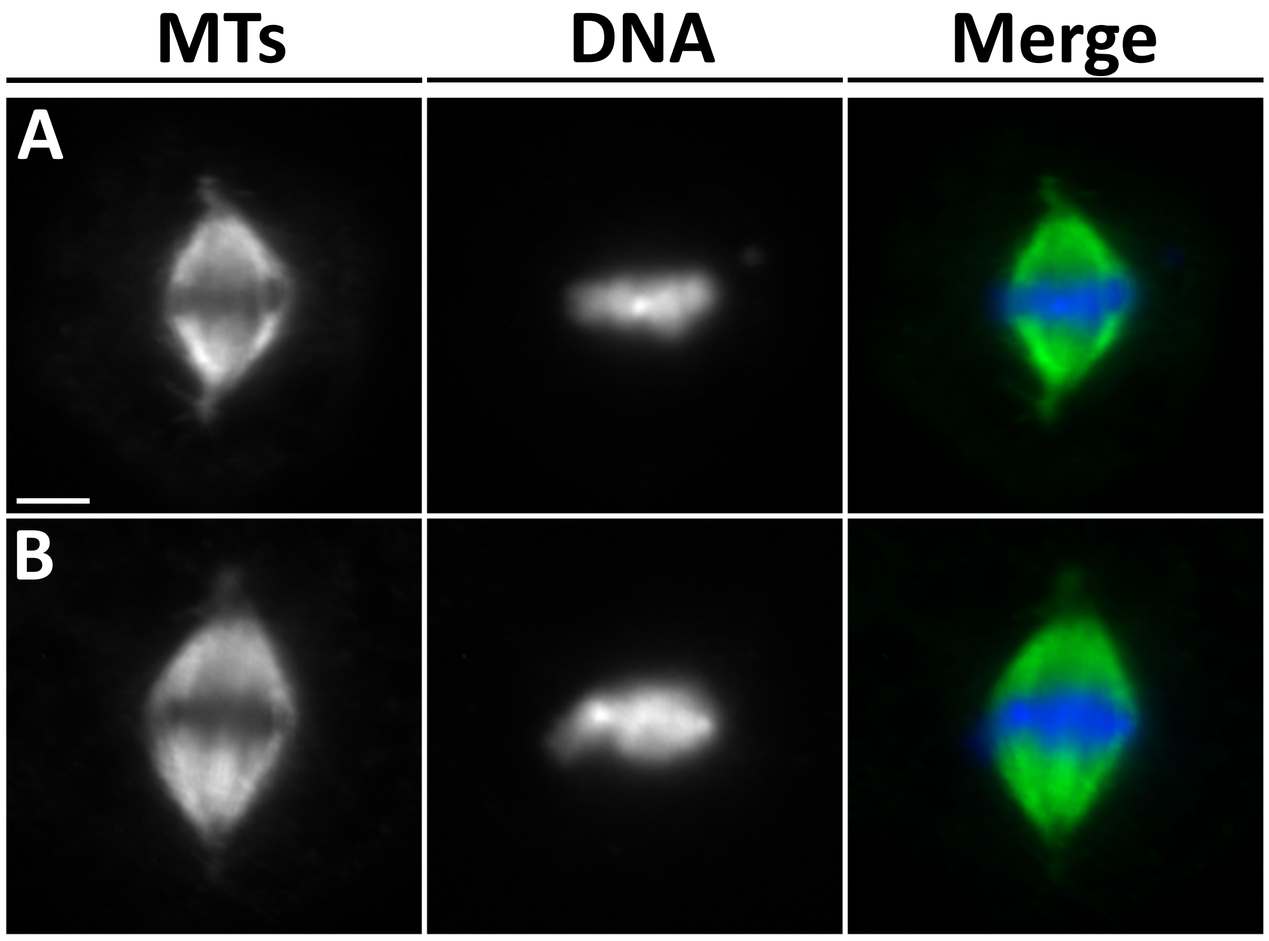


Figure 3-35. Double knock-down of *dTD-60* and *bj1* has no clear phenotype.
S2 cells were treated for 5d with dsRNA, fixed in methanol, and stained for α-Tubulin (Green) and DNA (Blue). (A) Control metaphase cell treated with *β-lac* dsRNA shows a robust bipolar spindle. (B) Metaphase cell treated with *dTD-60* and *bj1* dsRNA has no observable spindle defects compared with controls. Scale bar = 5µm.

3.4.7. Large Scale Co-Immunoprecipitation Shows dTD-60 Interactors via Mass-Spectrometry

GFP-dTD-60 was immunoprecipitated on a large scale to identify interactors. Proteins of interest were selected from the initial dataset by subtracting common false positives that were identified in previous immunoprecipitation experiments with GFP-fusion proteins in the Wakefield lab. While no members of the CPC were identified, 2 distinct peptides from short spindles 4 (Ssp4) were present in the pellet in multiple runs, and 4 unknown genes were also identified. Further investigation of these novel interactors will identify whether they are involved in combination with dTD-60 in spindle formation (Table 7).

Peptide	Symbol	Comments	No. Peptides	MS Score
α-Tubulin	α-Tub	Constituent of MTs	3	67.27
β-Tubulin	β-Tub	Constituent of MTs	10	136.53
Short Spindle 4	Ssp4	RNAi causes short spindle	3	15.68
CG6084	CG6084	Uncharacterised Gene	2	102.50
CG8036	CG8036	Uncharacterised Gene	2	17.60
CG1943	CG1943	Uncharacterised Gene	1	16.27
CG5791	CG5791	Uncharacterised Gene	1	17.34

Table 7. GFP-dTD-60 Interactors.

3.4.8. Preliminary RNAi screen of dTD-60 interactors

To further investigate the role of dTD-60 interactors identified by mass-spectrometry, RNAi was performed on each individual gene to investigate its function (Figure 3-36). Preliminary characterisations showed no effect on spindle bipolarity in any treatment. However, a short-spindle phenotype, as measured by inter-centrosomal distance (ImageJ), was observed in *ssp4* and *CG5791* knock-downs (Figure 3-37). Spindles were not significantly shorter in either *CG6084* or *CG1943*

knock-downs. Clearly, repetition of these experiments is necessary to fully elucidate the role of dTD-60 interactors in maintenance of spindle length. However, the short-spindle phenotype of *ssp4* knock-down is consistent with published observations (Goshima *et. al,* 2008).

Loss of function of these genes indicates an intriguing possibility that dTD-60 is involved in spindle length maintenance. A logical next step, therefore, would be to investigate whether a double knock-down of *dTD-60* and these genes displays an additive effect on spindle organisation.

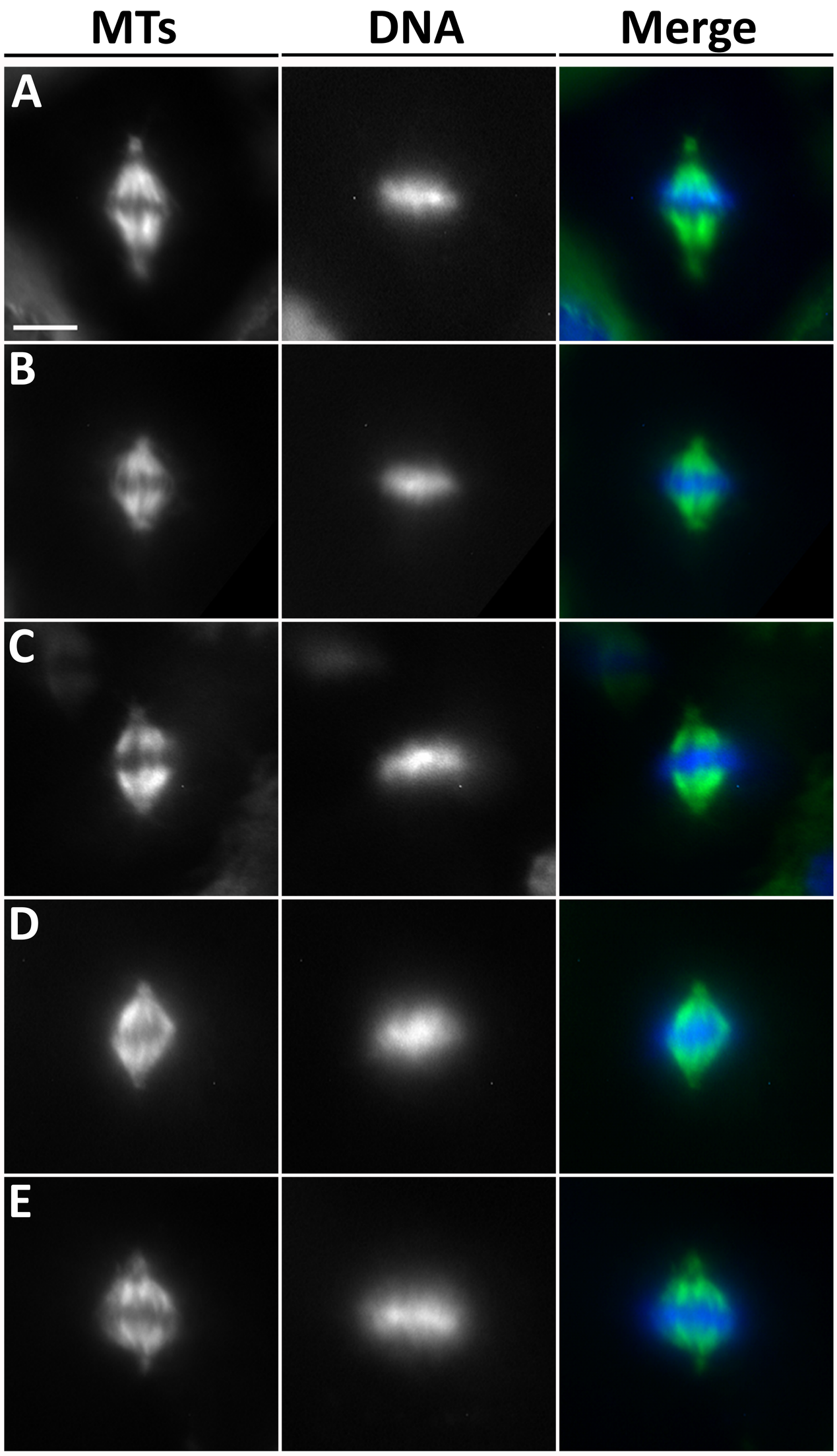


Figure 3-36. RNAi analysis of dTD-60 interactors.
S2 cells were treated for 5 days with dsRNA specific to genes identified as dTD-60 interactors by mass spectrometry. Cells were fixed in methanol and stained for α-Tubulin (Green) and DNA (Blue). (A) *β-lac* (B) *ssp4* (C) CG*6084* (D) CG*5791* (E) CG*1943*. No treatment disrupted spindle bipolarity, but cells treated with *ssp4* and CG*5791* dsRNA exhibited significantly shorter spindles than control-treated cells (see figure 3-37). Scale bar = 5µm.

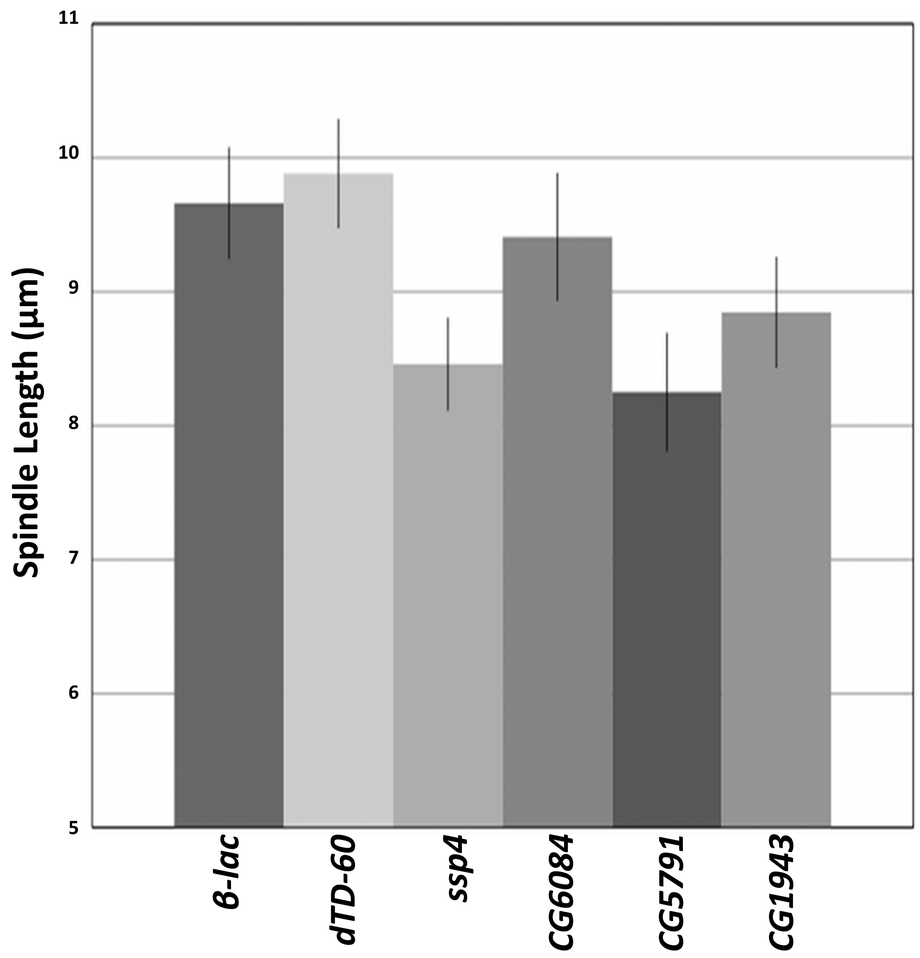


Figure 3-37. dTD-60 Interactors have a role in spindle length regulation.

Average pole-to-pole metaphase spindle lengths were measured following dsRNA treatment with dTD-60 interacting proteins identified via mass spectrometry. Cells treated with *dTD-60, CG6084* and *CG1943* dsRNA showed no significant difference in spindle length compared to control-treated cells (*β-lac* = 9.66µm ±0.41SEM, dTD-60 = 9.88µm±0.41SEM, CG*6084* = 8.46µm±0.47SEM, CG*1943* = 8.85µm±0.42SEM. $p>0.05$ in all). Cells treated with *ssp4* and CG*5791* dsRNA were significantly shorter than control-treated cells (*ssp4* = 8.46µm±0.35SEM, CG*5791* = 8.25µm±0.44SEM. $p<0.02$ in both).

3.4.9. Mutant Generation Using FRT-Directed Recombination

However, the direct effect of these proteins on the levels and localisation of dTD-60 is yet to be seen. A null mutation at the *CG9135* locus would provide an essential tool to elucidate the function of dTD-60. In an attempt to generate a mutant at this locus, two P-elements compatible with FRT-directed P-element recombination (Figure 3-38) were recombined as described in Figure 2-5 (Parks *et. al,* 2004). Flies that were trans-heterozygous for the two elements were crossed into a flipase background under the heat shock promoter. 3rd instar larvae were then heat shocked for 1 hour/day for 5 days. 20 lethal, white-eyed lines were generated and this phenotype was tested using deficiency complementation using *w^{1118};*Df(2L)ED353 (Table 8). The lethal phenotype did not complement with the deficiency, and therefore lethality in all 20 lines is not associated with an aberration at this genomic locus. Furthermore, none of the aberrations exhibited either female or male sterility when trans-heterozygous with the deficiency.

Clearly, molecular studies at the *CG9135* locus would elucidate the nature of these deletions. However, this study was undertaken early in the project and the deletion lines were lost prior to molecular characterisation. Subsequently, the w^{1118};PBac{CG9135^{f03307}} FRT element is no longer available at the Bloomington stock center, and repetition of the experiment is thus impossible.

Line	Lethal?	Lethal/Df?	Female Sterile/DF?	Male Sterile/Df?
1	Yes	No	No	No
2	Yes	No	No	No
3	Yes	No	No	No
4	Yes	No	No	No
5	Yes	No	No	No
6	Yes	No	No	No
7	Yes	No	No	No
8	Yes	No	No	No
9	Yes	No	No	No
10	Yes	No	No	No
11	Yes	No	No	No
12	Yes	No	No	No
13	Yes	No	No	No
14	Yes	No	No	No
15	Yes	No	No	No
16	Yes	No	No	No
17	Yes	No	No	No
18	Yes	No	No	No
19	Yes	No	No	No
20	Yes	No	No	No

Table 7. FRT Recombination Lines

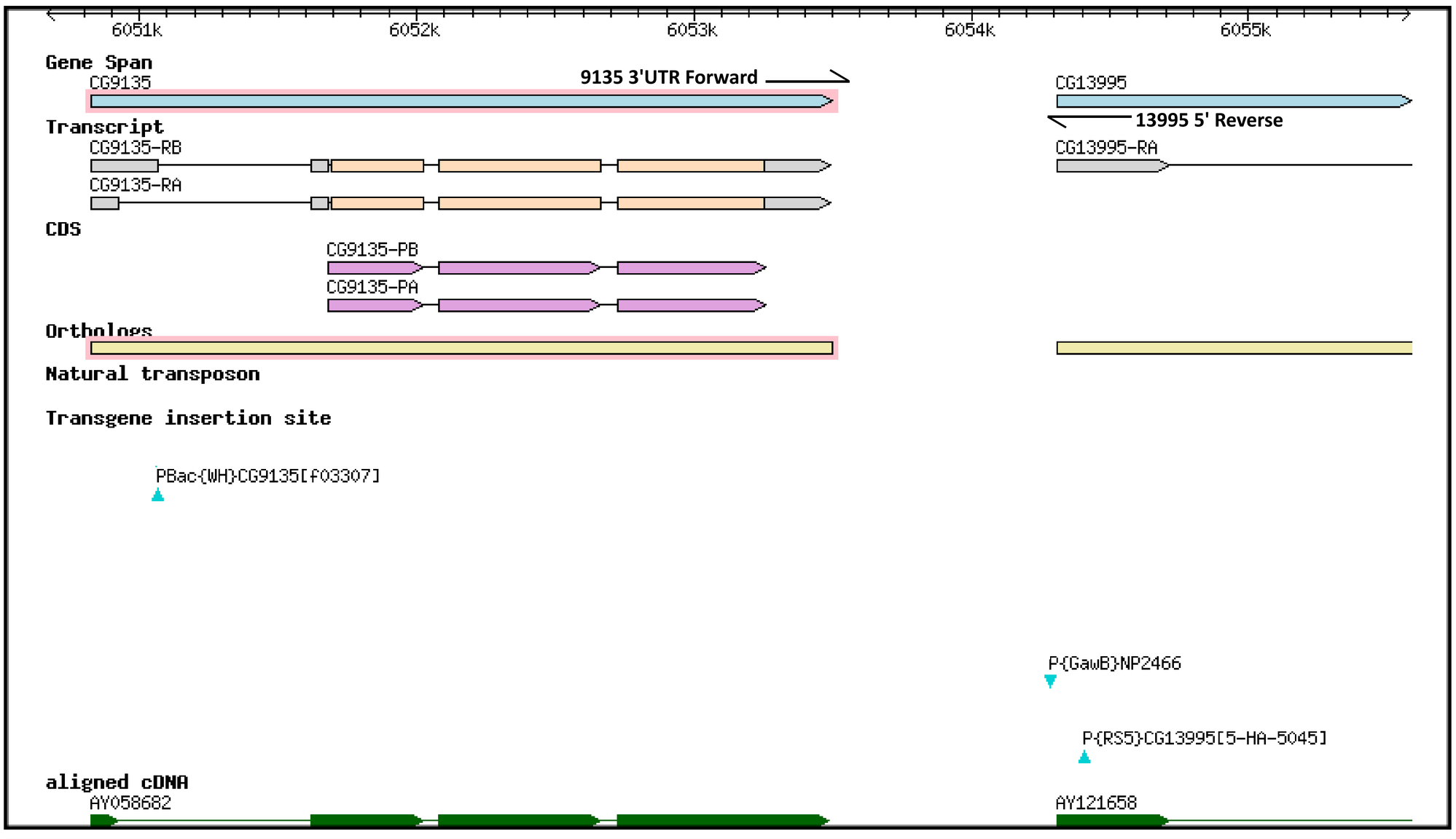


Figure 3-38. Genetic elements utilised at the *CG9135* genomic locus.

The presence of genetic elements available in the *CG9135* genomic locus (chromosome 2L) was investigated using Flybase. PBac {CG9135^{f03307}} and P{RS5}CG13995$^{5\text{-HA-}5045}$ were utilised for FRT-based recombination, and P-{GawB}-NP2466 was excised using imprecise excision. Primers spanning the insertion locus for element P-{GawB}-NP2466 for use in molecular analysis are depicted.

3.4.10. Imprecise Excision of P-element P{GawB}NP2466

The P-element w; P{GawB}NP2466 / CyO is inserted at the genomic locus 26B3 downstream of *CG9135* (Figure 3-38; Kyoto DGRC). Imprecise excision of this element was used to generate chromosomal aberrations in this region using the cross that is depicted in Figure 2-6. Male flies trans-heterozygous for the P-element and a Δ2-3 transposase generated 70 individual white-eyed males from which stocks were made. Individual males were isolated, and their gDNA extracted. No deletions were apparent from initial characterisation of this genomic locus using primers (9135_3'UTR Forward; 13995_5'UTR Reverse; Figure 3-38; Table 2) that span the P-element region. However, stocks were made of all lines, and will be further characterised in the Wakefield lab following this project.

3.4.11. Discussion

The role of dTD-60 during mitosis remains unclear. Characterisation of dTD-60 in S2 cells and embryos strongly refutes that dTD-60 has an identical role in *Drosophila* to that in human cells. While it is clear that dTD-60 is homologous to its human counterpart, its localisation is distinct from that of the CPC and also of hTD-60. In S2 cells, dTD-60 localised to the chromatin, rather than specifically to the inner centromere, at metaphase, and to the mid-body in late telophase, as opposed to the central spindle as it formed during anaphase. Similarly, GFP-dTD-60 localised to chromatin from prophase to metaphase in embryos. Little fluorescence was observed during telophase in these nuclei, however.

The absence of a detectable phenotype in dTD-60 knock-down cells despite a clear reduction in dTD-60 protein, as determined by Western Blotting, again suggests that dTD-60 is not required for prometaphase-metaphase progression as in humans (Mollinari *et. al,* 2003). Furthermore, because CPC localisation is unperturbed in these cells, dTD-60 is not required to localise CPC members dynamically throughout mitosis. This is perhaps unsurprising given that no CPC subunits were detected as dTD-60 interactors by co-immunoprecipitation. Furthermore, *dTD-60* has not been identified in genome-wide RNAi screens for genes required during mitotic spindle assembly (Goshima *et. al,* 2008; Hughes *et. al,* 2008).

Redundancy of function between homologues does not explain the dTD-60 phenotype. RCC1, the GEF required to generate high Ran.GTP concentration at the chromatin, localises to this region in a similar way to dTD-60 during metaphase. Despite this similarity, double knock-down experiments showed no effect on spindle morphology.

Finally, four proteins were identified as dTD-60 interactors via co-immunoprecipitation. Upon preliminary investigation using RNAi, two of these exhibited a short-spindle phenotype. First, the *ssp4* phenotype is unsurprising, since it is consistent with previous findings (Goshima *et. al,* 2008). However, the role of *CG5791* in spindle-length maintenance is uncharacterised. Further characterisation of these genes to investigate their localisation, and the dependence of this localisation on dTD-60 activity would be crucial to understanding this interaction.

4. Discussion

4.1. Msd1 – A novel MAP required for MT-templated MT nucleation

The experiments in this thesis initially involved a full characterisation of the function of a novel MAP, Msd1, originally identified in a proteomic screen (Hughes *et. al,* 2008). As a result of this thesis, Msd1 is now established as a component of the conserved Augmin complex, required for mitotic spindle-templated MT nucleation (Goshima *et. al,* 2008, Wainman *et. al,* 2009). In combination with the work described here, the role of Msd1, and the Augmin complex as a whole, has been demonstrated to be redundant with the centrosomal contribution of MTs (Figure 4-1; Section 3.1; 3.2). The possibility of other unidentified mechanisms for spindle assembly is fascinating, and underlines the necessity for a cell to possess mechanistic redundancy in this vital process.

A deeper insight into the MT nucleating capacity of Augmin would be very valuable. *In vitro* studies with a reconstituted Augmin complex would demonstrate first whether Augmin alone has MT nucleating capability, as is observed with numerous protein complexes involved in mitotic spindle formation. Furthermore, the dependence of Augmin-directed MT nucleation on both γ-Tubulin and γ-TuRC would become clear. Other *in vitro* experiments that visualise new MT formation at high resolution would demonstrate whether Augmin acts with any periodicity or directionality upon a MT template.

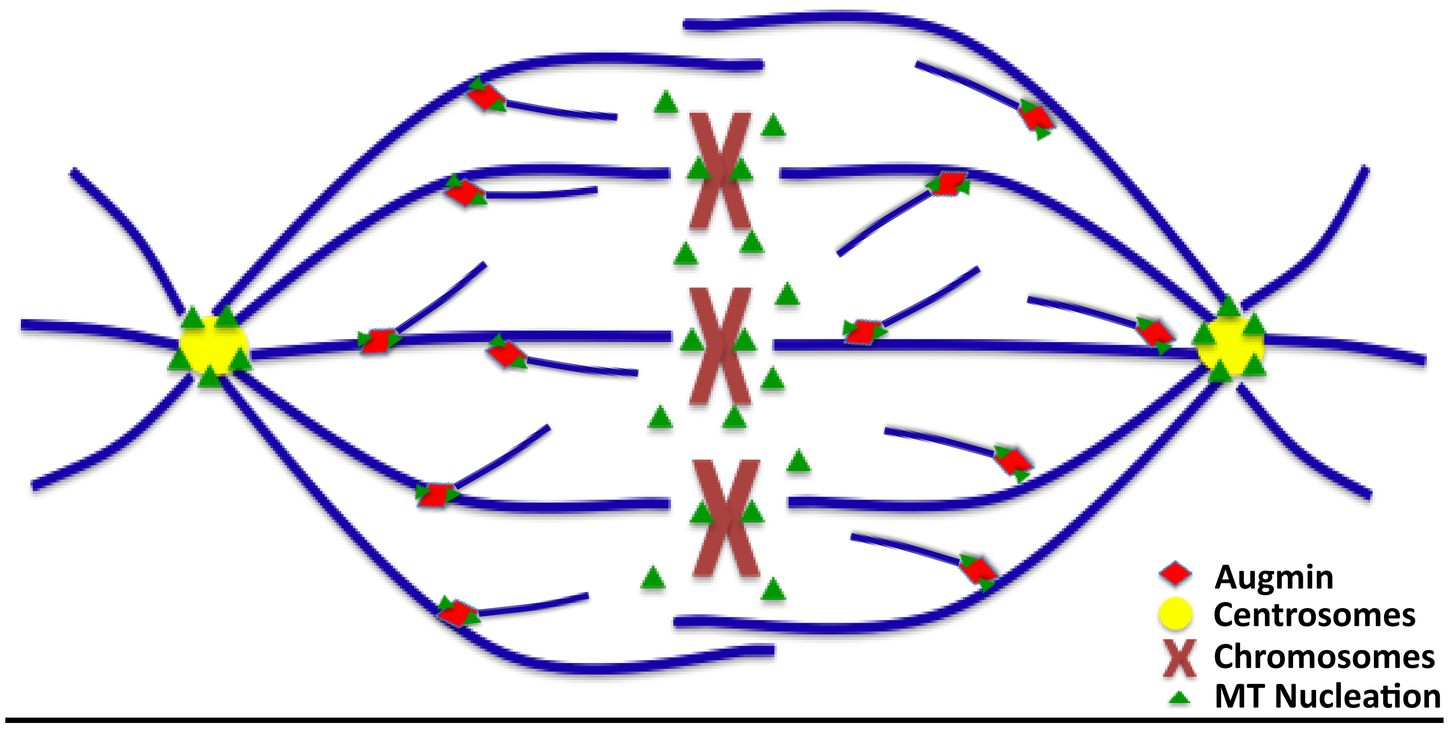


Figure 4-1. Redundancy of MT nucleation pathways in the mitotic spindle.
Numerous pathways work redundantly to support bipolar spindle assembly. MTs are not only nucleated from the centrosomes (Yellow) and from near the chromatin (Maroon), but the novel protein complex Augmin (Red) binds to existing MTs and acts to localise γ-TuRC here to initiate new MT formation (Green).

Aside from the requirement of a Polo phosphorylation on FAM29A/HAUS6 to localise NEDD1 to the spindle in human cells (Zhu *et. al,* 2009), the extent of cell cycle regulation of the Augmin complex is not clear. Comparative Mass Spectrometry studies to identify post-translational modifications upon Augmin subunits in both mitosis and interphase would reveal candidate amino acid sequences that are required for Augmin modulation. The presence of an 'activating' phosphorylation, for example, that serves to localise Augmin to spindle MTs would provide a Spatio-temporal dimension to Augmin activity that might vary between cell types, and could be utilised to demonstrate the relative importance of different MT generating mechanisms to different cell types.

In addition to initial characterisation of *msd1*, this thesis has provided insight into the importance of Msd1 during animal development. The $msd1^{ex51}$ allele demonstrated that in the absence of Augmin function, embryogenesis cannot proceed in *Drosophila.* The hypomorphic nature of the $msd1^{ex51}$ allele provided a useful tool for live analyses otherwise impossible to carry out. With Augmin activity compromised, embryogenesis was severely delayed, and nuclei showed a high degree of aneuploidy.

Further work in *Drosophila* is especially important in relation to this project, because Augmin is acting redundantly with other pathways to assist mitotic spindle formation. Because of this, genetic analysis is an invaluable tool for uncovering the extent of these redundancies. While the $msd1^{ex51}$*;cnn* double mutant elegantly demonstrated that mitotic spindle assembly, and *Drosophila* development, cannot

be supported in the absence of major pathways, there is no evidence to suggest that other MT generating pathways exist that have a comparable role in *Drosophila* development. A mutant screen for candidate genes in the *msd1*^{ex51} background might not only expose other mechanisms for MT amplification, but also the inter-relationships between other mechanisms of spindle assembly and MT generation. Moreover, generating 'synthetic lethality' with double mutants which are not lethal alone would again demonstrate redundancy within this system.

While *Drosophila* is an excellent system for studying this redundancy, another intriguing prospect would be to investigate the role of Augmin complex in spindle assembly *in vitro* using *Xenopus* egg extracts. Addition of mitotic chromatin to active extracts in the absence of centrosomes can support bipolar spindle assembly (Heald *et. al,* 1996), but whether spindle assembly in this system can be supported upon depletion of Msd1 would be very interesting.

Finally, the experiments in Section 3.3 of this thesis establish a role for Msd1 in central spindle assembly. Live analysis of S2 cells expressing α-Tubulin-GFP showed that central spindle assembly is disrupted in the absence of Msd1. This was caused by a reduced fluorescence recovery plateau in knock-down cells. A role for MT turnover during central spindle assembly is not well established, but this work is supported by recent experiments demonstrating a requirement for *de novo* MT nucleation directed by the HAUS complex during anaphase (Uehara *et. al,* 2010).

A similar study in anaphase to the analysis of nucleation events within the mitotic spindle using EB1-GFP comets in metaphase (Wainman *et. al,* 2009), would more directly demonstrate a role for Augmin in MT nucleation here. Furthermore, a comet profile would identify any localised regions of MT nucleation during anaphase, and also any directional bias of comets.

Again, it would be interesting to establish whether temporal regulation of Augmin exists between metaphase and anaphase. Analysis of post-translational modifications of Augmin subunits before and after metaphase might expose interactions with upstream proteins that are responsible for organising the mitotic and central spindles.

Drosophila spermatocytes provide a well-characterised system for studying cytokinesis phenotypes, and should be utilised for further analysis of the function of Augmin in anaphase. *wac* null mutant males are fertile, and exhibit no gross defects in cytokinesis, but appear to be lacking a 'central population' of MTs during anaphase and contractile ring organisation (M.Giansanti Pers. Comm.). Similarly, *spd-2* null mutant spermatocytes form anastral spindles that organise a central spindle and complete cytokinesis (M.Giansanti *et. al,* 2008). These observations again indicate a role for redundancy in this process, and double-mutant analysis with spindle assembly factors in an Augmin background might uncover new mechanisms during central spindle assembly.

In summary, this thesis has contributed to our understanding of the novel MAP Msd1 and its role in the Augmin complex. This thesis provides the first demonstration of the role of an Augmin complex subunit during *Drosophila* development, and furthermore describes a novel role for Msd1 in central spindle assembly – a mechanism that has not been demonstrated previously in *Drosophila.*

4.2. A divergent role for TD-60 in *Drosophila*

Section 3.4 of this thesis explores the role of CG9135, the *Drosophila* homologue of hTD-60. As a result of these experiments, it is very clear that dTD-60 does not perform an identical role in *Drosophila* as it does in human cells. Since the localisation, phenotype, and interactions of dTD-60 diverge from humans, further experiments were performed to ascertain the role of this protein. Initially, identification of, and subsequent RNAi analyses of the homologous *bj1* did not uncover a role for dTD-60 that was previously masked. To uncover the role of dTD-60 in *Drosophila,* generating a null mutant at the *CG9135* locus is important. This would eliminate the possibility that knock-down of dTD-60 is insufficient to produce a phenotype in S2 cells. Upon obtaining this mutant, genetic studies would more easily uncover the role that dTD-60 might have in concert with other proteins during development.

A preliminary RNAi screen of dTD-60 interactors did, however, uncover a number of genes that appear to have a function in mitosis. These studies provide a realistic, and exciting possibility that dTD-60 does have a role in mitotic spindle assembly, albeit different from that previously characterised in other organisms. Further

investigation into these interactions is necessary. Whether the localisations of these proteins and dTD-60 are reciprocally dependent remains to be seen, and requires antibody generation for the novel, and recently characterised genes.

Thus, this thesis does not support the hypothesis that CG9135 has a homologous role to hTD-60 in *Drosophila.* In contrast, a role for dTD-60 in spindle length regulation, via interacting proteins identified by Mass Spectrometry, is suggested.

5. References

Andersen, S., Ashford, A., Tournebize, R., Gavet, O., Sobel, A., Hyman, A., et al. (1997). Mitotic chromatin regulates phosphorylation of Stathmin/Op18. *Nature , 389* (6651), 640-3.

Ban, R., Irino, Y., Fukami, K., & Tanaka, H. (2004). Human mitotic spindle-associated protein PRC1 inhibits MgcRacGAP activity toward Cdc42 during the metaphase. *The Journal of biological chemistry , 279* (16), 16394-402.

Basto, R., Brunk, K., Vinadogrova, T., Peel, N., Franz, A., Khodjakov, A., et al. (2008). Centrosome amplification can initiate tumorigenesis in flies. *Cell , 133* (6), 1032-42.

Basto, R., Lau, J., Vinogradova, T., Gardiol, A., Woods, C., Khodjakov, A., et al. (2006). Flies without centrioles. *Cell , 125* (7), 1375-86.

Bischoff, F., & Ponstingl, H. (1991). Catalysis of guanine nucleotide exchange on Ran by the mitotic regulator RCC1. *Nature , 354* (6348), 80-2.

Bobinnec, Y., Khodjakov, A., Mir, L., Rieder, C., Eddé, B., & Bornens, M. (1998). Centriole disassembly in vivo and its effect on centrosome structure and function in vertebrate cells. *The Journal of cell biology , 143* (6), 1575-89.

Brinkley, B., Zinkowski, R., Mollon, W., & Davis, F. (1988, Jan 1). Movement and segregation of kinetochores experimentally detached from mammalian chromosomes. *nature.com* .

Brown, R., Lemmon, B., & Horio, T. (2004). Gamma-tubulin localization changes from discrete polar organizers to anastral spindles and phragmoplasts in mitosis of Marchantia polymorpha L. *Protoplasma , 224* (3-4), 187-93.

Bucciarelli, E., Pellacani, C., Naim, V., Palena, A., Gatti, M., & Somma, M. (2009, Oct 14). *Drosophila* Dgt6 Interacts with Ndc80, Msps/XMAP215, and gamma-Tubulin to Promote Kinetochore-Driven MT Formation. *Current biology : CB* .

Buffin, E., Emre, D., & Karess, R. (2007). Flies without a spindle checkpoint. *Nature cell biology , 9* (5), 565-72.

Burbank, K., Groen, A., Perlman, Z., Fisher, D., & Mitchison, T. (2006). A new method reveals microtubule minus ends throughout the meiotic spindle. *The Journal of cell biology , 175* (3), 369-75.

Calarco-Gillam, P., Siebert, M., Hubble, R., Mitchison, T., & Kirschner, M. (1983). Centrosome development in early mouse embryos as defined by an autoantibody against pericentriolar material. *Cell , 35* (3 Pt 2), 621-9.

Casanova, C., Rybina, S., Yokoyama, H., Karsenti, E., & Mattaj, I. (2008). Hepatoma up-regulated protein is required for chromatin-induced microtubule assembly independently of TPX2. *Molecular biology of the cell , 19* (11), 4900-8.

Cheeseman, I., Chappie, J., Wilson-Kubalek, E., & Desai, A. (2006). The conserved KMN network constitutes the core microtubule-binding site of the kinetochore. *Cell , 127* (5), 983-97.

Colombié, N., Cullen, C., Brittle, A., Jang, J., Earnshaw, W., Carmena, M., et al. (2008). Dual roles of Incenp crucial to the assembly of the acentrosomal metaphase spindle in female meiosis. *Development (Cambridge, England) , 135* (19), 3239-46.

DeLuca, J., Dong, Y., Hergert, P., Strauss, J., Hickey, J., Salmon, E., et al. (2005). Hec1 and nuf2 are core components of the kinetochore outer plate essential for organizing microtubule attachment sites. *Molecular biology of the cell , 16* (2), 519-31.

DeLuca, J., Moree, B., Hickey, J., Kilmartin, J., & Salmon, E. (2002). hNuf2 inhibition blocks stable kinetochore-microtubule attachment and induces mitotic cell death in HeLa cells. *The Journal of cell biology , 159* (4), 549-55.

Desai, A., & Mitchison, T. (1997). Microtubule polymerization dynamics. *Annual review of cell and developmental biology , 13*, 83-117.

Dix, C., & Raff, J. (2007). *Drosophila* Spd-2 recruits PCM to the sperm centriole, but is dispensable for centriole duplication. *Current biology : CB , 17* (20), 1759-64.

Dutta, D., Bloor, J., Ruiz-Gomez, M., VijayRaghavan, K., & Kiehart, D. (2002). Real-time imaging of morphogenetic movements in *Drosophila* using Gal4-UAS-driven expression of GFP fused to the actin-binding domain of moesin. *Genesis (New York, NY : 2000) , 34* (1-2), 146-51.

do Carmo Avides, M., & Glover, D. (1999). Abnormal spindle protein, Asp, and the integrity of mitotic centrosomal microtubule organizing centers. *Science (New York, NY) , 283* (5408), 1733-5.

do Carmo Avides, M., Tavares, A., & Glover, D. (2001). Polo kinase and Asp are needed to promote the mitotic organizing activity of centrosomes. *Nature cell biology , 3* (4), 421-4.

Dobbelaere, J., Josué, F., Suijkerbuijk, S., Baum, B., Tapon, N., & Raff, J. (2008). A genome-wide RNAi screen to dissect centriole duplication and centrosome maturation in *Drosophila*. *PLoS biology , 6* (9), e224.

Duncan, T & Wakefield, JG. (2007). Investigating the function of *CG9135* in *Drosophila melanogaster.* Undergraduate thesis. University of Oxford.

Foe, V., & Alberts, B. (1983). Studies of nuclear and cytoplasmic behaviour during the five mitotic cycles that precede gastrulation in *Drosophila* embryogenesis. *Journal of cell science , 61*, 31-70.

Foe, V., & Odell, G. (1989). Mitotic domains partition fly embryos, reflecting early cell biological consequences of determination in progress. *Integrative and Comparative Biology* .

Gadea, B., & Ruderman, J. (2006). Aurora B is required for mitotic chromatin-induced phosphorylation of Op18/Stathmin. *Proceedings of the National Academy of Sciences of the United States of America , 103* (12), 4493-8.

Gergely, F., Kidd, D., Jeffers, K., Wakefield, J., & Raff, J. (2000). D-TACC: a novel centrosomal protein required for normal spindle function in the early *Drosophila* embryo. *The EMBO journal , 19* (2), 241-52.

Giansanti, M., Bucciarelli, E., Bonaccorsi, S., & Gatti, M. (2008). *Drosophila* SPD-2 is an essential centriole component required for PCM recruitment and astral-microtubule nucleation. *Current biology : CB , 18* (4), 303-9.

Giet, R., McLean, D., Descamps, S., Lee, M., Raff, J., Prigent, C., et al. (2002). *Drosophila* Aurora A kinase is required to localize D-TACC to centrosomes and to regulate astral microtubules. *The Journal of cell biology , 156* (3), 437-51.

Glotzer, M. (2005). The molecular requirements for cytokinesis. *Science (New York, NY) , 307* (5716), 1735-9.

Gonzalez, C., Saunders, R., Casal, J., Molina, I., Carmena, M., Ripoll, P., et al. (1990). Mutations at the asp locus of *Drosophila* lead to multiple free centrosomes in syncytial embryos, but restrict centrosome duplication in larval neuroblasts. *Journal of cell science , 96 (Pt 4)*, 605-16.

Gonzalez, C., Sunkel, C., & Glover, D. (1998, Jan 1). Interactions between mgr, asp, and polo: asp function modulated by polo and needed to maintain the poles of monopolar and bipolar spindles. *Chromosoma* .

Goshima, G., Wollman, R., Stuurman, N., Scholey, J., & Vale, R. (2005). Length control of the metaphase spindle. *Current biology : CB , 15* (22), 1979-88.

Goshima, G., Mayer, M., Zhang, N., Stuurman, N., & Vale, R. (2008). Augmin: a protein complex required for centrosome-independent microtubule generation within the spindle. *The Journal of cell biology , 181* (3), 421-9.

Groen, A., Cameron, L., Coughlin, M., Miyamoto, D., Mitchison, T., & Ohi, R. (2004). XRHAMM functions in ran-dependent microtubule nucleation and pole formation during anastral spindle assembly. *Current biology : CB , 14* (20), 1801-11.

Gruss, O., Carazo-Salas, R., Schatz, C., Guarguaglini, G., Kast, J., Wilm, M., et al. (2001). Ran induces spindle assembly by reversing the inhibitory effect of importin alpha on TPX2 activity. *Cell , 104* (1), 83-93.

Gruss, O., Wittmann, M., Yokoyama, H., Pepperkok, R., Kufer, T., Silljé, H., et al. (2002). Chromosome-induced microtubule assembly mediated by TPX2 is required for spindle formation in HeLa cells. *Nature cell biology , 4* (11), 871-9.

Hannak, E., & Heald, R. (2006). Xorbit/CLASP links dynamic microtubules to chromosomes in the *Xenopus* meiotic spindle. *The Journal of cell biology , 172* (1), 19-25.

Hannak, E., Oegema, K., Kirkham, M., Gönczy, P., Habermann, B., & Hyman, A. (2002). The kinetically dominant assembly pathway for centrosomal asters in Caenorhabditis elegans is gamma-tubulin dependent. *The Journal of cell biology , 157* (4), 591-602.

Heald, R., Tournebize, R., Blank, T., Sandaltzopoulos, R., Becker, P., Hyman, A., et al. (1996). Self-organization of microtubules into bipolar spindles around artificial chromosomes in *Xenopus* egg extracts. *Nature , 382* (6590), 420-5.

Heald, R., Tournebize, R., Habermann, A., Karsenti, E., & Hyman, A. (1997). Spindle assembly in *Xenopus* egg extracts: respective roles of centrosomes and microtubule self-organization. *The Journal of cell biology , 138* (3), 615-28.

Horio, T., & Hotani, H. (1986, Jan 1). Visualization of the dynamic instability of individual microtubules by dark-field microscopy. *nature.com* .

Hughes, J., Meireles, A., Fisher, K., Garcia, A., Antrobus, P., Wainman, A., et al. (2008). A microtubule interactome: complexes with roles in cell cycle and mitosis. *PLoS biology , 6* (4), e98.

Hyman, A., & Mitchison, T. (1990). Modulation of microtubule stability by kinetochores in vitro. *The Journal of cell biology , 110* (5), 1607-16.

Kaláb, P., Pralle, A., Isacoff, E., Heald, R., & Weis, K. (2006). Analysis of a RanGTP-regulated gradient in mitotic somatic cells. *Nature , 440* (7084), 697-701.

Kalab, P., Weis, K., & Heald, R. (2002). Visualization of a Ran-GTP gradient in interphase and mitotic *Xenopus* egg extracts. *Science (New York, NY) , 295* (5564), 2452-6.

Kao, L.-R., & Megraw, T. (2009). Centrocortin cooperates with centrosomin to organize *Drosophila* embryonic cleavage furrows. *Current biology : CB , 19* (11), 937-42.

Kelly, A., Sampath, S., Maniar, T., Woo, E., Chait, B., & Funabiki, H. (2007). Chromosomal enrichment and activation of the aurora B pathway are coupled to spatially regulate spindle assembly. *Developmental cell , 12* (1), 31-43.

Khodjakov, A., & Rieder, C. (1999). The sudden recruitment of gamma-tubulin to the centrosome at the onset of mitosis and its dynamic exchange throughout the cell cycle, do not require microtubules. *The Journal of cell biology , 146* (3), 585-96.

Khodjakov, A., Cole, R., Oakley, B., & Rieder, C. (2000). Centrosome-independent mitotic spindle formation in vertebrates. *Current biology : CB , 10* (2), 59-67.

Khodjakov, A., Copenagle, L., Gordon, M., Compton, D., & Kapoor, T. (2003). Minus-end capture of preformed kinetochore fibers contributes to spindle morphogenesis. *The Journal of cell biology , 160* (5), 671-83.

Koffa, M., Casanova, C., Santarella, R., Köcher, T., Wilm, M., & Mattaj, I. (2006). HURP is part of a Ran-dependent complex involved in spindle formation. *Current biology : CB , 16* (8), 743-54.

Lampson, M., Renduchitala, K., Khodjakov, A., & Kapoor, T. (2004). Correcting improper chromosome-spindle attachments during cell division. *Nature cell biology , 6* (3), 232-7.

Lane, H., & Nigg, E. (1996). Antibody microinjection reveals an essential role for human polo-like kinase 1 (Plk1) in the functional maturation of mitotic centrosomes. *The Journal of cell biology , 135* (6 Pt 2), 1701-13.

Leber, B., Maier, B., Fuchs, F., Chi, J., Riffel, P., Anderhub, S., et al. (2010). Proteins required for centrosome clustering in cancer cells. *Science translational medicine , 2* (33), 33ra38.

Lee, M., Gergely, F., Jeffers, K., Peak-Chew, S., & Raff, J. (2001). Msps/XMAP215 interacts with the centrosomal protein D-TACC to regulate microtubule behaviour. *Nature cell biology , 3* (7), 643-9.

Liu, D., Vader, G., Vromans, M., Lampson, M., & Lens, S. (2009). Sensing chromosome bi-orientation by spatial separation of aurora B kinase from kinetochore substrates. *Science (New York, NY) , 323* (5919), 1350-3.

Lüders, J., & Stearns, T. (2007). Microtubule-organizing centres: a re-evaluation. *Nature reviews Molecular cell biology , 8* (2), 161-7.

Mahoney, N., Goshima, G., Douglass, A., & Vale, R. (2006). Making microtubules and mitotic spindles in cells without functional centrosomes. *Current biology : CB , 16* (6), 564-9.

Maiato, H., Rieder, C., & Khodjakov, A. (2004). Kinetochore-driven formation of kinetochore fibers contributes to spindle assembly during animal mitosis. *The Journal of cell biology , 167* (5), 831-40.

Maller, J., Poccia, D., Nishioka, D., Kidd, P., Gerhart, J., & Hartman, H. (1976). Spindle formation and cleavage in *Xenopus* eggs injected with centriole-containing fractions from sperm. *Experimental cell research , 99* (2), 285-94.

Maresca, T., Groen, A., Gatlin, J., Ohi, R., Mitchison, T., & Salmon, E. (2009). Spindle assembly in the absence of a RanGTP gradient requires localized CPC activity. *Current biology : CB , 19* (14), 1210-5.

Marumoto, T., Hirota, T., Morisaki, T., Kunitoku, N., Zhang, D., Ichikawa, Y., et al. (2002). Roles of aurora-A kinase in mitotic entry and G2 checkpoint in mammalian cells. *Genes to cells : devoted to molecular & cellular mechanisms , 7* (11), 1173-82.

McCleland, M., Gardner, R., Kallio, M., Daum, J., Gorbsky, G., Burke, D., et al. (2003). The highly conserved Ndc80 complex is required for kinetochore assembly, chromosome congression, and spindle checkpoint activity. *Genes & development , 17* (1), 101-14.

Megraw, T., Kao, L., & Kaufman, T. (2001). Zygotic development without functional mitotic centrosomes. *Current biology : CB , 11* (2), 116-20.

Megraw, T., Li, K., Kao, L., & Kaufman, T. (1999). The centrosomin protein is required for centrosome assembly and function during cleavage in *Drosophila*. *Development (Cambridge, England) , 126* (13), 2829-39.

Meireles, A., Fisher, K., Colombié, N., Wakefield, J., & Ohkura, H. (2009). Wac: a new Augmin subunit required for chromosome alignment but not for acentrosomal microtubule assembly in female meiosis. *The Journal of cell biology , 184* (6), 777-84.

Mishra, R., Chakraborty, P., Arnaoutov, A., Fontoura, B., & Dasso, M. (2010). The Nup107-160 complex and gamma-TuRC regulate microtubule polymerization at kinetochores. *Nature cell biology , 12* (2), 164-9.

Mitchison, T., & Kirschner, M. (1984, Jan 1). Dynamic instability of microtubule growth. *Nature* .

Moutinho-Pereira, S., Debec, A., & Maiato, H. (2009). Microtubule cytoskeleton remodeling by acentriolar microtubule-organizing centers at the entry and exit from mitosis in *Drosophila* somatic cells. *Molecular biology of the cell , 20* (11), 2796-808.

Nachury, M., Maresca, T., Salmon, W., Waterman-Storer, C., Heald, R., & Weis, K. (2001). Importin beta is a mitotic target of the small GTPase Ran in spindle assembly. *Cell , 104* (1), 95-106.

Nicklas, R., & Ward, S. (1994). Elements of error correction in mitosis: microtubule capture, release, and tension. *The Journal of cell biology , 126* (5), 1241-53.

Nigg, E., & Raff, J. (2009). Centrioles, centrosomes, and cilia in health and disease. *Cell , 139* (4), 663-78.

Nogales, E., & Downing, K. (2008). Tubulin and Microtubule Structures. *The Role of Microtubules in Cell Biology*.

O'Connell, C., Loncarek, J., Kaláb, P., & Khodjakov, A. (2009). Relative contributions of chromatin and kinetochores to mitotic spindle assembly. *The Journal of cell biology , 187* (1), 43-51.

Ohba, T., Nakamura, M., Nishitani, H., & Nishimoto, T. (1999). Self-organization of microtubule asters induced in *Xenopus* egg extracts by GTP-bound Ran. *Science (New York, NY) , 284* (5418), 1356-8.

Ohtsubo, M., Okazaki, H., & Nishimoto, T. (1989). The RCC1 protein, a regulator for the onset of chromosome condensation locates in the nucleus and binds to DNA. *The Journal of cell biology , 109* (4 Pt 1), 1389-97.

Parks, A., Cook, K., Belvin, M., Dompe, N., Fawcett, R., Huppert, K., et al. (2004). Systematic generation of high-resolution deletion coverage of the *Drosophila* melanogaster genome. *Nature genetics , 36* (3), 288-92.

Raff, J. (2001). Centrosomes: Central no more? *Current biology : CB , 11* (5), R159-61.

Rebollo, E., Llamazares, S., & Reina…, J. (2004, Jan 1). Contribution of noncentrosomal microtubules to spindle assembly in *Drosophila* spermatocytes. *PLoS biology* .

Riparbelli, M., Callaini, G., Glover, D., & Avides, M. (2002). A requirement for the Abnormal Spindle protein to organise microtubules of the central spindle for cytokinesis in *Drosophila*. *Journal of cell science , 115* (Pt 5), 913-22.

Rogers, G., Rusan, N., Peifer, M., & Rogers, S. (2008). A multicomponent assembly pathway contributes to the formation of acentrosomal microtubule arrays in interphase *Drosophila* cells. *Molecular biology of the cell , 19* (7), 3163-78.

Rosa, J., Canovas, P., Islam, A., Altieri, D., & Doxsey, S. (2006). Survivin modulates microtubule dynamics and nucleation throughout the cell cycle. *Molecular biology of the cell , 17* (3), 1483-93.

Ruchaud, S., Carmena, M., & Earnshaw, W. (2007). Chromosomal passengers: conducting cell division. *Nature reviews Molecular cell biology , 8* (10), 798-812.

Sampath, S., Ohi, R., Leismann, O., Salic, A., Pozniakovski, A., & Funabiki, H. (2004). The chromosomal passenger complex is required for chromatin-induced microtubule stabilization and spindle assembly. *Cell , 118* (2), 187-202.

Sawin, K., & Mitchison, T. (1991). Mitotic spindle assembly by two different pathways in vitro. *The Journal of cell biology , 112* (5), 925-40.

Saxton, W., & McIntosh, J. (1987). Interzone microtubule behavior in late anaphase and telophase spindles. *The Journal of cell biology , 105* (2), 875-86.

Schatz, C., Santarella, R., Hoenger, A., Karsenti, E., Mattaj, I., Gruss, O., et al. (2003). Importin alpha-regulated nucleation of microtubules by TPX2. *The EMBO journal , 22* (9), 2060-70.

Sharp, D., Rogers, G., & Scholey, J. (2000). Microtubule motors in mitosis. *Nature , 407* (6800), 41-7.

Shaw, S., Kamyar, R., & Ehrhardt, D. (2003). Sustained microtubule treadmilling in Arabidopsis cortical arrays. *Science (New York, NY) , 300* (5626), 1715-8.

Shelden, E., & Wadsworth, P. (1990). Interzonal microtubules are dynamic during spindle elongation. *Journal of cell science , 97 (Pt 2)*, 273-81.

Shi, W.-Y., & Skeath, J. (2004). The *Drosophila* RCC1 homolog, Bj1, regulates nucleocytoplasmic transport and neural differentiation during *Drosophila* development. *Developmental biology , 270* (1), 106-21.

Shimamura, M., Brown, R., Lemmon, B., Akashi, T., Mizuno, K., Nishihara, N., et al. (2004). Gamma-tubulin in basal land plants: characterization, localization, and implication in the evolution of acentriolar microtubule organizing centers. *The Plant cell , 16* (1), 45-59.

Silljé, H., Nagel, S., Körner, R., & Nigg, E. (2006). HURP is a Ran-importin beta-regulated protein that stabilizes kinetochore microtubules in the vicinity of chromosomes. *Current biology : CB , 16* (8), 731-42.

Stratmann, R., & Lehner, C. (1996). Separation of sister chromatids in mitosis requires the *Drosophila* pimples product, a protein degraded after the metaphase/anaphase transition. *Cell , 84* (1), 25-35.

Teixidó-Travesa, N., Villén, J., Lacasa, C., Bertran, M., Archinti, M., Gygi, S., et al. (2010). The gammaTuRC revisited: a comparative analysis of interphase and mitotic human gammaTuRC redefines the set of core components and identifies the novel subunit GCP8. *Molecular biology of the cell , 21* (22), 3963-72.

Theurkauf, W., & Hawley, R. (1992). Meiotic spindle assembly in *Drosophila* females: behavior of nonexchange chromosomes and the effects of mutations in the nod kinesin-like protein. *The Journal of cell biology , 116* (5), 1167-80.

Theurkauf, W. (1994). Microtubules and cytoplasm organization during *Drosophila* oogenesis. *Developmental biology , 165* (2), 352-60.

Torosantucci, L., De Luca, M., Guarguaglini, G., Lavia, P., & Degrassi, F. (2008). Localized RanGTP accumulation promotes microtubule nucleation at kinetochores in somatic mammalian cells. *Molecular biology of the cell , 19* (5), 1873-82.

Trieselmann, N., & Wilde, A. (2002). Ran localizes around the microtubule spindle in vivo during mitosis in *Drosophila* embryos. *Current biology : CB , 12* (13), 1124-9.

Tsai, M.-Y., Wiese, C., Cao, K., Martin, O., Donovan, P., Ruderman, J., et al. (2003). A Ran signalling pathway mediated by the mitotic kinase Aurora A in spindle assembly. *Nature cell biology , 5* (3), 242-8.

Tseng, B., Tan, L., Kapoor, T., & Funabiki, H. (2010). Dual detection of chromosomes and microtubules by the chromosomal passenger complex drives spindle assembly. *Developmental cell , 18* (6), 903-12.

Tulu, U., Fagerstrom, C., Ferenz, N., & Wadsworth, P. (2006). Molecular requirements for kinetochore-associated microtubule formation in mammalian cells. *Current biology : CB , 16* (5), 536-41.

Uehara, R., Nozawa, R.-s., Tomioka, A., Petry, S., Vale, R., Obuse, C., et al. (2009). The augmin complex plays a critical role in spindle microtubule generation for mitotic progression and cytokinesis in human cells. *Proceedings of the National Academy of Sciences of the United States of America , 106* (17), 6998-7003.

Uehara, R., & Goshima, G. (2010). Functional central spindle assembly requires de novo microtubule generation in the interchromosomal region during anaphase. *The Journal of cell biology , 191* (2), 259-67.

Vernì, F., Somma, M., Gunsalus, K., Bonaccorsi, S., Belloni, G., Goldberg, M., et al. (2004). Feo, the *Drosophila* homolog of PRC1, is required for central-spindle formation and cytokinesis. *Current biology : CB , 14* (17), 1569-75.

Wainman, A., Buster, D., Duncan, T., Metz, J., Ma, A., Sharp, D., et al. (2009). A new Augmin subunit, Msd1, demonstrates the importance of mitotic spindle-templated microtubule nucleation in the absence of functioning centrosomes. *Genes & development , 23* (16), 1876-81.

Wheatley, S., & Wang, Y. (1996). Midzone microtubule bundles are continuously required for cytokinesis in cultured epithelial cells. *The Journal of cell biology , 135* (4), 981-9.

Wheatley, S., Carvalho, A., Vagnarelli, P., & Earnshaw, W. (2001). INCENP is required for proper targeting of Survivin to the centromeres and the anaphase spindle during mitosis. *Current biology : CB , 11* (11), 886-90.

Wiese, C., Wilde, A., Moore, M., Adam, S., Merdes, A., & Zheng, Y. (2001). Role of importin-beta in coupling Ran to downstream targets in microtubule assembly. *Science (New York, NY) , 291* (5504), 653-6.

Wilde, A., & Zheng, Y. (1999). Stimulation of microtubule aster formation and spindle assembly by the small GTPase Ran. *Science (New York, NY) , 284* (5418), 1359-62.

Witt, P., Ris, H., & Borisy, G. (1980). Origin of kinetochore microtubules in Chinese hamster ovary cells. *Chromosoma , 81* (3), 483-505.

Wittmann, T., Wilm, M., Karsenti, E., & Vernos, I. (2000). TPX2, A novel *Xenopus* MAP involved in spindle pole organization. *The Journal of cell biology , 149* (7), 1405-18.

Wong, J., & Fang, G. (2006). HURP controls spindle dynamics to promote proper interkinetochore tension and efficient kinetochore capture. *The Journal of cell biology , 173* (6), 879-91.

Yokoyama, H., Rybina, S., Santarella-Mellwig, R., Mattaj, I., & Karsenti, E. (2009). ISWI is a RanGTP-dependent MAP required for chromosome segregation. *The Journal of cell biology , 187* (6), 813-29.

Zhu, C., & Jiang, W. (2005). Cell cycle-dependent translocation of PRC1 on the spindle by Kif4 is essential for midzone formation and cytokinesis. *Proceedings of the National Academy of Sciences of the United States of America , 102* (2), 343-8.

Zhu, H., Coppinger, J., Jang, C.-Y., Yates, J., & Fang, G. (2008). FAM29A promotes microtubule amplification via recruitment of the NEDD1-gamma-tubulin complex to the mitotic spindle. *The Journal of cell biology , 183* (5), 835-48.

Zhu, H., Fang, K., & Fang, G. (2009). FAM29A, a target of Plk1 regulation, controls the partitioning of NEDD1 between the mitotic spindle and the centrosomes. *Journal of cell science , 122* (Pt 15), 2750-9.

Zimmerman, W., Sillibourne, J., Rosa, J., & Doxsey, S. (2004). Mitosis-specific anchoring of gamma tubulin complexes by pericentrin controls spindle organization and mitotic entry. *Molecular biology of the cell , 15* (8), 3642-57.